THE UNIVERSITY OF CHICAGO

TRANSITION METAL MEDIATED TRANSFORMATIONS IN SMALL MOLECULE AND ENZYMATIC SYSTEMS

A DISSERTATION SUBMITTED TO

THE FACULTY OF THE DIVISION OF THE PHYSICAL SCIENCES

IN CANDIDACY FOR THE DEGREE OF

DOCTOR OF PHILOSOPHY

DEPARTMENT OF CHEMISTRY

BY

NATALIE H. CHAN

CHICAGO, ILLINOIS

DECEMBER 2021

Table of contents

List of Figures

List of Tables

Acknowledgements

I would like to thank those who have contributed to the research in this dissertation. I would foremost like to thank my advisor, Prof. Jared Lewis, for his guidance and consistent pressure to achieve ambitious goals. I have reached new levels of my potential and become a more resilient person under his mentoring.

It is a privilege to be mentored by and collaborate with Joe Gair. Joe's dedication to the scientific process and his work ethic hugely motivated me in my own work and inspired me to be a better mentor to junior students in the lab. Joe's friendship and support kept me afloat in the many difficult times during graduate school. For all this, I cannot thank him enough.

The Lewis lab would not be such an enjoyable place to work at without its amazing former and current group members, many of whom supported me scientifically and/ or personally. I thank everyone I have interacted with, specifically Christian Gomez, Harrison Snodgrass, Atreyi Bhattacharya, David Upp, Brian Fisher, Rui Huang, Xinhang Yang, Yasmine Zubi, and Mary Andorfer.

The work in this dissertation was only made possible with the help from many people outside of my lab. For instrumental assistance at UChicago and Argonne, I thank Antoni Jurkiewicz, Jin Qin, Alex Filatov, and Sun Yin Grass. I am thankful for the instrumental help I received at IU, specifically the Flood lab, the Dann lab, Rob Pepin, Angie Hansen, Jon Trinidad, and Frank Gao. I would also like to thank my thesis committee, Prof. John Anderson and Prof. Joseph Piccirilli, for their helpful questions and comments on this work.

Lastly, I would not have survived and thrived in this Ph.D. program without the support of my friends and family. My friends from the UChicago chemistry cohort kept me sane with competitive innertube water polo and our many adventures in Chicago. My in-laws, Joe, Jeanne, and Marc Maguire, became my family in the US and always cheer me on. My husband, Jack Maguire, has been a constant source of love and support in the last few years that had been extremely difficult for me. Most of all, I am grateful to my parents. They instilled in me the importance of hard work, and have always supported and believed in me no matter what path I take.

A note on numbering

Compounds in each chapter of this dissertation are numbered independently. Figures, tables and references are numbered continuously across chapters.

Abstract

This dissertation describes efforts toward achieving transformations in organic molecules – in particular, C–H functionalization and hydrosilylation, mediated by transition metal catalysts in small molecule, enzymatic, and artificial metalloenzyme systems.

In Chapter 1, a proposed dual catalytic cycle system using two transition metal catalysts for non-directed C–H functionalization was introduced. The system may have the potential to achieve C–H functionalization via one-pot substrate C–H activation by a first metal catalyst, followed by functionalization of the activated substrate catalyzed by a second metal catalyst. Transmetallation of a hydrocarbyl fragment between the two metal intermediates is the lesser-known process in this system and was studied in this chapter. Several novel pre-formed metal precursors of transmetallation were synthesized and tested. The best transmetallation yield of this project was obtained with the preformed metal complexes ^{iPr}(PNP)RhPh and (SPhos)Pt(*p*-Tol)(Cl). Efforts to complete the dual catalytic system were also described.

In Chapter 2, C–H functionalization of *N*-succinylated leucine (NsL) by Fe(II) α-KG-dependent hydroxylase SadA was explored. This work was built upon literature precedent of non-native chlorination of NsL by mutant SadA D157G in the presence of NaCl by exploiting the mechanistic similarities between Fe(II) α-KG-dependent hydroxylases and halogenase. The binding between exogenous anions and Fe(II) in SadA D157G was studied in this chapter via anion activity assay, steady-state kinetics, and UV-vis titration assay of the mutant in the presence of different anions. These studies provide several lines of evidence of anion binding to Fe(II) in the enzyme.

In Chapter 3, the development toward an artificial metalloenzyme (ArM) comprising of streptavidin (SAV) and a bioconjugated Ni(II) salicylaldiminato catalyst was described. This ArM has the potential to perform olefin hydrosilylation or polymerization in aqueous medium. A small molecule Ni(II) salicylaldimine catalyst for aqueous olefin hydrosilylation was identified. A biotinylated analogue was synthesized and shown to bioconjugate to SAV. The resulting ArM has yet to demonstrate olefin hydrosilylation activity. Control reactions point to detrimental interaction between residue(s) in binding pocket of SAV and Ni(II) as cause for inactivity. Efforts to circumvent this issue are ongoing.

Chapter 1 Transmetallation of hydrocarbyl fragments between two transition metal complexes

Introduction

Chemical synthesis is central to improving the quality of the modern life – from pharmaceutical drugs to materials in manufacturing, and agrochemicals. All of these materials require the synthesis of organic compounds with functional groups that provide the desired characteristics for their end use. Most functional group installation relies on an existing functional group in the precursor to act as a synthetic handle that can be transformed into a new functional group. In order to achieve this, the existing functional group on the precursor oftentimes needs to be pre-installed and is not inherently useful for the end use, creating waste and inefficiencies. Examples of transformation reliant of pre-functionalized substrates include cross coupling and electrophilic aromatic substitution (EAS).

C–H bonds are ubiquitous in organic molecules. Functionalizing a C–H bond obviates the need to pre-functionalize the targeted site on the precursor, making C–H functionalization a very attractive approach to organic synthesis.[1,2] There are two major challenges to successful C–H functionalization. Many C–H bonds are quite stable and energetically similar to each other within the same precursor molecule such that it is not a trivial task to (i) activate and functionalize a C–H bond and, (ii) to do so selectively. Common tactics used to address these challenges include:

1. Relying on an electronic bias to make a certain C–H bond more electron rich (**Figure 1A** and **B**)[3,4] or more acidic (**Figure 1C**)[5,6] than its neighboring sites to favor functionalization there.

2. Relying on an existing directing group (usually also a functional group) to direct the installation of the new functional group at a proximal location (**Figure 1D**).[7,8]

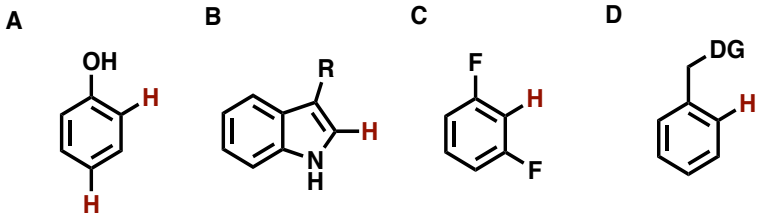

Figure 1. Common tactics to achieve site-selective C–H functionalization.

While these approaches have contributed significantly to the toolkit of synthetic chemists, there is still much potential within C–H functionalization that is not exploited by these approaches. The tactics listed above require prefunctionalized substrates in order to target a specific site. This limits the substrate scope of the transformations; substrates without these pre-installed functional group cannot be functionalized selectively, if at all. The prefunctionalized substrate approach also restricts the functionalization to occur at one (or sometimes two) C–H bonds within the same substrate. It would be difficult to override the inherently more favorable C–H bond(s) in such a substrate to functionalize a different C–H bond selectively.

An appealing alternative approach that complements the prefunctionalized substrate tactic is non-directed C–H functionalization. Such functionalization does not achieve selectivity by relying on directing groups; rather, it takes advantage of the subtle

differences in electronic effects and steric accessibility between the substrate and other reagents to favor certain C–H bond(s) for functionalization.[9] With the exception of H/D exchange in a substrate, examples of non-directed, catalytic C–H functionalization are rather rare compared to the ones using the other aforementioned approaches. One notable example is the C–H borylation of arenes reported by Hartwig and Smith concurrently.[10,11] These researchers independently showed that borylation with iridium catalysts favors the *meta* position on an arene regardless of whether the arene bears an electron withdrawing or donating group.

In general, non-directed C–H functionalization can be split into two processes: C–H activation, and functionalization of the activated carbon. There are many different mechanisms through which C–H activation occurs. One example of C–H activation involves a high-valent transition metal complex acting as an electrophile while the C–H bond acts as the nucleophile. Another example of C–H activation occurs via a low-valent transition metal complex and an electron-poor substrate undergoing C–H activation via concerted metallation deprotonation (CMD). There have been examples of stoichiometric C–H activation of unactivated arenes by transition metal complex in the last few decades (**Figure 2**).[12–14] These examples involve generating a highly active transition metal complexes that can cleave an inert C–H bond to form a relatively stable C–H activation complex that can be observed spectroscopically. Functionalizing the stable and isolable activated substrates in these cases would require harsh reagents given the stability of these complexes. For example, Bergman was able to functionalize a neopentyl group on the C–H activation complex (Cp*)(PMe_3)Ir(neopentyl)(H) using fluorosulfonic acid or

mercury(II) chloride followed by bromine.[14] The use of such harsh reagents results in transition metal complexes that are incapable of turning over for another C–H activation, rendering the reaction stoichiometric.

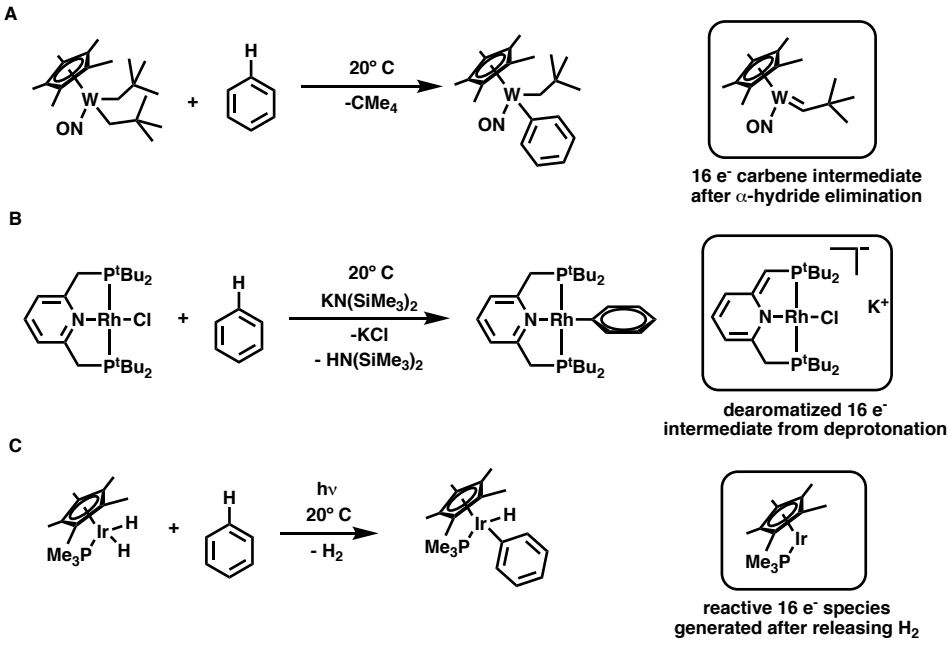

Figure 2. Examples of stoichiometric C–H activation by transition metal complexes.

The Lewis group envisioned that two transition metal catalysts could be used to create a dual catalytic cycle to achieve both C–H activation and the subsequent functionalization steps catalytically in a one-pot fashion and without the need for harsh reagents (**Figure 3**). On the left of the scheme, we hope to harness one of the transition metal complexes (M1) listed in **Figure 2** to form the activated M1 complex after C–H activation of the substrate. To avoid the use of harsh reagents for functionalizing the hydrocarbyl fragment on M1, we propose using another transition metal complex (M2) known to catalyze cross coupling reactions for the final functionalization, such as some combination of Pd(0) precursor with ligand(s). There are some examples in the literature showing it is possible

to transfer a hydrocarbyl group from one transition metal complex to another under relatively mild conditions.[15–18] In our dual catalytic cycle proposal, M2 would (i) undergo oxidative addition of R–X (where R is the desired functional group in the final product and X is a leaving group), (ii) carry out transmetallation with the activated M1 species to exchange the X group for the hydrocarbyl group on M1, and (iii) undergo reductive elimination of the final functionalized product. While the cross-coupling aspect in the functionalization cycle in **Figure 3** is well-established, the transmetallation of a hydrocarbyl group between two transition metal complexes and the turning over of the C–H activation cycle are less explored aspects of our proposed system. Our group first set out to investigate transmetallation of a hydrocarbyl group between two transition metal complexes, hoping a better understanding of this step would ultimately enable dual catalytic cycle for C–H functionalization in the future.

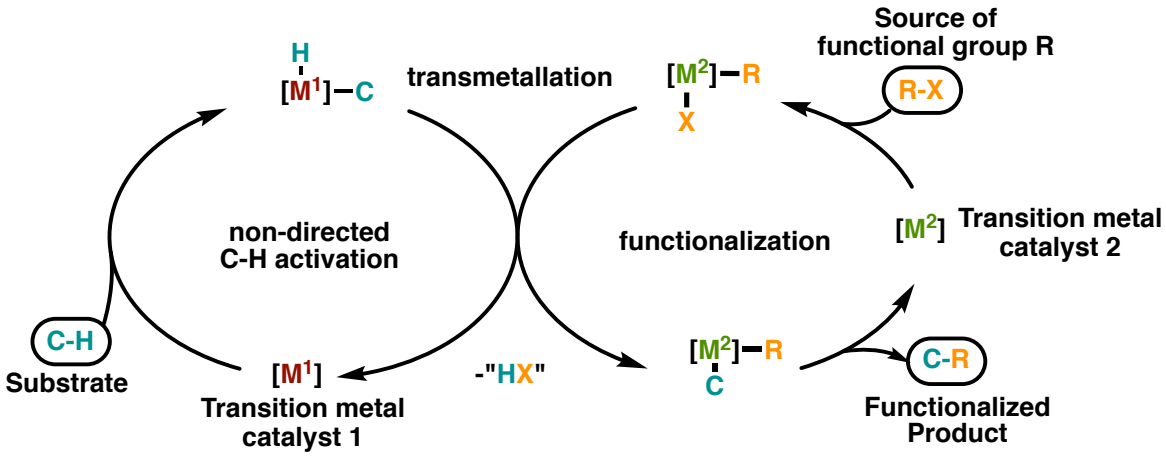

Figure 3. Proposed dual catalytic cycle for C–H functionalization

Previous work

The effort to explore the feasibility of transmetallation in the context of the proposed dual catalytic system was spearheaded by former members of the group, Dr. Landon Durak and Dr. Joe Gair. To eliminate complications arising from the reactions preceding transmetallation, and for ease of observation by spectroscopy, preformed M1 and M2 complexes were used for studying transmetallation. The preformed M1 complexes are known products of C–H activation or structural analogues to such products, while the preformed M2 complexes are analogous to those resulting from oxidative addition of an alkyl or aryl halide to a low valent Pd or Pt complex (hereinafter, preformed M1 and M2 are referred to as "M1" and "M2", respectively).

Dr. Durak extensively studied a model transmetallation between Ir(III) and Pt(II) complexes.[19] Inspired by Bergman's heavily studied complex Cp*Ir(PMe_3)$(H)_2$ (**Figure 2C**), Cp*Ir(PMe_3)$(benzyl)_2$ was chosen as M1. (cod)Pt(Me)(X), where X is a less coordinated anionic ligand, was chosen as M2 on account of extensive precedent for transmetallation to d^8 square planar Pt(II) complexes and the stability of Pt(II)-dialkyl complexes that do not undergo reductive elimination as easily as Pd(II) complexes.[20,21] Upon heating, this pair of M1 and M2 underwent stoichiometric transmetallation of a benzyl group (**Figure 4A**). Dr. Durak observed a higher yield of the transmetallated product when a more labile X group was initially installed on (cod)Pt(Me)(X). This suggests a potential ionization equilibrium between (cod)Pt(Me)(X) and its Pt(II) cation preceding transmetallation (**Figure 4B**). This hypothesis was supported by three lines of evidence: (I) The transmetallation reaction is first order in (cod)Pt(Me)(X). (II) The reaction

exhibits saturation behavior for Cp*Ir(PMe$_3$)(benzyl)$_2$. (III) The k_{obs} of the reaction is positively correlated to the polarity of reaction solvent used.

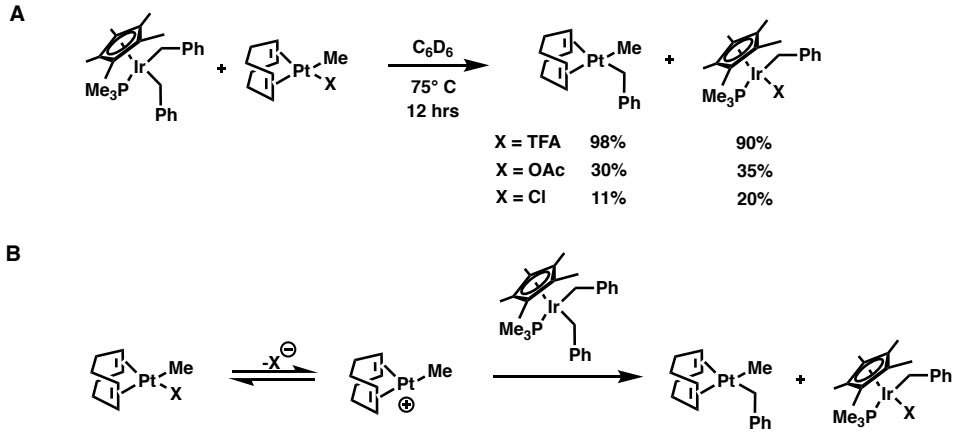

Figure 4. Stoichiometric transmetallation of benzyl group between Ir(III) and Pt(II)

Dr. Durak then sought to render the system catalytic for M2 (**Figure 3**).[22] Dr. Durak developed a system for direct arylation of simple arenes such as 1,2-dichlorobenzene with stoichiometric Cp*Ir(PMe$_3$)(Me)(Cl) as M1 and catalytic Pd[P(^{t}Bu)$_3$]$_2$ as M2 in the presence of KB(Ar^F)$_4$ (**Figure 5A**). The reaction works for a range of arenes with electron withdrawing or donating substituent(s) and site selectivity of the arylation appears to be primarily based on steric accessibility as opposed to electronic effects.

While we could not observe spectroscopically the fleeting intermediates of this reaction to aid us in delineating a mechanism, a putative mechanism of the reaction was proposed based on our other observations and the known reactivity of similar Ir complexes toward hydrocarbons (**Figure 5B**).[23–25] We proposed that Cp*Ir(PMe$_3$)(Me)(I) is first ionized by KB(Ar^F)$_4$ and water to form the cationic species [Cp*Ir(PMe$_3$)(Me)]$^+$. C–H activation of the arene substrate is then driven by the formation of methane to form another cationic species [Cp*Ir(PMe$_3$)(Ar)]$^+$. Transmetallation of the arene fragment could

occur from the cationic or the neutral Ir species to the cationic, post-oxidative-addition Pd(II) species. The final biaryl product is obtained after reductive elimination from the diaryl Pd(II) complex. Unfortunately, the M1 transmetallation product, $Cp^*Ir(PMe_3)(I)_2$ could not be transformed back into $Cp^*Ir(PMe_3)(Me)(I)$ for another round of C–H activation and transmetallation.

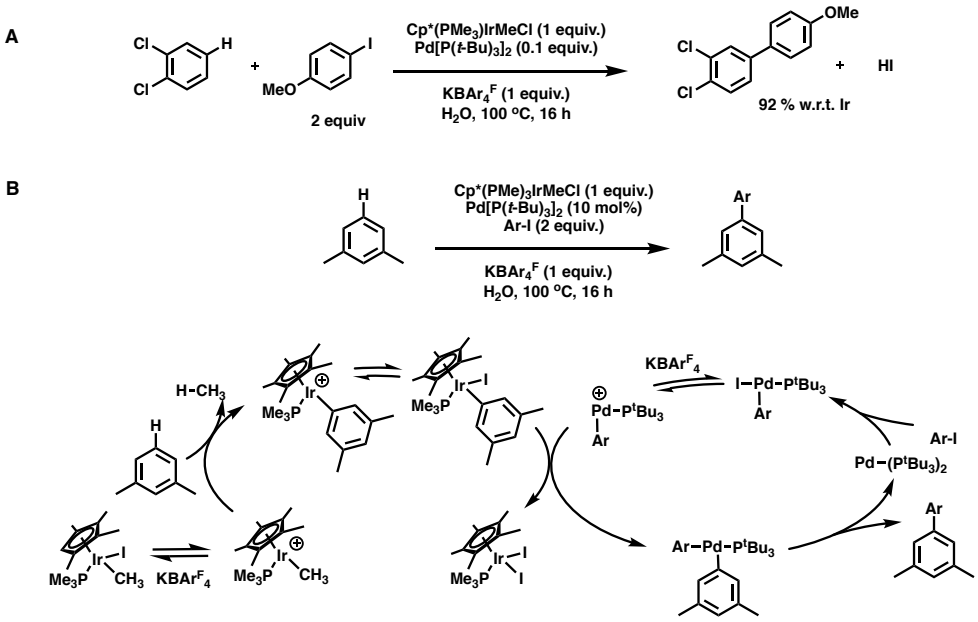

Figure 5. Direct arylation using catalytic amount of Pd(II) and stoichiometric Ir(III).

In search of a different platform that enables the turning over of C–H activation, Dr. Gair then investigated other potential hydrocarbyl donor complexes M1 including $(Cp)Mo(NO)(R)_2$, $(Cp)W(NO)(R)_2$, and pincer Rh complexes that are known to carry out activation of unactivated C–H bonds under mild conditions (**Figure 2A** and **B**).[26]

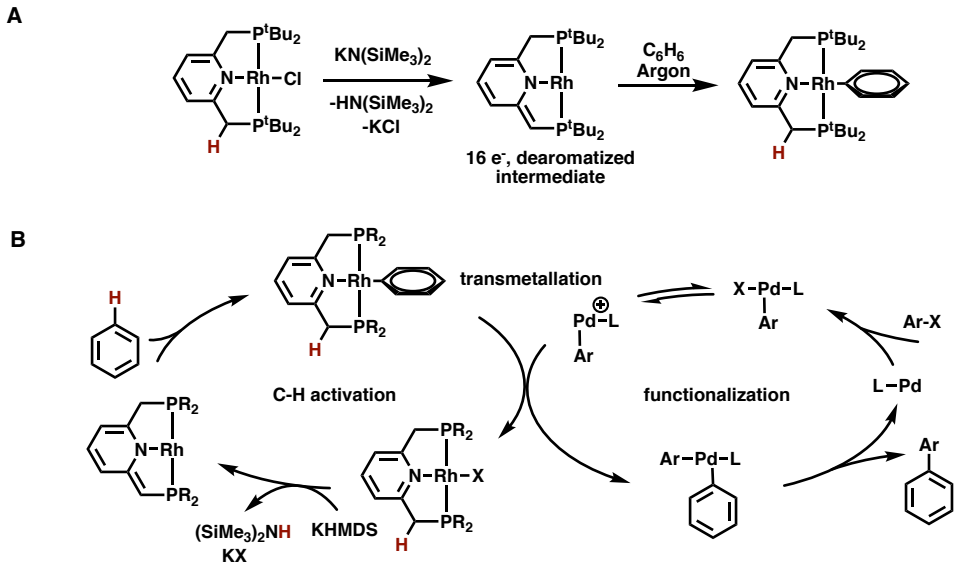

Figure 6. (PNP)Rh system capable of C-H activation and how it is envisioned to turnover in the proposed dual cycle system.

In particular, the family of Rh complexes with 2,6-bis(di-alkylphosphinomethyl)pyridine ligand (hereinafter "^{R}(PNP)", where R= alkyl groups on phosphines) developed by the Milstein group is an attractive choice for M1. The transmetallation product ^{tBu}(PNP)RhCl has been shown to be capable of activating benzene in the presence of a base via a 16-electron dearomatized intermediate (**Figure 6A**).[13] This is potentially a way to achieve turnover in the C–H activation cycle within the proposed dual catalytic system (**Figure 6B**). In our system, the ^{R}(PNP)RhCl can be formed again after transmetallation of the phenyl group from Rh to M2. The turnover of the Rh cycle relies on base KHMDS to deprotonate the methylene arm of the PNP ligand and abstraction of chloride from Rh by potassium cation. This result is promising to us because such strong bases are commonly used with cross coupling catalyzed by palladium complexes, suggesting cross-compatibility of these bases across the two

catalytic cycles in our system to be likely. The dearomatized Rh intermediate can then carry out another round of C–H activation.

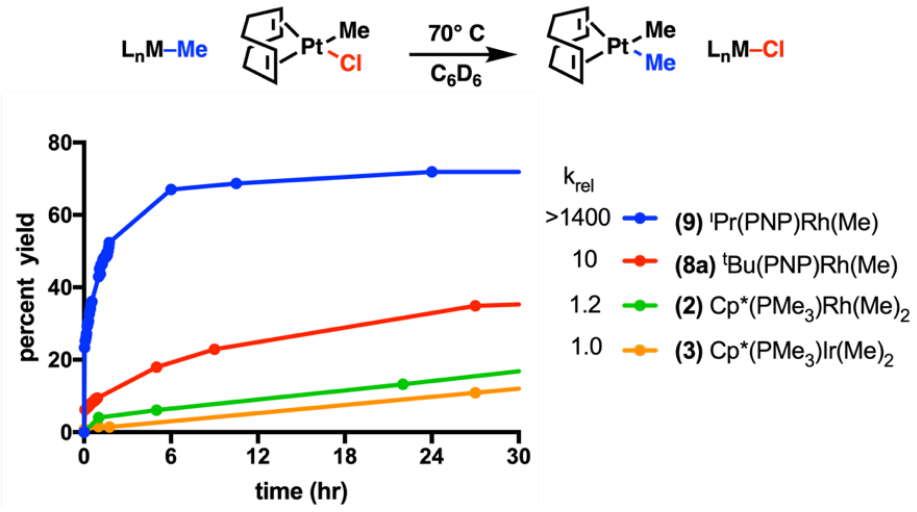

Figure 7. Qualitative comparison of transmetallation rates of different hydrocarbyl donors to (cod)Pt(Me)(Cl).The k_{rel} values are initial rates determined by [Pt]-dimethyl product formation at <10% conversion. In the fastest cases, the reactions achieved >10% conversion by the first time point (ca. 2 min after mixing). For these fast reactions, the k_{rel} represents a lower bound on the initial rate and was defined as the slope between the origin and the concentration of product at the first time point.

To compare the transmetallation competency of these M1 candidates with previously used systems, Dr. Gair conducted stoichiometric transmetallation reactions between (cod)Pt(Me)(Cl) and different M1 complexes and monitored the formation of transmetallation products over the course of the reaction (**Figure 7**). Pt(II) was used instead of Pd(II) such that the more stable transmetallation products can be observed spectroscopically and their yields calculated using 1H NMR peak integrations. The rates of transmetallation were compared across the different hydrocarbyl donors qualitatively. Results show that (i) (PNP)Rh complexes are by far the best candidates for transmetallation compared to donors with the Cp*(PMe3) ligand platform, and (ii)

decreasing the steric bulk on the (PNP) ligand from *tert*-butyl to isopropyl significantly enhances rate of transmetallation. Similar trends were observed in benzyl group transfer reactions.[26]

With the promising results of ^{iPr}(PNP)RhMe, Dr. Gair screened potential M2 candidates for transmetallation with ^{iPr}(PNP)RhPh (**Figure 8**). The phenyl group on Rh was chosen because aromatic substrates have the lowest C–H activation energy barriers among all the substrates our group has studied.[27] Good yields of the transmetallation Pt(II) product were observed for (cod)Pt(Me)(X) and (cod)Pt(*p*-tolyl)(X) for a number of X groups under room temperature or at 70 ^{o}C (**Figure 8A, B)**. We had hoped that Pd complexes would produce good yields of the reductive elimination biaryl products given the large body of Pd cross coupling literature. Surprisingly, none of the five Pd(II) complexes tested afforded any desired organic cross coupling or transmetallation products, whether the ancillary ligand is cod, a monodentate, bidentate, or hemilabile phosphine (**Figure 8C**).

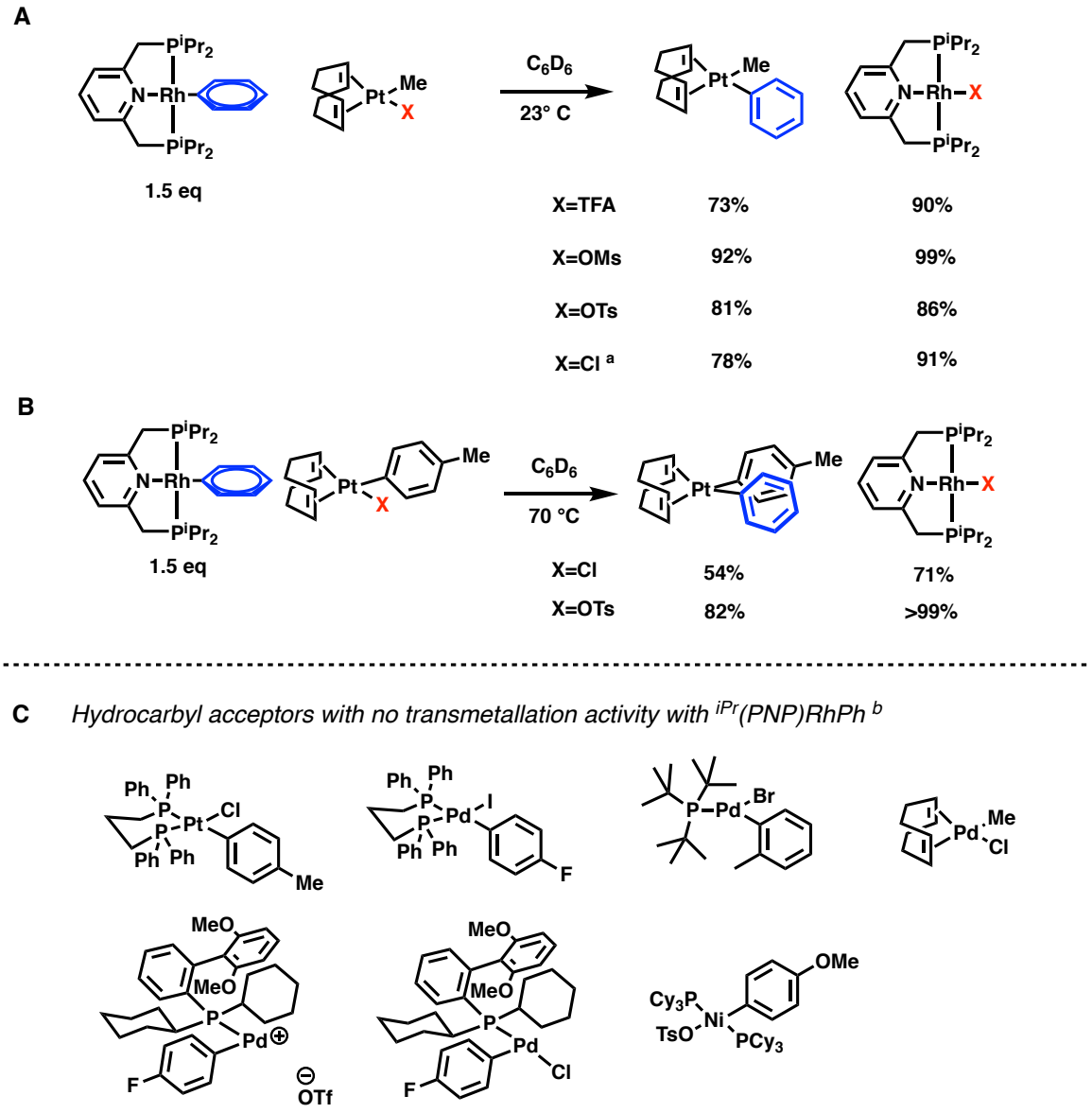

Figure 8. Scope of hydrocarbyl acceptors for transmetallation with iPr(PNP)RhPh.NMR yields are reported. [a.] Reaction was carried out at 70 °C. [b] Transmetallation carried out in C_6D_6 from 20 °C to 120 °C, with or without the following were attempted: co-solvent, excess aryl halide, ^{t}BuOK, ionizing additives. No clean transfer of Ph group observed.

Dr. Gair also investigated what types of bases could be used to turn over the C–H activation cycle of (PNP)RhX (**Figure 6B**). So far, only KHMDS and *tert*-butoxides of alkali metal cations (Na^+ or K^+) have been shown to turn over this cycle. We were aware of the chemistry of salt metathesis between alkali metal bases and halides on Pt(II) centers. [28,29]

KHMDS and *tert*-butoxides will likely undergo salt metathesis with our Pt(II) hydrocarbyl acceptors to generate substitution products with new, less labile X groups, which we have shown to be less conducive for transmetallation (**Figure 4A**, **8B**).[19,26] Alternative milder and/or bulkier bases that could potentially be compatible with Pt(II) or Pd(II) complexes were tested for the ability to deprotonate the benzylic proton on ^{iPr}(PNP)RhCl to generate the dearomatized Rh intermediate that can activate a C–D or C–H bond in the reaction solvent, benzene, to form ^{iPr}(PNP)RhPh (**Figure 9A**). We included bulky bases such as 2,6-di-*tert*-butyl-4-methoxyphenoxide in the hopes that it would remain on the outer sphere of the cationic group 10 complex after salt metathesis with the alkali metal ion such that the group 10 metal center could still undergo transmetallation from iPr(PNP)RhPh. Unfortunately, this base and other ones we tried showed no or trace conversion of ^{iPr}(PNP)RhCl to ^{iPr}(PNP)RhPh, even at elevated temperatures. However, the bulky phenoxide base showed desired activity with ^{iPr}(PNP)RhOMs to form ^{iPr}(PNP)RhPh (**Figure 9B**). At this time, we had yet to test whether the two types of viable bases would undergo salt metathesis with (cod)Pt(R)(X) to form the substitution product. Given the observed correlation between the lability of the leaving group on Pt and transmetallation yield, successful transmetallation between the substitution product with a less labile X group and the Rh hydrocarbyl donor may require extra optimization of conditions, which we have yet to attempt (**Figure 9B**).

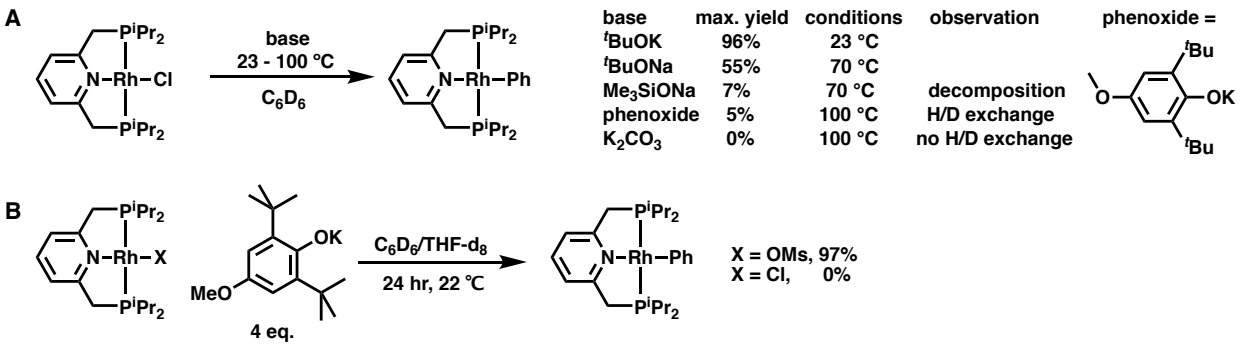

Figure 9. Screening of compatible bases for dual catalytic system. Figure adapted from Dr. Gair's thesis.[27]

When I first joined this project, I had the following goals given this body of work by Dr. Durak and Dr. Gair: (I) To better understand the mechanism by which the hydrocarbyl fragment is transferred between a group 9 donor and group 10 acceptor using a stereochemical probe. (II) To improve transmetallation by exploring alternatives of M1 and M2. (III) To test out base compatibility for a dual catalytic system.

Stereochemical probe

To better understand transmetallation between group 9 hydrocarbyl donors (M1) and group 10 hydrocarbyl acceptors (M2), we started investigating whether the hydrocarbyl group is transferred over from M1 to M2 via retention or inversion of stereochemistry. We designed a stereochemical probe (Cp*)(PMe_3)Ir(Ph)(*syn*-d_2-neohex) based on a similar one, (Cp*)(PMe3)Ir(Cl)(*anti*-neohex-d_2) synthesized in the literature.[30] (Hereinafter [Ir]=(Cp*)(PMe_3)Ir fragment.) The deuterium labeled neohexyl ligand on [Ir](Ph)(*syn*-neohex-d_2) can be used to assess the stereochemical course of transmetallation via the diagnostic difference in $^3J_{HH}$ coupling constants for *syn* versus

anti protons on ^{1}H NMR (**Figure 10**).[30] We chose to install a phenyl group on the probe as preliminary results from Dr. Durak showed exclusive transmetallation of an alkyl group from [Ir](alkyl)(aryl) complexes to (cod)Pt(Me)(TFA).[31] The *syn*-neohex-d_2 fragment was used instead of the *anti* one due to the relative ease of synthesizing the precursor compared to the former.

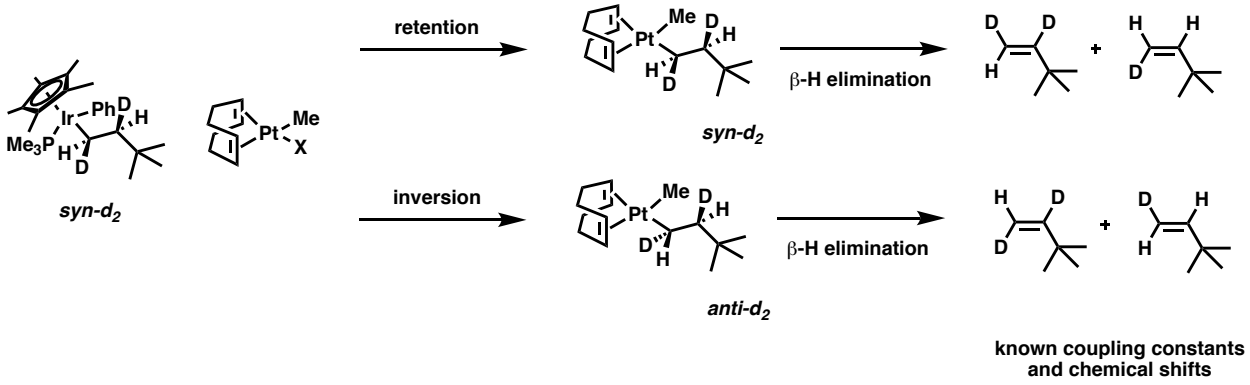

Figure 10. Proposed stereochemical probe for transmetallation of neohexyl group to (cod)Pt(Me)(X), where X = TFA, Cl, or OMs.

Michael Roy synthesized the per-protio version of the stereochemical probe and found the optimized conditions (X=OMs, $CDCl_3$, 70 ^{o}C) to carry out the transmetallation for maximum yield of Pt(II) product within 8 hours. His results also reveal that beta-hydride elimination occurred shortly after transfer of the neohexyl group, resulting in olefin product(s) (**Figure 10**). Due to the syn co-planar arrangement between the hydride and platinum that is required for beta-hydride elimination, the stereochemistry of the transfer is presumed to be preserved during the elimination. The production of olefin works in our favor as the $^{3}J_{HH}$ coupling constants and chemical shifts for the olefin proton peaks in these products are known; we could reach an easy conclusion of whether the neohexyl group transfer occurs with retention or inversion of stereochemistry.

I came into the project synthesizing the deuterated probe via a 9-step synthesis. The >94% enriched stereochemical probe and its crystal structure were obtained. Using Mr. Roy's optimized conditions, transmetallation between this probe and (cod)Pt(Me)(OMs) afforded several beta-hydride eliminated olefin products (**Figure 11A**). It would appear that some sort of H/D exchange of the product(s) occurred after transmetallation and/ or beta-hydride elimination, obscuring the stereochemistry of the neohexyl group transfer. Changing the reaction solvent from $CDCl_3$ to the less polar dichlorobenzene-d_4 did not prevent the H/D scrambling, nor did using less labile X group on (cod)Pt(Me)(X) such as chloride and trifluoroacetate. Control reactions show that an authentic product of >99% enriched (*E*)-1-deuterio-3,3-dimethyl-1-butene undergoes H/D scrambling in the presence of (i) $[Ir](Ph)^+$ (generated *in situ* from ionization of [Ir](Ph)(Cl) by $KB(Ar^F)_4$), (ii) (cod)Pt(Me)(OMs), or (iii) (cod)Pt(Me)(neohex) to afford similar olefin mixtures seen in the transmetallation (**Figure 11B**). Efforts to distill the volatile olefin products into a cold trap during the course of the reaction – hopefully before H/D exchange with other species occurs – still resulted in scrambled olefins in the distillate. Due to these difficulties, gleaning the stereochemistry of the transfer between these two complexes was not achieved, and further efforts to correct these issues were not pursued.

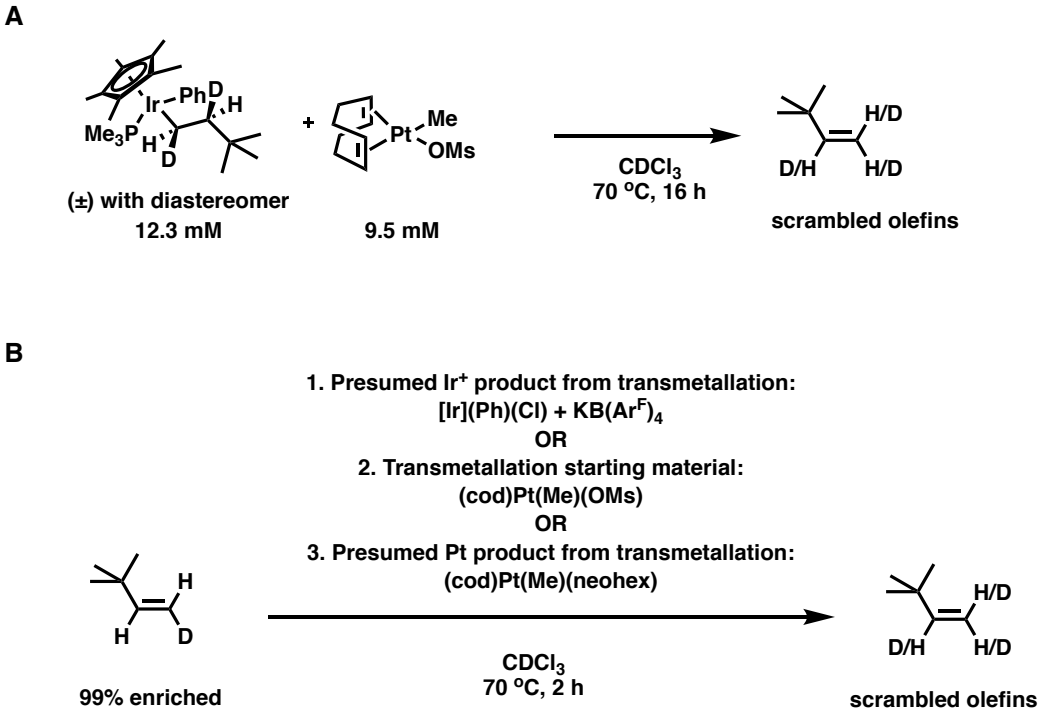

Figure 11. Transmetallation between stereochemical probe and (cod)Pt(Me)(OMs).(A) Transmetallation resulted in scrambled olefin products. (B) Control reactions between an authentic potential product and a presumed transmetallation product or the Pt starting material.

I considered using (cod)Pt(aryl)(X) as the acceptor instead. The aryl group in its transmetallation product (cod)Pt(aryl)(neohex) provides a little more steric hindrance around Pt than the methyl group does in (cod)Pt(Me)(neohex) and thus (cod)Pt(aryl)(X) may be less likely to undergo beta-hydride elimination to give the olefin product that is prone to H/D exchange. The neohexyl group may be less likely to undergo H/D exchange if it is still bound to Pt(II) so that the ^{1}H NMR peaks associated with the methylene protons can be analyzed to reveal the stereochemistry of the transfer. Control experiments were run before any transmetallation with the stereochemical probe was attempted. Upon heating, the presumed product (cod)Pt(*p*-tolyl)(neohex) afforded some beta-hydride elimination product. The experiment also shows that the ^{1}H NMR peaks associated with

the diagnostic methylene protons in the transmetallation product overlap with its own (cod) olefin peaks significantly. At this point, switching direction from Pt(II) to a different soft electrophile was perhaps a better way forward.

I turned my attention to $HgCl_2$ as a potential M2 candidate. $HgCl_2$ is known to (i) accept a neopentyl group from [Ir](Br)(neopentyl), and (ii) be a stereochemical probe acceptor for neohexyl group transfer with established $^3J_{HH}$ coupling values for the deuterated products.[14,32] Successful group transfer between [Ir](Ph)(syn-neohex-d_2) and two equivalents of $HgCl_2$ was observed. The $^3J_{HH}$ coupling constant of 5.5 Hz of the vicinal protons from the resulting HgCl(neohex-d_2) on ^{1}H NMR spectrum match with literature values for *threo*-3,3-dimethyl-1-butyl-1,2-d_2 mercuric chloride, whereas the erythro diastereomer has a reported $^3J_{HH}$ coupling constant of 12.3 Hz (**Figure 12A**).[32] This seems to point to retention in stereochemistry of the group transfer, consistent with a bent 3c2e bimolecular electrophilic substitution transition state. Upon closer inspection of the ^{1}H and ^{31}P NMRs of the first few hours of the reaction, we found that the phenyl group on [Ir](Ph)(syn-neohex-d_2) was first transferred to the first equivalent of $HgCl_2$ to form PhHgCl and [Ir](Cl)(syn-neohex-d_2) within the first hour which was confirmed by the spiking in of authentic [Ir](Cl)(syn-neohex-d_2). Only after all [Ir](Ph)(syn-neohex-d_2) had been converted to [Ir](Cl)(*syn*-neohex-d_2), was the neohexyl group transferred to another equivalent of $HgCl_2$ to form ClHg(neohex-d_2) and [Ir]Cl_2.The formation of [Ir]Cl_2 was confirmed by spiking in authentic [Ir]Cl_2. When an authentic sample of the presumed intermediate [Ir](Cl)(*syn*-neohex-d_2) was heated with excess $HgCl_2$, the same *threo*-3,3-

dimethyl-1-butyl-1,2-d_2 mercuric chloride product was observed along with [Ir](Cl)$_2$ within two hours, consistent with the retention of stereochemistry in the transfer (**Figure 12B)**.

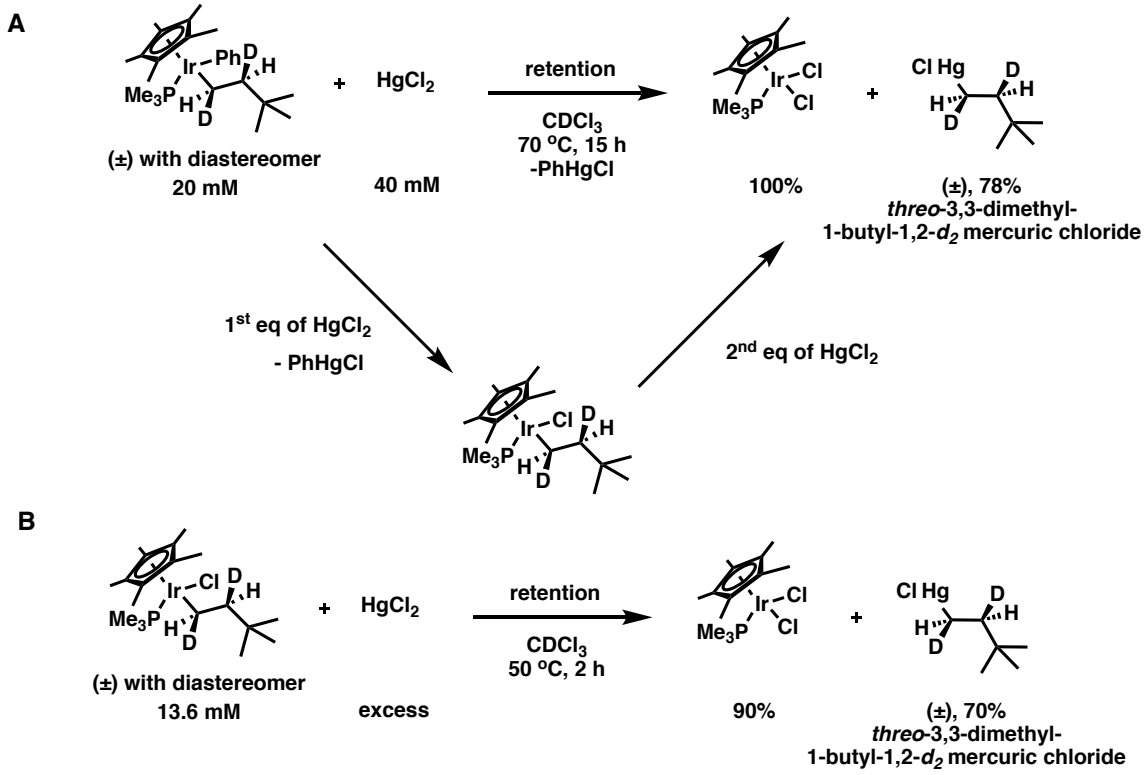

Figure 12. Transmetallation between stereochemical probe and $HgCl_2$.(A) Transmetallation with probe occurred in two steps via [Ir](Cl)(neohex-d_2). (B) Transmetallation of presume intermediate with $HgCl_2$.

Given the two-step group transfer, Hg(II) behaves very differently from Pt(II) which accepts only the neohexyl group, presumably via direct transfer from [Ir](Ph)(neohex) based on prior studies.[31] Although the $HgCl_2$ results do not offer us more information on the transmetallation between groups 9 and 10 metal centers, they provide insights on the complementary nature of the transfers to soft electrophiles. Transfer of the phenyl group is more favored in the case of Hg(II) while the alkyl group is preferred for Pt(II) in the intramolecular competition for transmetallation from [Ir](Aryl)(Alkyl).

Tuning the hydrocarbyl donor M1 to improve transmetallation

With Dr. Gair's excellent results showing M1 with ^{R}(PNP)Rh fragment outperforming those with the fragments (Cp*)(PMe_3)Ir or (Cp*)(PMe_3)Rh by 3 orders of magnitude in transmetallation of a methyl group (**Figure 7**), I sought ways to further improve transmetallation performance of M1 using the ^{R}(PNP)Rh platform. There were two promising preformed M1 candidates based on our existing data: (i) ^{Et}(PNP)RhPh where the isopropyl groups on the phosphines are replaced with ethyl, and (ii) a (PNP)RhPh where the PNP ligand is 2,6-bis(di-isopropylphosphinomethyl)-4-*N*-pyrrolidinyl-pyridine (hereinafter "pyrr-^{iPr}(PNP)") (**Figure 13**). Dr. Gair's data showed that when the R in ^{R}(PNP)RhMe was changed from *tert*-butyl to isopropyl, the qualitative initial rate of transmetallation of the methyl group to (cod)Pt(Me)(X) increased by over 100-fold (**Figure 7**). We speculated that the isopropyl groups open up more space for the methyl to be transferred to Pt. The natural next step would be to test the ^{Et}(PNP) ligand, which has never been synthesized before. We picked pyrr-^{iPr}(PNP)RhPh for electronic reasons – the *para*-pyrrolidinyl group would push more electron density onto Rh via the conjugated pincer ligand. Chirik and co-workers reported that substituting the *para*-hydrogen on the pyridine ring of ^{iPr}(PNP)Co(Cl) with a pyrrolidinyl group significantly lowers the redox potential of the complex, i.e., the complex is more electron rich at the metal center.[33] A more nucleophilic Rh for our system should in theory be better at transferring the phenyl group over to the electrophilic M2. The phenyl group was chosen for both candidates as a starting point due to our perceived ease of synthesis as ^{iPr}(PNP)RhPh was much more stable for handling compared to the methyl or benzyl analogs.

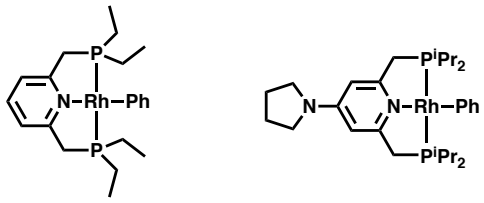

^{Et}(PNP)RhPh pyrr-^{iPr}(PNP)RhPh

Figure 13. Promising preformed hydrocarbyl donor candidates.

I attempted to synthesize the novel ^{Et}(PNP)RhPh and pyrr-^{iPr}(PNP)RhPh in order to test their abilities to transmetallate a phenyl group in the model reaction ^{iPr}(PNP)RhPh and (cod)Pt(Tol)(Cl). The novel ^{Et}PNP ligand was synthesized in high purity after testing several synthetic approaches (**Figure 14A**). I envisioned the final product ^{Et}(PNP)RhPh can be obtained using the same or similar protocols as those for ^{iPr}(PNP)RhPh (**Figure 14B**). Unfortunately, in my many attempts of metalating the ^{Et}PNP ligand with $[(coe)_2RhCl]_2$, black insoluble product(s) in benzene or THF were obtained, unlike the red soluble product from the iPr or tBu analogue. The $^{31}P\{^1H\}$ NMR of this product dissolved in DMSO showed one doublet of doublet peak and one doublet of triplet peak in 2:1 ratio (**Figure 14D**). Taking into account of ^{103}Rh and ^{31}P couplings in these peaks, it appears that each Rh center of two [κ^3-^{Et}(PNP)]Rh fragment coordinates to one of the phosphines on another ^{Et}(PNP) ligand in monodentate fashion, with the two chlorides in the outer sphere (**Figure 14C**). The ^{Et}PNP ligand seems to provide too much room for the Rh center in this case such that another ^{Et}PNP can be coordinated to Rh, forcing the chloride anion to stay in the outer sphere.

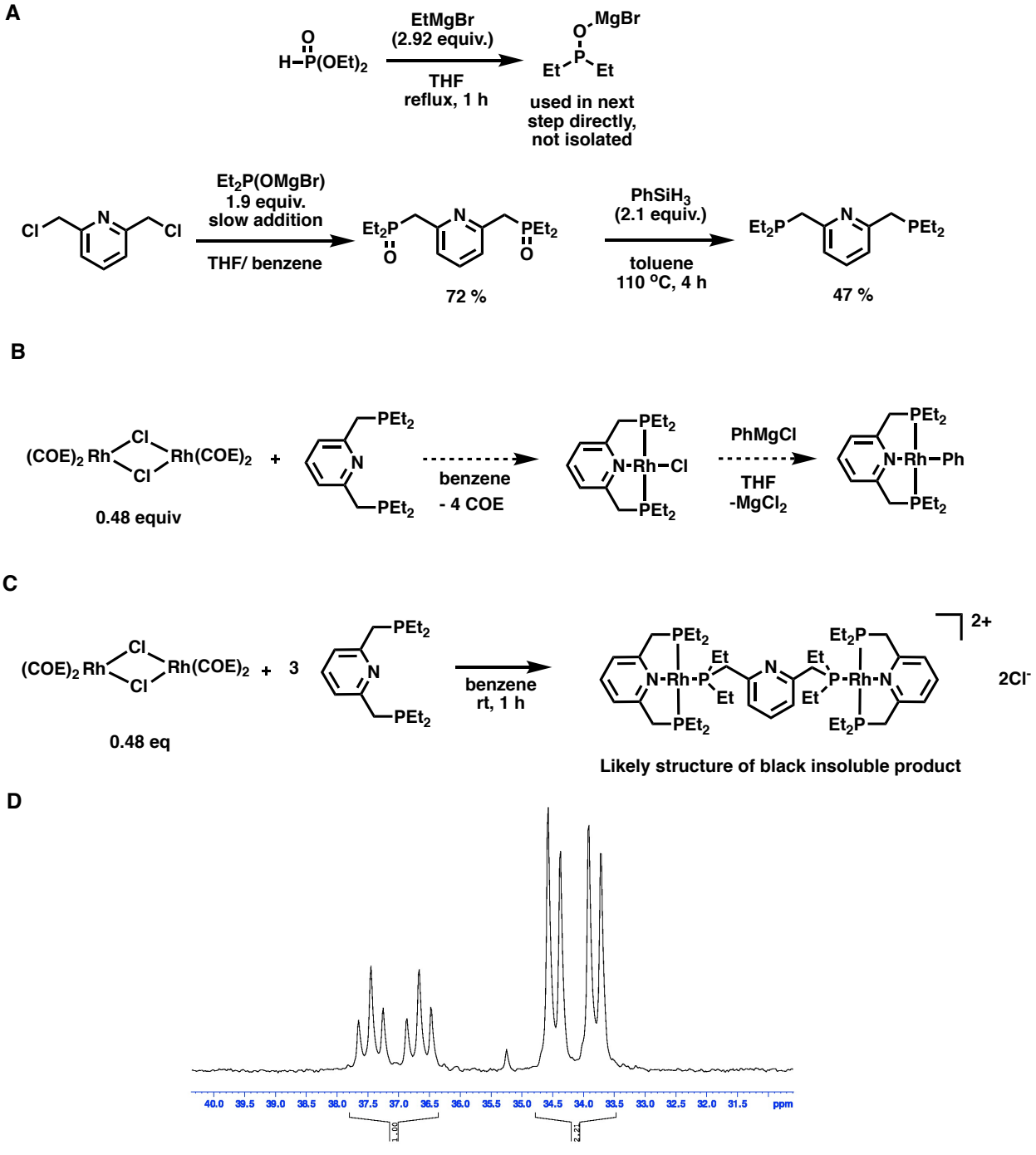

Figure 14. Efforts to synthesize Et(PNP)RhPh.(A) Synthesis of ^{Et}(PNP) ligand. (B) Proposed synthesis of ^{Et}(PNP)RhPh via metalation of ligand and subsequent Grignard reaction. (C) Dominant competitive pathway of metalation with proposed structure of product. (D) ^{31}P NMR of that product dissolved in DMSO.

Addition of a very dilute solution of the ^{Et}PNP ligand to $[(coe)_2RhCl]_2$ did appear to yield the desired ^{Et}(PNP)RhCl by ^{31}P NMR of the crude mixture but attempts to isolate the product resulted in the insoluble 3-ligand-2-metal product again. After many failed attempts of isolating ^{Et}(PNP)RhCl, I decided to focus my energy on other aspects of the project since the final M1 complex ^{Et}(PNP)RhPh will likely be too unstable to carry out transmetallation under the general conditions we use even if I was able to isolate it.

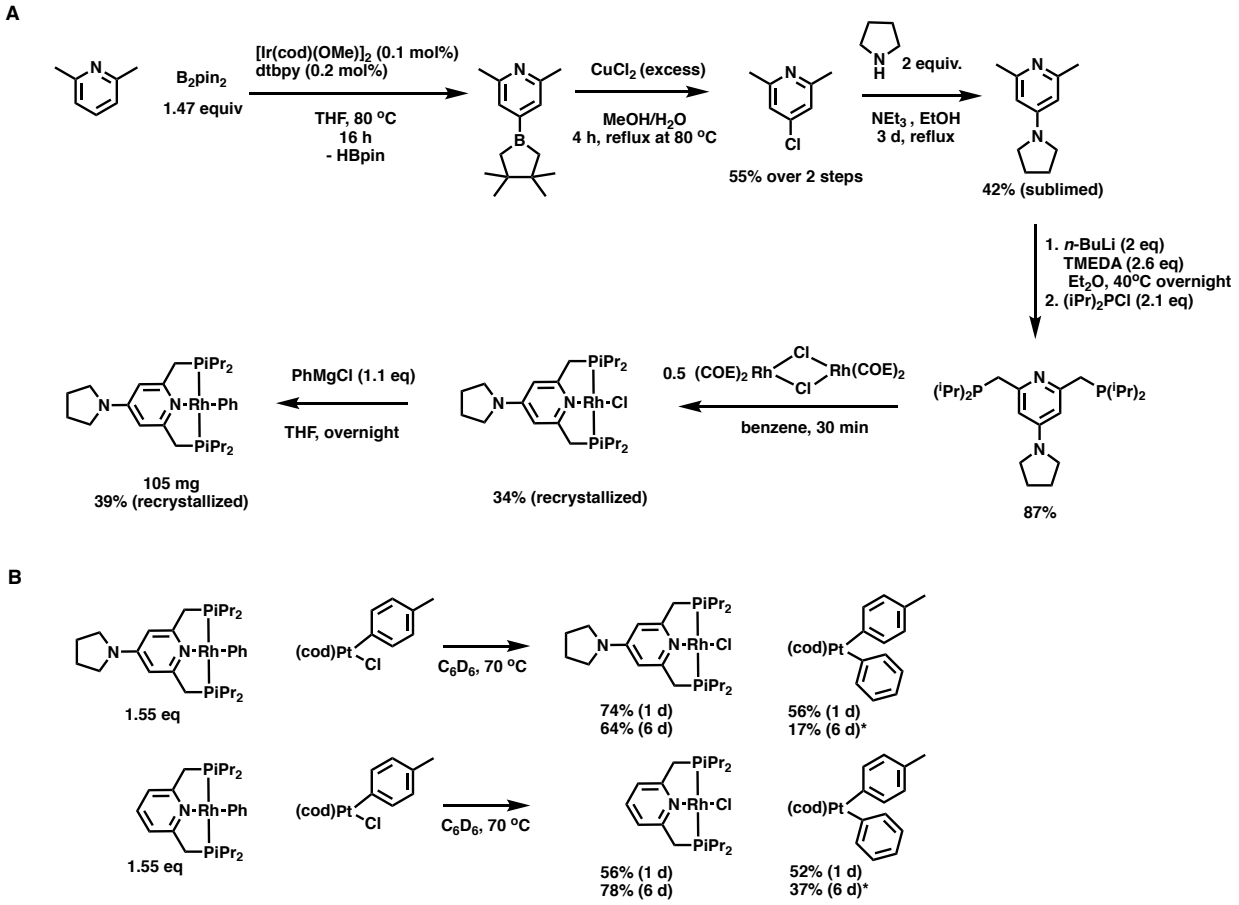

Figure 15. Synthesis and transmetallation reaction of pyrr-iPr(PNP)RhPh.

(A) Synthesis of pyrr-iPr(PNP)RhPh. (B) Transmetallation between pyrr-iPr(PNP)RhPh and (cod)Pt(p-Tol)(Cl) against model reaction using iPr(PNP)RhPh. *Desired reductive elimination product 4-phenyltoluene was observed by GC-MS in both reactions, accounting for the drop in Pt product yield over time.

In the case of the novel 4-pyrr-^{iPr}(PNP)RhPh, pure product was obtained in a 6-step synthesis and a crystal structure was obtained, confirming the product's structure (**Figure 15A**). When tested for transmetallation to (cod)Pt(*p*-Tol)(Cl) side by side with model reaction using ^{iPr}(PNP)RhPh, some improvement was observed but it was not as significant as we had hoped for. Within one day of heating, the pyrr-^{iPr}(PNP)RhPh reaction gave 74% and 56% NMR conversions to pyrr-^{iPr}(PNP)RhCl and (cod)Pt(*p*-Tol)(Ph), whereas the model reactions afforded 56% and 52% of the analogous products, respectively (**Figure 15B**). After six days of heating, the yields of both Rh products were roughly the same, whereas a drop in the yield of Pt products was observed. GC-MS analysis of both reactions on the sixth day showed the presence of reductive elimination product 4-phenyltoluene. Given the large amount of ^{iPr}(PNP)RhPh that was already on hand and the modest improvement provided by pyrr-^{iPr}(PNP)RhPh, we decided to carry out future transmetallations with ^{iPr}(PNP)RhPh. While some progress to enhance transmetallation was made by tuning the PNP ligand, more significant developments were produced on the hydrocarbyl acceptor's front.

Tuning hydrocarbyl acceptor M2 to improve transmetallation

The choice of ancillary ligand on the hydrocarbyl acceptor M2 was explored simultaneously. In the context of the proposed dual catalytic system (**Figure 3**), the ancillary ligand on M2 needs to provide just the right amount of electron density to M2 such that M2 is electron rich enough to carry out oxidative addition of the aryl halide substrate, but electron deficient enough to accept the hydrocarbyl transfer from the nucleophilic M1 in the transmetallation step. In Dr. Gair's studies, he explored transmetallation activity of Pt(II) bearing the ligands cod or dppp, which represent two ends of this spectrum: (cod)Pt(*p*-Tol)(Cl) with the less electron-donating bis-olefin ligand can transmetallate well but (cod)Pt systems are not known to carry out oxidative additions; (dppp)Pt(*p*-Tol)(Cl) with the more electron-donating bis-phosphine ligand was not able to transmetallate in our experiments although there have been reports of oxidative addition of aryl halide by Pt(0) complexes bearing bulky phosphine ligands (**Figure 8B, C**).[34–36] I came into the project exploring the ligands on Pt(II) that likely fall between these two extremes, in particular 4,4'-di-*tert*-butyl-2,2'-bipyridine (dtbpy), and the phosphine-containing hemilabile ligands (*Z*)-1-*tert*-butyl-2,3,6,7-tetrahydrophosphepine ("phosphepine" hereinafter) and SPhos (**Figure 16A**). My main focus was placed on using preformed $(L_n)Pt(Ar)(X)$ for transmetallation as Pt(II) does not carry out reductive elimination as easily as Pd(II) does, allowing for the observation of the buildup of M2 transmetallation product by NMR.

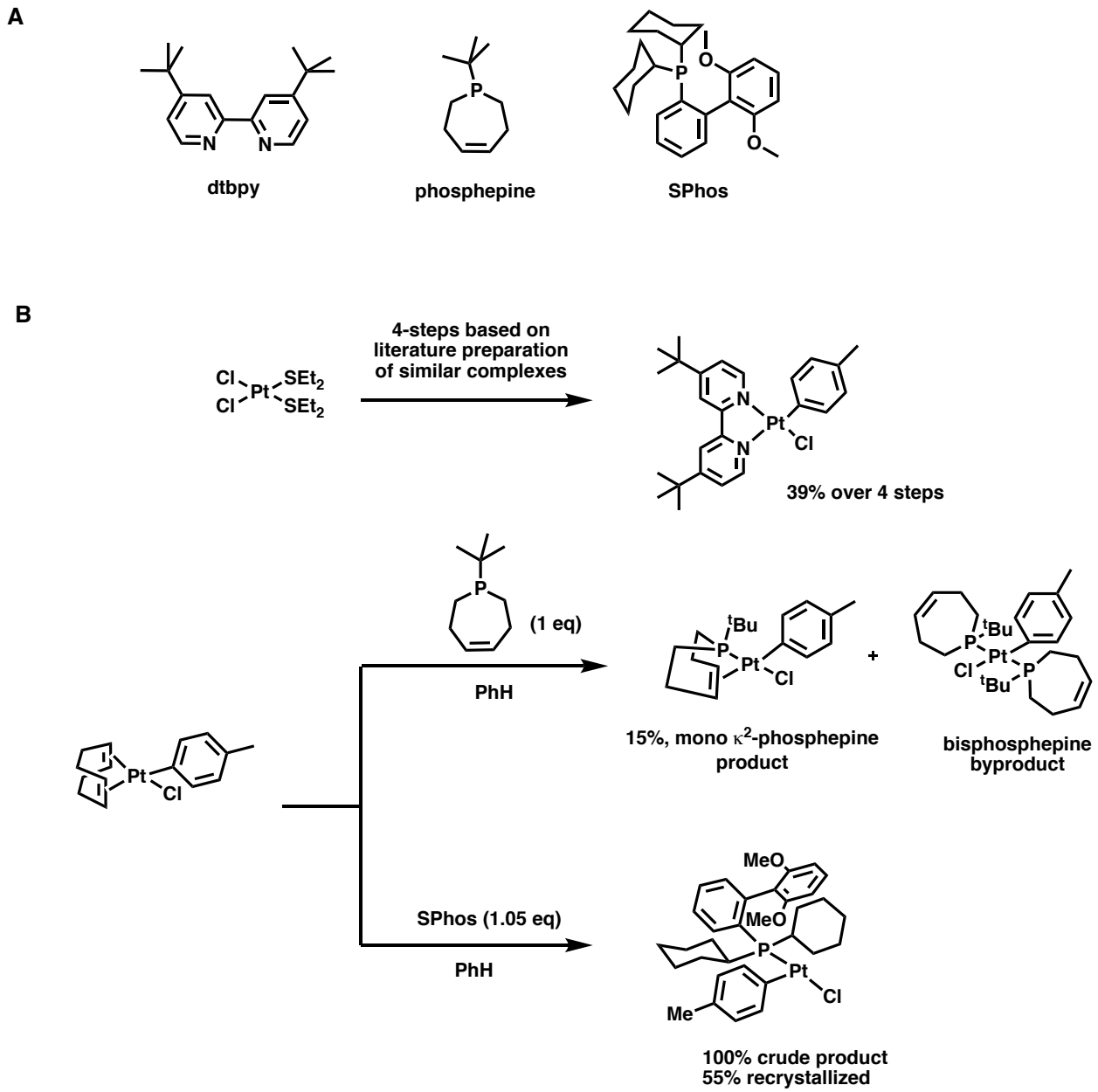

Figure 16. Choice of ancillary ligands for M2 complex (Ln)Pt(p-Tol)(Cl).(A) Promising ancillary ligands for Pt(II) transmetallation. (B) Syntheses of (L_n)Pt(*p*-Tol)(Cl) complexes

All three complexes of (L_n)Pt(*p*-Tol)(Cl) were synthesized with varying levels of difficulty (**Figure 16B**). Crystal structures of the novel (κ^2-phosphepine)Pt(*p*-Tol)(Cl) and (SPhos)Pt(*p*-Tol)(Cl) were obtained, confirming their structures. As far as we know,

(SPhos)Pt(*p*-Tol)(Cl) is the first reported complex in which a Buchwald ligand is to coordinate to Pt(II).

The three complexes were each tested against the model M2 complex, (cod)Pt(*p*-Tol)(Cl), in their abilities to accept the phenyl group from ^{iPr}(PNP)RhPh (**Figure 17A**). The (dtbpy) complex was even worse than the (cod) complex at transmetallation; the bipyridyl ligand likely provides more electron density to Pt(II) than (cod) does. Both phosphepine and SPhos ligands were superior to cod in product yields. Despite our initial worries that reductive elimination would be difficult on a Pt complex, both complexes underwent the process and afforded >50% yield of biaryl products from cross- or homo-coupling. The phosphepine complex gave an equal mix of biphenyl, bitolyl, and 4-phenyltoluene, indicating an unproductive transmetallation between two molecules of (phosphepine)Pt(*p*-Tol)(Ph) competing with reductive elimination of *p*-phenyltoluene. The SPhos complex, however, afforded the desired *p*-phenyltoluene product almost exclusively with 58% yield. This result was quite surprising to us as Dr. Gair had attempted transmetallation to a similar Pd congener, (SPhos)Pd(*p*-F-Ph)(Cl), which did not result in any of the desired product, 4-fluorobiphenyl (**Figure 8C**).

A

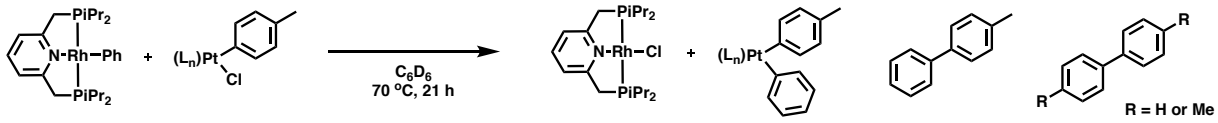

Ligand (L_n)	% Rh product	% Pt product	% 4-phenyl-toluene	% homo-coupling products
cod	32	40	10	7
dtbpy*	7	10	N.A.	N.A.
phosphepine	79	52	17	37
SPhos	70	N.A.**	58	2

NMR yields are reported for Rh and Pt product while GC-MS yields are reported for the organic products. * Reaction with (dtbpy) on (L_n)Pt(*p*-Tol)(Cl) was run in THF-d_8 and its reported yields above were measured at 24 hours. Further heating for another 6 days of the reaction did not afford significantly more products. The reaction was not checked on the GC-MS for organic products **The Pt product was not observed by ^{1}H NMR, likely due to low net accumulation of this species before reductive elimination such that overlapping NMR peaks from other species obscure the Pt product's.

B

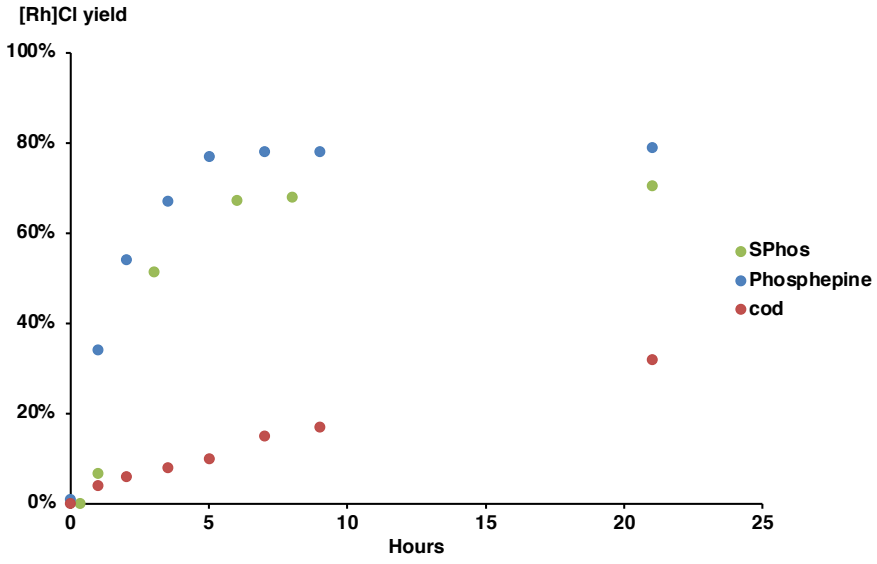

Figure 17. Transmetallation performance for different ancillary ligands on (L_n)Pt(*p*-Tol)(Cl) with ^{iPr}(PNP)RhPh.

(A) NMR yields of organometallic products and GCMS yields of organic products at 21 hours. (B) Time course study showing yield ^{iPr}(PNP)RhCl for (L_n)Pt(*p*-Tol)(Cl) where L_n is SPhos, phosphepine, or cod.

A time course study of the transmetallation using Pt(II) complexes with cod, SPhos, and phosphepine was carried out as well to qualitatively compare transmetallation rates (**Figure 17B**). Since the Pt transmetallation product undergoes reductive elimination at different rates depending on the ancillary ligand, the NMR yield of the other transmetallation product ^{iPr}(PNP)RhCl was measured instead to provide qualitative transmetallation rates for this study. I was delighted to find that both phosphepine and SPhos ligands significantly enhance transmetallation rates. Compared to the sluggish model reaction with (cod)Pt(*p*-Tol)(Cl) with only 10% of the ^{iPr}(PNP)RhCl product at five hours, reactions with phosphepine and SPhos complexes both reached maximum yields of around 70 to 80% within that time frame. Given the significant synthetic challenges in isolating the (κ^2-phosphepine)Pt(*p*-Tol)(Cl) complex and its lack of coupling selectivity, I placed my focus on the air-stable and easily isolable SPhos complex in moving forward with my attempt in completing the dual catalytic cycle system.

Given our hypothesis that a cationic (or electrophilic) Pt(II) is involved in the transmetallation step, and the trend observed for (cod)Pt(*p*-Tol)(X) where a more labile X group improves transmetallation yields (**Figure 8B**), the natural next step would be to test whether this trend extends to the (SPhos)Pt(*p*-Tol)(X) complexes. Four such other complexes were synthesized and tested against (SPhos)Pt(*p*-Tol)(Cl) in transmetallation with ^{iPr}(PNP)RhPh (**Table 1**). All reactions produced very little Pt product for yield calculation, presumably due to facile reductive elimination to form 4-phenyltoluene. Surprisingly, the chloride complex still produced the most desired product by a wide margin; all other Pt complexes afforded dismal amounts of product. We have yet to

produce an explanation of this trend reversal. Perhaps the hemilability of the SPhos ligand enables the (SPhos)Pt(Ar)(X) platform to accept the phenyl group from ^{iPr}(PNP)RhPh without the need to generate the cationic species, unlike in the case of (cod)Pt(Ar)(X). If this were the case, the reaction would be even more driven by the energies of the Rh products. From our experience in handling complexes containing the ^{iPr}(PNP)Rh fragment, ^{iPr}(PNP)RhX is more stable when X=Cl than OTs or OMs. Although this is mostly speculation at this stage, this observation would be consistent with the energy argument that the formation of ^{iPr}(PNP)RhCl is more energetically favored than other ^{iPr}(PNP)RhX, translating to higher transmetallation yields. Further investigation, both experimental and computational, could be carried out in the future to better understand this trend reversal. At the time, determining whether there is a C–H activation-enabling base that is compatible with (SPhos)Pt(*p*-Tol)(Cl) was a more interesting question to address.

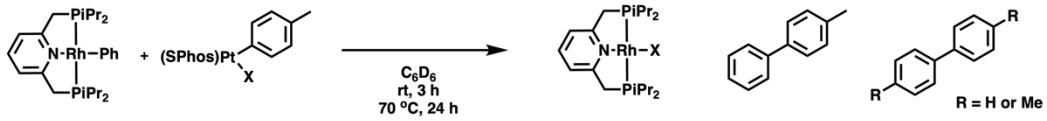

Leaving group X	% Rh product	% 4-phenyl-toluene	% homo-coupling products
Cl	41	53	1.3
OMs	20	4.6	4.4
TFA	12	2.0	3.8
OTs	31*	3.2	7.2
OTf	**	0.4	3.4

Table 1. Transmetallation yields of (SPhos)Pt(p-Tol)(X) with iPr(PNP)RhPh.

Yields of organic products were obtained on the GCMS. Yields of ^{iPr}(PNP)Rh(X) were obtained by NMR integrations. *An extra 8% of the Rh(III)-orthometallated product was observed. **^{iPr}(PNP)Rh(Ph) was all converted to ^{iPr}(PNP)Rh(OTf)(N_2) which precipitated out of solution at t=0.

Efforts on completing the dual catalytic cycle

Having found the best preformed M2 and M1 pairing for transmetallation with (SPhos)Pt(*p*-Tol)(Cl) and ^{iPr}(PNP)RhPh, I investigated whether the dual catalytic cycle proposed in **Figure 6B** can be completed. There are two missing puzzles: (i) what kind of base can turnover the C–H activation cycle without crippling M2's ability to accept a hydrocarbyl group during transmetallation, and (ii) whether the (SPhos)Pt platform can perform oxidative addition of aryl halides to turn over the cross-coupling cycle.

In **Figure 8A**, Dr. Gair showed that KO^{t}Bu can deprotonate the methylene proton on the PNP ligand of ^{iPr}(PNP)RhCl to form a 16-electron, dearomatized intermediate capable of activating benzene to form ^{iPr}(PNP)RhPh. The challenge with using KO^{t}Bu is the likely salt metathesis with (L_n)Pt(Ar)(X) to form KX and (L_n)Pt(Ar)(O^{t}Bu), rendering Pt less electrophilic to accept a phenyl group from ^{iPr}(PNP)RhPh. With the bulky SPhos ligand, we hoped that the steric bulk might reduce the level of salt metathesis, and if the metathesis were to occur, the ^{t}BuO anion might stay in the outer sphere such that the cationic Pt species could still carry out transmetallation. When 5 equivalents of KO^{t}Bu was added to (SPhos)Pt(*p*-Tol)(Cl), about 40% of Pt was converted to a new product within minutes at room temperature, likely (SPhos)Pt(*p*-Tol)(O^{t}Bu), judging from the shifted but similar ^{1}H NMR peak patterns of this new product, compared to the starting material (**Figure 18A**). This new product is not the cationic (SPhos)Pt(*p*-Tol) species, which has been independently generated *in situ* by the addition of ionizing reagent KB(Ar^F)$_4$ to (SPhos)Pt(*p*-Tol)(Cl), and characterized by NMR. When this mixture of KO^{t}Bu and (SPhos)Pt(*p*-Tol)(Cl) was heated to 70 ^{o}C, the temperature that enables

transmetallation, all (SPhos)Pt(*p*-Tol) species at around 22-25 ppm on ^{31}P NMR were converted to two new broad overlapping peaks at -37 ppm within an hour. No free SPhos ligand was observed. I have yet to identify this unknown product as its ^{1}H NMR also contained broad peaks.

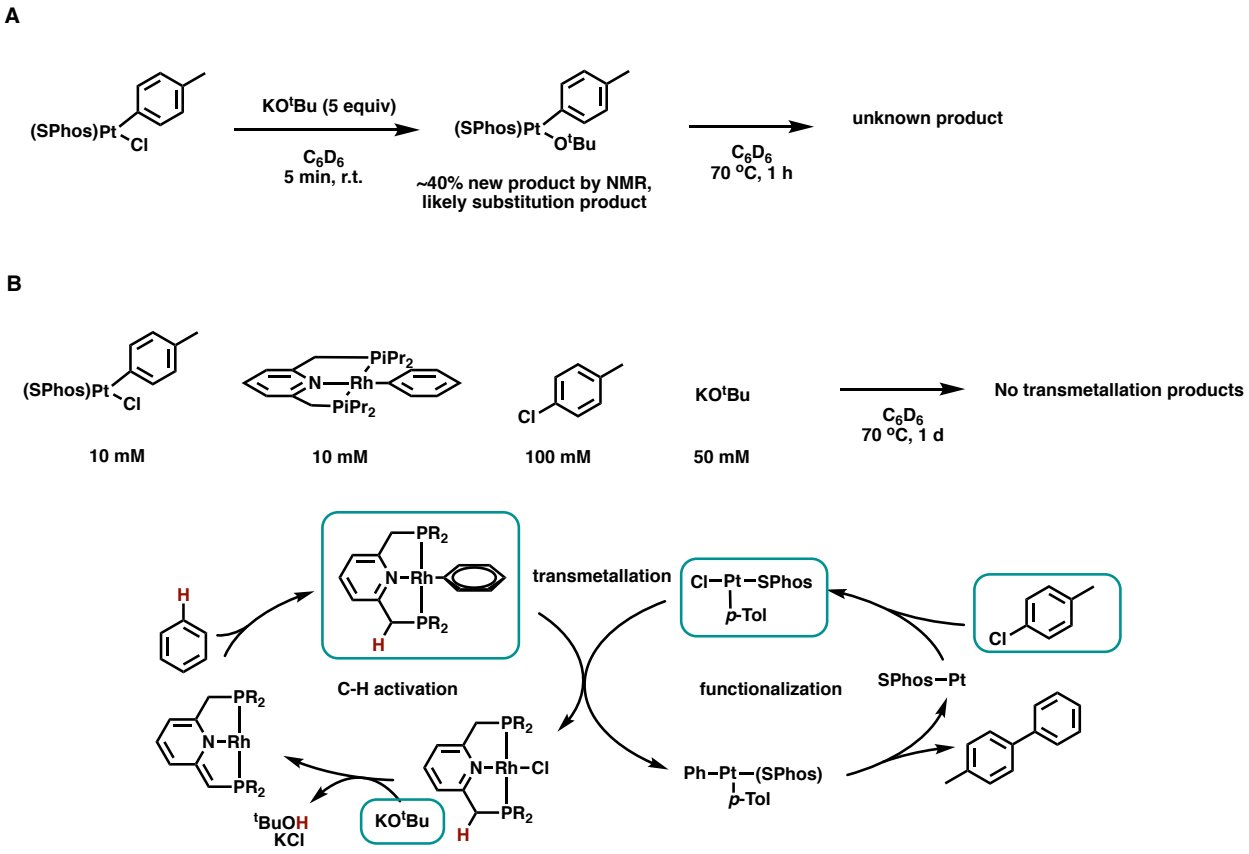

Figure 18. Using KO^{t}Bu as base for dual catalytic system.

(A) Effect of KOtBu on (SPhos)Pt(p-Tol)(Cl). (B) Attempt of dual catalytic cycle using KOtBu and preformed M1 and M2 complexes resulted in no transmetallation products. Species in teal boxes were reagents added at the start of the reaction.

The dual catalytic cycle with M1, ^{iPr}(PNP)RhPh, and M2, (SPhos)Pt(*p*-Tol)(Cl), in the presence of five equivalents of KO^{t}Bu and ten equivalents of 4-chlorotoluene was attempted as well (**Figure 18B**). I hoped that even with the formation of (SPhos)Pt(*p*-

Tol)(O^{t}Bu), this species could still undergo transmetallation. Unfortunately, no transmetallation products, ^{iPr}(PNP)RhCl or 4-phenyltoluene, was observed after heating for 24 hours. H/D exchange of ^{iPr}(PNP)RhPh was observed, likely due to the presence of base. (SPhos)Pt(*p*-Tol)(Cl) underwent the same two step processes as seen in the prior reaction in **Figure 18A** of partial salt metathesis followed by complete conversion to an unknown product. The complete shutdown of transmetallation by KO^{t}Bu was not an unexpected result. I moved on to experiment with a different base.

In **Figure 8B**, Dr. Gair showed that a bulky phenoxide base could in fact deprotonate the ligand sidearm of ^{iPr}(PNP)Rh(OMs) such that a benzene molecule can be activated afterwards; however, this does not work in the case of ^{iPr}(PNP)Rh(Cl). This is not an ideal situation for the (SPhos)Pt(Ar)(X) platform I developed as this limits the choice of the less coordinated anionic ligand X on Pt. In my study of (SPhos)Pt(*p*-Tol)(X), transmetallation with any X group other than chloride afforded paltry yields of transmetallation products (**Table 1**). Nonetheless, a set of dual catalytic cycle reactions were set up for X=OMs with two different phenoxides, 4-tolyl mesylate, (SPhos)Pt(*p*-Tol)(OMs) and ^{iPr}(PNP)RhPh to create an analogous system of the one I envisioned with KO^{t}Bu (**Figure 18B**, **Table 1**). As expected, the transmetallation reaction in the absence of base afforded very little cross coupling product, consistent with previous results (**Table 1** entry 3). The two dual catalytic cycle reactions afforded trace amounts of 4-phenyltoluene products, while formation of the substitution product, (SPhos)Pt(*p*-Tol)(phenoxide), was observed over time (**Table 2,** entries 1-2). Formation of the substitution product was confirmed by independent *in situ* generation of (SPhos)Pt(*p*-

Tol)(phenoxide) when excess phenoxide was heated with (SPhos)Pt(*p*-Tol)(Cl). While the substitution product can be observed by ^{31}P NMR and ^{1}H NMR, efforts to isolate the product via recrystallization or chromatography resulted in mixed crystals containing the phenol side product or decomposed materials, respectively. Reaction between ^{iPr}(PNP)RhPh and the *in situ* generated substitution product (SPhos)Pt(*p*-Tol)(phenoxide) did not result in any transmetallation product even with extended periods of heating.

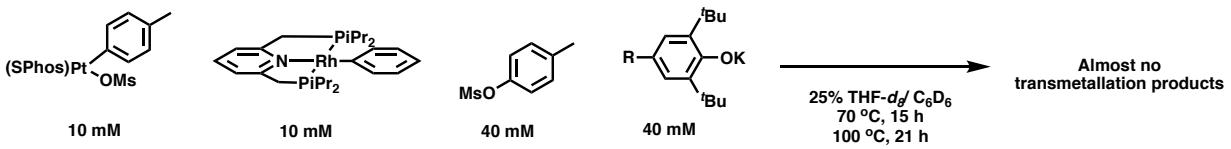

Entry	^{iPr}(PNP) RhPh	(SPhos)Pt (*p*-Tol)(Cl)	Phenoxide (R)	*p*-TsOMs	biphenyl	4-phenyl-toluene	bitolyl
1	10 mM	10 mM	OMe	40 mM	-	trace	2.0%
2	10 mM	10 mM	H	40 mM	-	trace	0.5%
3	10 mM	10 mM	No base	40 mM	-	1.9%	0.4%

Table 2. Transmetallation results with an attempted dual catalytic cycle with ^{iPr}(PNP)RhPh, (SPhos)Pt(*p*-Tol)(OMs), 4-tolyl mesylate, and phenoxide base.

Yields of tolyl-containing products were calculated based on total amount of tolyl fragments in each reaction, i.e., the sum of (SPhos)Pt(*p*-Tol)(OMs) and 4-tolyl mesylate.

Obstacles and Outlook

Although my last contribution toward identifying a compatible base yielded disappointing results (**Table 2**), there are still possibilities to enable the dual catalytic cycle for a future student. One current major obstacle is the mismatch between which base and X group afford the best outcomes for C–H activation turnover and transmetallation (**Table 3**). While using chloride as the less coordinating anionic ligand on Pt facilitates transmetallation, it also easily undergoes salt metathesis with a potassium base, especially with the sterically less hindered KO^{t}Bu (**Table 3**, entries 1-2). However, the stronger KO^{t}Bu base does enable turnover for C–H activation from ^{iPr}(PNP)RhCl, which cannot be achieved with potassium phenoxides. On the other side of this conundrum is the switch to mesylate from chloride on Pt. While the transmetallation product ^{iPr}(PNP)Rh(OMs) can be deprotonated by the bulkier and weaker phenoxide base for C–H activation, transmetallation between (SPhos)Pt(*p*-Tol)(OMs) and ^{iPr}(PNP)RhPh yields very little product (**Table 3**, entries 3-4).

One possible solution is to use *tert*-butoxide bases with non-coordinating cations such as tetramethylammonium, or even tetra-*n*-butylammonium. In the case of X=Cl with a *tert*-butoxide base (**Table 3**, entry 1), the only problem is salt metathesis with Pt driven by the formation of KCl. With a non-coordinating cation instead of potassium cation, salt metathesis of (SPhos)Pt(*p*-Tol)(Cl) may become less competitive compared to transmetallation.

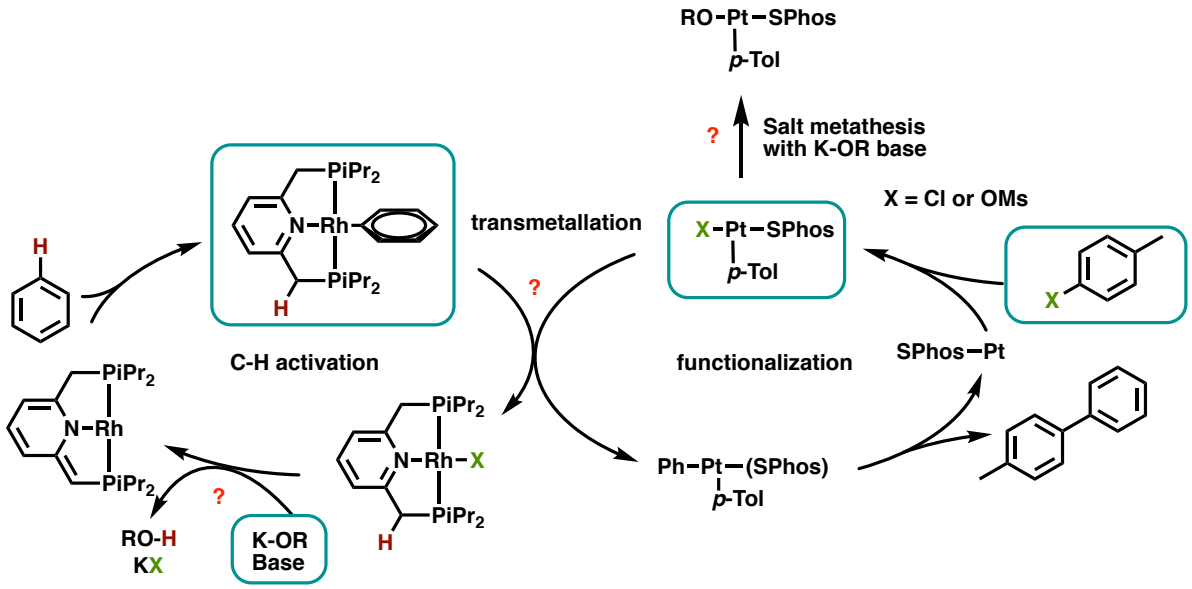

Entry	X	Base	C–H activation	Transmetallation & Salt metathesis
1	Cl	KO^{t}Bu	Turnover	Good transmetallation yields in the absence of base. Facile salt
2	Cl	K(phenoxide)	No turnover	metathesis with base prevents transmetallation
3	OMs	KO^{t}Bu	Turnover	Very little transmetallation even in the absence of base.
4	OMs	K(phenoxide)	Turnover	Slower salt metathesis with base

Table 3. Transmetallation and C–H activation outcomes for different leaving X groups and bases.

Another possible avenue to explore would be to acidify the methylene proton on the PNP ligand such that even ^{iPr}(PNP)RhCl can be deprotonated with the weaker phenoxide base (**Table 3**, entry 2). One could imagine tuning the electronics of the PNP ligand by installing electron-withdrawing substituents on its pyridine ring, such as a *para*-trifluoromethyl group. One drawback of this approach is the likely compromise in transmetallation yield with a less nucleophilic Rh hydrocarbyl donor complex. Yet another potential solution is testing other ancillary ligands on Pt to see whether they possess the same X group trend observed with (cod), where a OMs on Pt is better at transmetallation than Cl so that the weaker phenoxide base can be used with this system (**Table 3**, entries

3 & 4). Aside from the obvious choice of other hemilabile Buchwald ligands, bulky monophosphine ligands such as tris(1-adamantyl)phosphine, $P(Ad)_3$, can also be good options. Carrow reported that the bulky $P(Ad)_3$ ligand stabilizes a very active cationic organopalladium species resulting from the oxidative addition of aryldiazondium tetraborofluorate salts.[37] This $[P(Ad)_3Pd(Ar)]^+$ species is so active that Suzuki-Miyaura coupling can be carried out in the absence of base. This is as opposed to using a less active organopalladium species generated from the oxidative addition of aryl halide which requires stoichiometric amount of base to drive the reaction forward. With regard to our system, one could imagine $[P(Ad)_3]Pt(Ar)(OMs)$ easily undergoing ionization to form the cationic species where the Pt^+ center is stabilized by the bulky phosphine ligand. Informed by Dr. Durak's extensive studies on Pt, this cationic species will likely be very conducive to transmetallation with Rh. Preliminary work in synthesizing the preformed $[P(Ad)_3]Pt(Ar)(X)$ was met with challenges posed by suboptimal conditions with regards to maintaining an air- and water-free environment in the early days following the relocation of our group. While this project was put on pause for the time being so as to focus on other projects within this dissertation, I believe a future student will likely find solutions to enable the dual catalytic system with some of the suggestions listed above.

One last issue remains to be addressed concerning the dual catalytic system – whether the (SPhos)Pt fragment has the ability to undergo oxidative addition of aryl halides to turnover the cross-coupling cycle. While this has yet to be tested explicitly, literature does offer a few examples of aryl iodide oxidative addition by Pt(0) with bulky

phosphines such as $(PPh_3)_4Pt(0)$ and (Me-DuPhos)(*trans*-stilbene)Pt(0).[34–36] The bulky hemilabile SPhos ligand or even the $P(Ad)_3$ ligand may very well enable Pt to do the same.

In conclusion, significant progress has been made since Dr. Durak's and Dr. Gair's studies on transmetallation between metal centers of groups 9 and 10 organometallic complexes. A stereochemical probe study revealed complementary selectivity of the transfer of either an aryl or an alkyl group from $Cp^*(PMe_3)Ir(Ph)$(neohex-d_2) to $HgCl_2$ or (cod)Pt(Me)(OMs), respectively. While results with the Pt compound was obscured by background H/D exchange of the final olefin product, transmetallation of the neohexyl group to $HgCl_2$ was found to proceed via retention of stereochemistry. Efforts to develop new preformed M1 and M2 complexes via ligand-tuning or experimenting with new ancillary ligands resulted in the best transmetallation yield of the reductive elimination product of this project so far, using ^{iPr}(PNP)RhPh and (SPhos)Pt(*p*-Tol)(Cl). Although issues of oxidative addition and base compatibility remain to be addressed, the progress made in this chapter takes us one step closer to completing the dual catalytic system for non-directed C–H functionalization.

Experimental

1. Materials

Unless otherwise noted, all reagents were obtained from commercial suppliers and used without further purification. Tetrahydrofuran (THF), diethyl ether, methylene chloride (DCM), toluene (PhMe), and pentane were obtained from an Innovative Technologies solvent purification system (solvent deoxygenated by N_2 sparge and dried over alumina). Methane sulfonic acid was dried by azeotropic distillation with anhydrous toluene and then vacuum distilled. Triflic anhydride and methanesulfonylchloride were distilled from P_2O_5. Benzene-*d6* was degassed by three freeze-pump-thaw cycles in a glass tube sealed with a Kontes stopper and stored over 3 Å molecular sieves. THF-*d8* was dried over sodium/benzophenone ketyl, and vacuum transferred to a glass storage vessel with a Kontes stopper. Methylene chloride-*d2* was dried over CaH_2, distilled into a Schlenk flask, and stored under N2. Molecular sieves were activated in a Schlenk flask under vacuum (<0.05mmHg) in a heating mantle set to 250°C for at least 12 hours. Alumina that was used in the glove box was dried in a Schlenk flask under vacuum in a heating mantle set to 250°C. Biotage reverse phase columns (SNAP-KP-C18-HS) were purchased from Biotage.

$IrCl_3 \cdot 3H_2O$ and $RhCl_3 \cdot 3H_2O$ were purchased from Pressure Chemicals. (cod)$PtCl_2$ was purchased from Strem. Complete analytical data and preparations have been reported for [Ir](Cl)(*syn*-neohex-*d2*),[26] [Ir](Ph)(*syn*-neohex-*d2*),[26] [Ir](Cl)$_2$,[38] (*E*)-1-deuterio-3,3-dimethyl-1-butene, (cod)Pt(Me)(Cl),[39] (cod)Pt(Me)(OMs),[26] (cod)Pt(*p*-Tol)$_2$,[40] (cod)Pt(*p*-

Tol)(Cl),[40] (cod)Pt(Ph)(*p*-Tol),[40] (SPhos)Pt(*p*-Tol)(Cl),[26] (*Z*)-1-*tert*-butyl-2,3,6,7-tetrahydrophosphepine (phosphepine),[41] $[Rh(coe)_2(Cl)]_2$,[42] pyrr-^{iPr}(PNP),[33] pyrr-^{iPr}(PNP)RhCl,[43] pyrr-^{iPr}(PNP)RhPh,[43] ^{iPr}(PNP)Rh(Ph),[43] ^{iPr}(PNP)Rh(Cl),[44] ^{iPr}(PNP)Rh(OMs),[45] potassium 2,6-bis(*tert*-butyl)-4-methoxy-phenolate.[46]

The fragments (Cp*)(PMe_3)Ir and pincer ligand 2,6-bis(di-alkylphosphinomethyl)pyridine are abbreviated as [Ir] and ^{R}(PNP), respectively, where R=alkyl groups on phosphines.

2. General Procedures

Unless otherwise noted, all reactions and manipulations were performed under a circulating nitrogen atmosphere in an anhydrous Innovative Technologies glove box, or using standard Schlenk technique. Glassware was dried in an oven set to 150 °C before use. Flash column chromatography was carried out using Silicycle 230-400 mesh silica gel. NMR spectra (^1H, ^{13}C, and ^{31}P) were obtained using a Bruker 500 MHz spectrometer, a Varian 500 MHz Inova NMR spectrometer, or a Varian 400 MHz Inova NMR Spectrometer at room temperature. Chemical shifts are reported in ppm and coupling constants are reported in Hz. Products of reactions monitored by *in situ* NMR were confirmed by comparison to authentic material prepared by either the procedures listed above in the materials section or below in the “Synthesis, Characterization and General Reaction Procedures” section. Reverse phase purifications were performed on a Biotage Isolera One with a SNAP-KP-C18-HS 30 g column. All alkyllithium and Grignard reagents

were titrated under N_2 with salicylaldehyde phenylhydrazone in THF according to the procedure described in literature.[47]

3. Synthesis, Characterization, and General Reaction Procedures

3.1 Stereochemical probe

Procedures for setting up transmetallation reactions with (i) [Ir](Ph)(*syn*-neohex-d_2) and (cod)Pt(Me)(OMs), and (ii) [Ir](Ph)(*syn*-neohex-d_2) and $HgCl_2$, have been reported previously.[26] Transmetallation reaction between [Ir](Cl)(*syn*-neohex-d_2) and $HgCl_2$ were performed using the same procedures as reported ones for the transmetallation between [Ir](Ph)(*syn*-neohex-d_2) and $HgCl_2$. ^{1}H NMR's of *erythro*- and *threo*-3,3-dimethyl-1-butyl-1,2-d_2 mercuric chloride have been previously reported as well.[32]

3.1a Control reactions to test for H/D scrambling in (*E*)-1-deuterio-3,3-dimethyl-1-butene

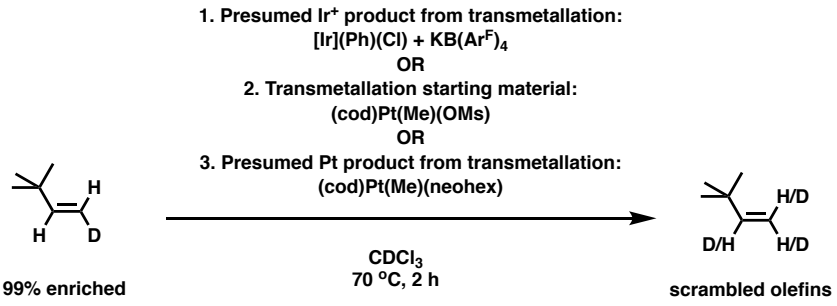

Reaction 1: A J. Young tube was charged with $KB(Ar^F)_4$ (15.6 mg, 21.7 μmol, 1.1 equiv.). To the J. Young tube was added a stock solution in $CDCl_3$ (500 μL) of [Ir](Ph)(Cl) (20 μmol, 40 mM, 1 equiv.) and internal standard 1,3,5,-trimethoxybenzene (56 μmol, 12 mM, 2.8 equiv.). To this solution was added *neat* (*E*)-1-deuterio-3,3-dimethyl-1-butene (30 μmol, 2.6 μL, 1.5 equiv.). The mixture in the sealed J. Young tube was heated at 70 °C and

monitored by ^{1}H NMR at t=0 and 2 h. 3,3-dimethyl-1-butene was observed after two hours of heating.

Reaction 2: To a J. Young tube were added a stock solution in $CDCl_3$ (500 µL) of (cod)Pt(Me)(OMs) (20 µmol, 40 mM, 1 equiv.) and internal standard 1,3,5,-trimethoxybenzene (56 µmol, 12 mM, 2.8 equiv.). To this solution was added *neat* (*E*)-1-deuterio-3,3-dimethyl-1-butene (30 µmol, 2.6 µL, 1.5 equiv.). The mixture in the sealed J. Young tube was heated at 70 °C and monitored by ^{1}H NMR at t=0 and 2 h. (*Z*)-1-deuterio-3,3-dimethyl-1-butene was observed after two hours of heating.

Reaction 3: To a J. Young tube were added a stock solution in $CDCl_3$ (500 µL) of (cod)Pt(Me)(neohex) (20 µmol, 40 mM, 1 equiv.) and internal standard 1,3,5,-trimethoxybenzene (56 µmol, 12 mM, 2.8 equiv.). To this solution was added *neat* (*E*)-1-deuterio-3,3-dimethyl-1-butene (30 µmol, 2.6 µL, 1.5 equiv.). The mixture in the sealed J. Young tube was heated at 70 °C and monitored by ^{1}H NMR at t=0 and 2 h. (*Z*)-1-deuterio-3,3-dimethyl-1-butene was observed after two hours of heating.

3.1b Synthesis of(*E*)-1-deuterio-3,3-dimethyl-1-butene

Precursor *B*-(trans-1-hexenyl)-9-borabicyclo(3,3,1)nonane was prepared according to literature procedures.[48] The precursor (7.3 g, 35.7 mmol, 1 equiv.) was briefly subjected to negative pressure inside an anhydrous, anaerobic glovebox to remove any 3,3-dimetyl-1-butene decomposition byproduct that may have formed while in storage. The precursor

was then dissolved in anhydrous and degassed tetradecane (60 mL). A 100mL Schlenk flask was charged with this solution, sealed, and brought outside of the glovebox. To the vigorously stirred solution of precursor, acetic acid-d_4 (2 mL, 35.7 mmol, 1 equiv.) was added dropwise under an N_2 atmosphere. Formation of solids in the reaction was observed after 0.6 equiv. of acetic acid-d_4 was added. The resulting suspension was sonicated for 1 hour and then stirred for 0.5 hour at room temperature under an N_2 atmosphere. The desired product was vacuum transferred to a 10mL Schlenk flask under static vacuum. A second vacuum transfer of the desired product from the distillate of the first one may be required to further remove any residual acetic acid-d_4. Yield: 1.32 g, 43%. Enrichment (as calculated by ^{1}H NMR integrations): >99%.

^{1}H NMR (500 MHz, $CDCl_3$) δ 5.86 (dt, J_{HH} = 17.4 Hz, J_{DH} = 1.58 Hz, 1H), 4.90 (d, J = 17.4 Hz, 1H), 1.01 (s, 9H).

^{2}H NMR (77 MHz, $CDCl_3$) δ 4.88 (d, J_{DH} = 1.6 Hz, 1D).

3.1c Synthesis of (cod)Pt(Me)(neohex)

A 50 mL round bottom flask was charged with (cod)Pt(Me)(Cl) (81.5 mg, 0.23 mmol, 1 equiv.) and a THF/Et_2O mixture in 1:3 v/v ratio (10 mL). To this stirring solution was added neohexylmagnesium chloride (0.34 mmol, 0.98 M, 0.35 mL, 1.5 equiv.) dropwise. After 1 hour of stirring at room temperature, the reaction was passed through a pad of basic alumina with THF. The filtrate was dried *in vacuo* to yield off white solids. The final yield was not measured.

^{1}H NMR (500 MHz, $CDCl_3$) δ 4.94 – 4.80 (m, 2H), 4.80 – 4.69 (m, 2H), 2.42 – 2.19 (m, 8H), 1.55 (s, 3H), 1.47 – 1.39 (m, 2H), 1.31 – 1.22 (m, 2H), 0.84 (s, 9H).

3.1d Synthesis of (cod)Pt(p-Tol)(neohex)

A 50 mL round bottom flask was charged with (cod)Pt(*p*-Tol)(Cl) (142.5 mg, 0.33 mmol, 1 equiv.) and a THF/Et_2O mixture in 1:3 v/v ratio (16 mL). To this stirring solution was added neohexylmagnesium chloride (0.5 mmol, 0.98 M, 0.51 mL, 1.5 equiv.) dropwise. After 1 hour of stirring at room temperature, the reaction was passed through a pad of basic alumina with diethyl ether. The filtrate was dried *in vacuo*. The product was dissolved in minimal amount of warm pentane and stored at -35 °C freezer overnight to allow the slow evaporation of solvent. The supernatant was decanted, and the resulting clear crystals were washed with cold pentane. Yield: 91.9 mg (58% yield).

^{1}H NMR (500 MHz, $CDCl_3$) δ 7.18 (d, *J* = 7.6 Hz, 2H), 6.93 (d, *J* = 7.5 Hz, 2H), 5.06 – 4.95 (m, 2H), 4.93 – 4.81 (m, 2H), 2.48 – 2.30 (m, 8H), 2.25 (s, 3H), 1.50 – 1.43 (m, 2H), 1.18 – 1.11 (m, 2H), 0.71 (s, 9H).

3.2. Tuning the hydrocarbyl donor M1 to improve transmetallation

3.2a General procedures for transmetallation

A stock containing (cod)Pt(*p*-Tol)(Cl) (9.25 mM, 4.6 µmol, 1 equiv) and internal standard 1,3,5-trimethoxybenzene (1.41 mM, 0.7 µmol, 0.15 equiv) in C_6D_6 (500 µL) was added to a J. Young tube kept at around -35 °C on cold aluminum beads. Another stock containing

^{R}(PNP)Rh(Ph) (24 mM, 7.2 µmol, 1.55 equiv) in C_6D_6 (300 µL) was added to the reaction. The J. Young tube was sealed, and the reaction was thawed right before the ^{1}H NMR of the first time point was recorded. The reaction was heated to 70 °C and monitored by ^{1}H NMR until all (cod)Pt(*p*-Tol)(Cl) was consumed. NMR yields were measured against the internal standard. The identities of the [Rh] and [Pt] products were confirmed either through comparison of NMR chemical shifts between experimental results with literature NMR spectra of the products.

3.2b Synthesis of bis(diethylphosphinomethyl)pyridine *P*,*P*′-dioxide

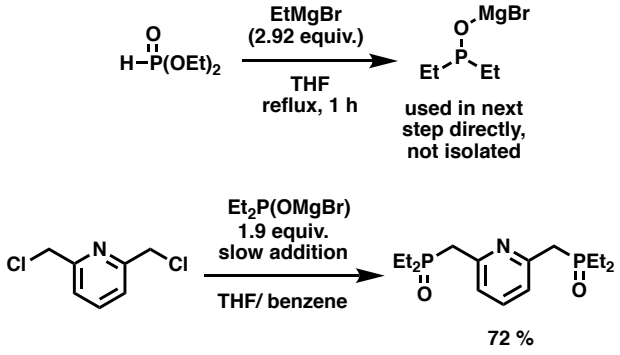

To a 250 mL Schlenk flask was charged THF (60 mL) and EtMgBr (2.82 M in Et_2O, 23.5 mL, 64.9 mmol, 5.7 eq) under an N_2 atmosphere. The majority of Et_2O was removed *in vacuo*. To the stirring Grignard solution was added diethyl phosphite (3.06 g, 2.86 mL, 22.2 mmol, 1.95 eq) in benzene (30 mL) was via a syringe pump over 2 h. At the end of the addition, a condenser was installed onto the 250 mL Schlenk flask containing reaction which was then refluxed at 75 °C for 1 h. The pale brown reaction turned yellow after the reflux. To a second 250 mL Schlenk flask was charged 2,6-bis(chloromethyl)pyridine (2

g, 11.4 mmol, 1 eq); the flask was degassed with three cycles of evacuation and purging with N_2. To 2,6-bis(chloromethyl)pyridine was added benzene (18 mL). The second Schlenk flask was fitted with an addition funnel capped with a septum under N_2. The yellow reaction mixture containing $PEt_2(OMgBr)$ in the first Schlenk flask was cannulated into the addition funnel on the second Schlenk flask. The $PEt_2(OMgBr)$ solution was slowly added to a vigorously stirred solution of 2,6-bis(chloromethyl)pyridine over 1 h. The initially clear reaction turned orange over the course of addition. Upon completion of $PEt_2(OMgBr)$ addition, solvents were removed *in vacuo* to afford yellow solid residues which was then quenched with a saturated solution of NH_4Cl in water (100 mL). The product was extracted with water (500 mL) and DCM (500 mL x 12) until the aqueous phase no longer contained any UV-active substance. NaCl may be added to the aqueous phase to aid extraction. The organic layers were combined, and DCM was removed under reduced pressure. The crude product was purified on a reverse phase column with the mobile phases of water and ACN (without formic acid or TFA). The product eluted with 10% ACN/water. Solvents were removed under reduced pressure to afford the final product as a clear oil. The oil was degassed with three cycles of freeze-pump-thaw and stored inside a glovebox. Yield: 2.6 g, 72%.

^{1}H NMR (500 MHz, CD_2Cl_2) δ 7.59 (t, J = 7.7 Hz, 1H), 7.17 (dt, J = 7.7, 1.7 Hz, 2H), 3.24 (d, J = 14.4 Hz, 4H), 1.74 – 1.60 (m, 8H), 1.12 (ddd, J = 17.1, 7.7 Hz, 12H).

^{31}P NMR (202 MHz, CD_2Cl_2) δ 48.15 (s, 2H).

3.2c Synthesis of ^{Et}PNP ligand

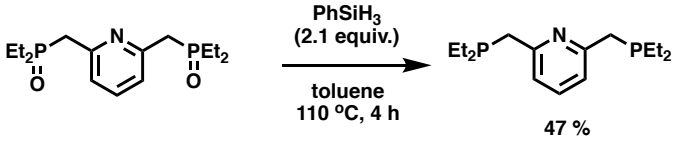

Inside a glovebox, bis(diethylphosphinomethyl)pyridine *P*,*P′*-dioxide (1.22 g, 3.9 mmol, 1 eq) was dissolved in toluene (8 mL). A 25 mL bomb was charged with this solution and phenylsilane (1 mL, 8.2 mmol, 2.1 eq). The bomb was sealed and refluxed at 110 °C for hours after which the reaction was transferred to a 50 mL round bottom flask Toluene was removed *in vacuo*. The byproduct from mono-reduction was first removed by Kugelrohr distillation at 75 °C over two hours under an active vacuum, leaving behind the final product. Further purification of final product may be carried out by distillation at 110 °C on the Kugelrohr to afford a clear oil distillate. Yield: 520 mg, 47%.

^{1}H NMR (500 MHz, C_6D_6) δ 7.07 (t, *J* = 7.7 Hz, 1H), 6.73 (d, *J* = 7.6 Hz, 2H), 2.89 (br s, 4H), 1.38 (dq, *J* = 14.7, 7.6 Hz, 4H), 1.28 (dq, *J* = 14.7, 7.6 Hz, 4H), 1.02 (ddd, *J* = 14.9, 7.6 Hz, 12H). *The two dq peaks correspond to the two diastereotopic methylene protons on each ethyl group.

^{31}P NMR (202 MHz, C_6D_6) δ -15.72 (s, 2H).

3.2d Metalation of ^{Et}PNP

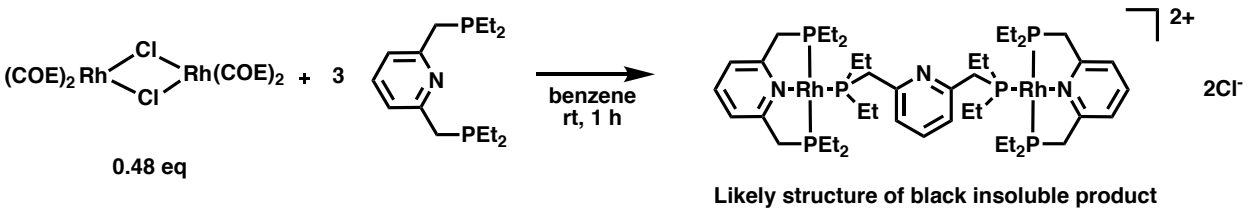

Likely structure of black insoluble product

A 250 mL round bottom flask was charged $[(COE)_2Rh(\mu\text{-}Cl)]_2$ in benzene (2 mM, 28 mL, 0.056 mmol, 0.5 eq.). To the vigorously stirred solution of $[(COE)_2Rh(\mu\text{-}Cl)]_2$ was added ^{Et}PNP (5 mM, 11.4 mL, 0.114 mmol, 1 eq.) dropwise. The reaction was stirred at room temperature for 1 h, after which benzene was removed *in vacuo*. The crude mixture was washed with pentane three times to remove residual cyclooctene. ^{31}P NMR of this red crude mixture indicated the likely formation of ^{Et}(PNP)RhCl. Attempts to purify the mixture via recrystallization resulted in precipitation of black solids that were insoluble in benzene or THF. ^{31}P NMR of this black solid in DMSO suggests the formation of a 3-ligand-2-metal salt shown in the above scheme.

^{31}P NMR of crude mixture (202 MHz, C_6D_6) δ 29.41 (d, J = 143.7 Hz).

^{31}P NMR of black product (202 MHz, DMSO) δ 37.07 (dt, J = 158.0, 40.2 Hz, 2P), 34.16 (dd, J = 133.6, 40.3 Hz, 4P).

3.3 Tuning hydrocarbyl acceptor M2 to improve transmetallation

3.3a General procedures for transmetallation

A stock containing ^{iPr}(PNP)Rh(Ph) (50 mM, 2.5 µmol, 1.25 equiv) and internal standard 1,3,5-trimethoxybenzene (8 mM, 0.4 µmol, 0.2 equiv) in C_6D_6 (50 µL) was added to a J. Young tube kept at around -35 °C on cold aluminum beads. Another stock containing the metal(oid) electrophile $L_nM(R)(X)$ (50 mM, 2 µmol, 1 equiv) and internal standard ferrocene (5 mM, 0.25 µmol, 0.125 equiv) in in C_6D_6 (40 µL) was added to the reaction. Finally, 460 µL of C_6D_6 was added to make up to 550 µL. The J. Young tube was sealed, and the reaction was thawed right before the ^{1}H NMR of the first time point was recorded. The reaction was either kept at room temperature or heated to 70 °C. The reaction was monitored by ^{1}H NMR until all $L_nM(R)(X)$ was consumed. NMR yields were measured against the internal standards. The identities of the [Pt] products (if observed) were confirmed either through comparison of NMR chemical shifts between experimental results with literature NMR spectra of the products. The yields of the biaryl products were measured on the GCMS using calibration curves of authentic biaryl products against internal standard *n*-decane.

Transmetallation between ^{iPr}(PNP)RhPh and (dtbpy)Pt(*p*-Tol)(Cl) was carried out in THF-d_8 due to poor solubility of the Pt complex in C_6D_6.

3.3b Synthesis of (dtbpy)Pt(p-Tol)(Cl)

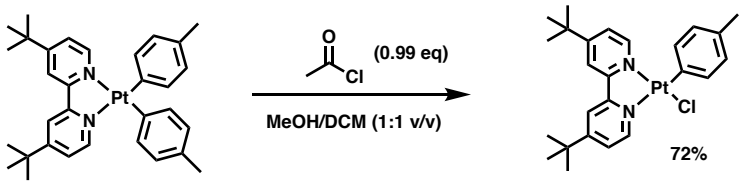

(dtbpy)Pt(*p*-Tol)$_2$ was prepared according to literature procedures.[49] In air, a 50 mL round bottom flask was charged with (dtbpy)Pt(*p*-Tol)$_2$ (96.2 mg, 0.149 mmol, 1 eq) and a MeOH/DCM mixture (15 mL, 1:1 v/v ratio). To the stirring solution of (dtbpy)Pt(*p*-Tol)$_2$ was added a solution of acetyl chloride in DCM (141 mM, 1.0 mL,0.145 mmol, 0.99 eq) dropwise. The reaction was stirred at room temperature for 15 minutes, after which volatiles were removed under reduced pressure. Product was purified by flash chromatography on silica gel eluting with 15% hexanes in DCM. The final product may be further purified by recrystallization in DCM with vapor diffusion of either pentane or diethyl ether. Yield: 63.3 mg, 72%.

^{1}H NMR (500 MHz, CD_2Cl_2) δ 9.38 (dd, *J* = 5.8, 0.7 Hz, 1H), 8.51 (m, *J* = 25.1, 6.2, 0.6 Hz, 2H), 8.00 (d, *J* = 1.9 Hz, 1H), 7.94 (d, *J* = 2.2 Hz, 1H), 7.67 (dd, *J* = 5.9, 1.9 Hz, 1H), 7.27 (dd, *J* = 6.3, 2.2 Hz, 1H), 7.22 (m, *J* = 8.0 Hz, 1H), 6.88 (dd, *J* = 8.1, 0.8 Hz, 1H), 2.30 (s, 3H), 1.43 (s, 8H), 1.38 (s, 8H).

3.3c Synthesis of (κ^2-phosphepine)Pt(*p*-Tol)(Cl)

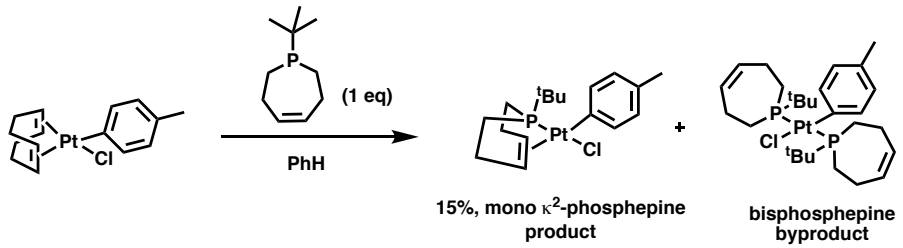

(*Z*)-1-*tert*-butyl-2,3,6,7-tetrahydrophosphepine was prepared according to literature procedures.[41] A 100 mL round bottom flask was charged with a solution of (cod)Pt(*p*-Tol)(Cl) (5 mM, 14 mL, 0.071 mmol, 1 eq) in benzene. To the stirred solution of (cod)Pt(*p*-Tol)(Cl) was added a solution of (*Z*)-1-*tert*-butyl-2,3,6,7-tetrahydrophosphepine (2 mM, 35 mL, 0.071 mmol, 1 eq)) in benzene dropwise over 15 minutes. Upon completion of the addition, benzene was removed *in vacuo*. The light brown crude solids were washed with pentane once. (κ^2-phosphepine)Pt(*p*-Tol)(Cl) was obtained after several iterations of recrystallization in benzene with vapor diffusion of pentane at -35 ^{o}C to remove most impurities including residual Pt precursor and the bisphosphepine Pt product . Yield: 5.1 mg, 15%.

Single crystal suitable for X-ray crystallography was prepared as follows. A brown crude mixture of product and a small amount of (cod)Pt(*p*-Tol)(Cl) (c.a. 30 mg) was suspended in benzene (200 μL) at room temperature. The brown supernatant containing more of (cod)Pt(*p*-Tol)(Cl) than product was removed. The remaining off white solids were dissolved in benzene (300 μL) at room temperature and filtered through a 20 μm syringe filter into a small shell vial placed inside a 20 mL scintillation vial containing 5-10 mL of pentane. The scintillation vial was capped. Vapor diffusion overnight at room temperature

followed by another 24 hours at -35 °C afforded small clear block crystals. The resolved structure confirms that the chloride ligand is *trans*- to the phosphine group.

^{1}H NMR (500 MHz, C_6D_6) δ 7.69 – 7.62 (m, *J* = 7.5, 2H), 6.88 (d, *J* = 7.8 Hz, 2H), 5.56 (m, 2H), 2.97 (m, 2H), 2.19 (s, 3H), 2.05 – 1.72 (m, 4H), 1.71 – 1.30 (m, 2H), 0.96 (d, *J* = 14.2, 9H).

^{31}P NMR (202 MHz, C_6D_6) δ 27.31 (t, J_{PtP} = 2447 Hz, 1P).

3.3d General procedures for preparation of (cod)Pt(p-Tol)(X)

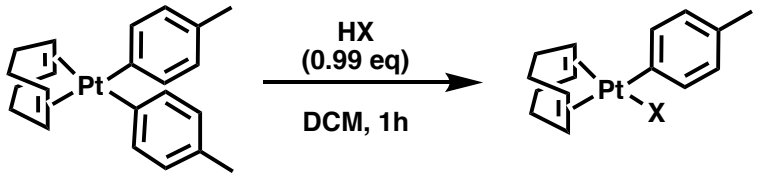

X=OMs —> methanesulfonic acid
X=TFA —> trifluoroacetic acid
X=OTs —> *p*-toluenesulfonic acid

(cod)Pt(*p*-Tol)$_2$ was prepared according to literature procedures.[40] To a 20 mL scintillation vial was added (cod)Pt(*p*-Tol)$_2$ (51 mg, 0.105 mmol, 1 eq) in DCM (5 – 10 mL). To the stirring solution of (cod)Pt(*p*-Tol)$_2$ was added HX (1 M, 99 μL, 0.103 mmol, 0.99 eq) in DCM dropwise. (For TsOH, it was dissolved as a 1 M solution in 10% MeOH in DCM.) After 0.5 – 1 h of stirring at room temperature, volatiles were removed under reduced pressure. Azeotroping with hexanes may be required to remove all volatiles. The product was recrystallized by dissolving the crude product in minimal amount of hot benzene which was then filtered through a 20 μm syringe filter into a small shell vial placed inside

a 20 mL scintillation vial containing 5-10 mL of pentane. The scintillation vial was capped; vapor diffusion overnight at room temperature afforded clear needle-like crystals.

3.3e (cod)Pt(*p*-Tol)(OMs)

Yield: 43 mg, 78%.

^{1}H NMR (500 MHz, C_6D_6) δ 7.32 (d, J = 7.7 Hz, 2H), 6.99 (d, J = 7.7 Hz, 2H), 6.28 (br s, 2H), 4.14 – 3.79 (m, J_{Pt-H} = 40.1 Hz, 2H), 2.56 (s, 3H), 2.20 (s, 3H), 1.74 – 1.66 (m, 4H), 1.45 – 1.17 (m, 4H).

3.3f (cod)Pt(p-Tol)(TFA)

Yield: 49.2 mg, 91%

^{1}H NMR (500 MHz, C_6D_6) δ 7.28 (d, J = 7.8 Hz, 2H), 6.95 (d, J = 7.7 Hz, 2H), 5.38 (br s, 2H), 4.09 (m, J_{PtH} = 39.0, 2H), 2.15 (s, 3H), 1.68 (dddt, J = 28.0, 17.1, 8.8, 3.5 Hz, 4H), 1.31 (dddd, J = 20.8, 14.1, 6.9, 3.3 Hz, 4H).

^{19}F NMR (470 MHz, C_6D_6) δ -73.68 (s, 3F).

3.3g (cod)Pt(p-Tol)(OTs)

Yield: 12.5 mg, 21%

The resulting crystals were not characterized by ^{1}H NMR and were used directly for the synthesis of (SPhos)Pt(*p*-Tol)(OTs)

3.3h General procedures for preparation of (SPhos)Pt(*p*-Tol)(X)

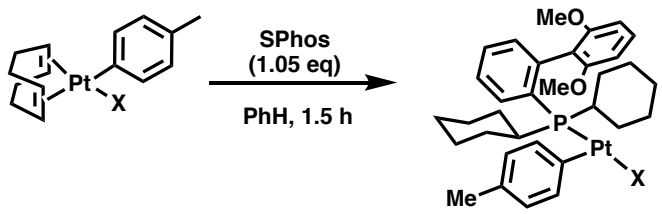

To a 20 mL scintillation vial was added (cod)Pt(*p*-Tol)(X) (0.022 – 0.097 mmol, 1 eq) in PhH (5 mL). To the stirring solution of (cod)Pt(*p*-Tol)(X) was added SPhos (1.05 eq) in PhH (5 mL). After 1.5 h of stirring at room temperature, volatiles were removed under reduced pressure. The crude product was washed with pentane. The product was recrystallized by dissolving the crude product in minimal amount of hot benzene which was then filtered through a 20 μm syringe filter into a small shell vial placed inside a 20 mL scintillation vial containing 5-10 mL of pentane. The scintillation vial was capped; vapor diffusion overnight at room temperature afforded crystals.

3.3i (SPhos)Pt(*p*-Tol)(OMs)

Yield: 32.0 mg, 46%

^{1}H NMR (500 MHz, C_6D_6) δ 8.19 (t, *J* = 8.4 Hz, 1H), 7.61 (dd, *J* = 7.9, 1.6 Hz, 2H), 7.23 (t, *J* = 7.4 Hz, 1H), 7.00 (tt, *J* = 7.5, 1.3 Hz, 1H), 6.93 (tt, *J* = 7.5, 1.7 Hz, 1H), 6.85 (d, *J* = 7.7 Hz, 2H), 6.80 (d, *J* = 8.5 Hz, 2H), 6.72 (ddd, *J* = 7.8, 2.9, 1.3 Hz, 1H), 3.54 (s, 6H), 2.18 (m, 2H), 2.09 (s, 3H), 1.95 (s, 3H), 1.80 – 0.82 (m, 20H).

^{31}P NMR (202 MHz, C_6D_6) δ 19.22 (t, J_{PtP} = 2372 Hz, 1P).

3.3j (SPhos)Pt(*p*-Tol)(TFA)

Yield: 40.1 mg, 51%

^{1}H NMR (500 MHz, C_6D_6) δ 7.57 (d, *J* = 7.8 Hz, 2H), 7.45 (t, *J* = 8.4 Hz, 1H), 7.25 (t, *J* = 7.5 Hz, 1H), 7.01 (t, *J* = 7.5 Hz, 1H), 6.94 (t, *J* = 7.4 Hz, 1H), 6.83 (d, *J* = 7.8 Hz, 2H), 6.71 (dd, *J* = 7.7, 2.6 Hz, 1H), 6.35 (d, *J* = 8.4 Hz, 2H), 3.42 (s, 6H), 2.20 (q, *J* = 11.6 Hz, 2H), 2.07 (s, 3H), 1.80 – 0.81 (m, 20H).

^{31}P NMR (202 MHz, C_6D_6) δ 20.41(t, J_{PtP} = 2265 Hz, 1P).

3.3k (SPhos)Pt(*p*-Tol)(OTs)

Yield: 7.5 mg, 39%

^{1}H NMR (500 MHz, C_6D_6) δ 8.20 (t, *J* = 8.4 Hz, 1H), 7.50 (d, *J* = 7.9 Hz, 2H), 7.38 (d, *J* = 7.7 Hz, 2H), 7.23 (t, *J* = 7.5 Hz, 1H), 7.01 (t, *J* = 7.5 Hz, 1H), 6.94 (ddd, *J* = 9.4, 4.7, 1.8 Hz, 1H), 6.90 (d, *J* = 8.4 Hz, 2H), 6.73 (dt, *J* = 7.8, 1.8 Hz, 1H), 6.58 (d, *J* = 7.9 Hz, 2H), 6.51 (d, *J* = 7.6 Hz, 2H), 3.60 (s, 6H), 2.25 – 2.10 (m, 2H), 2.01 (s, 3H), 1.95 (s, 3H), 1.75 – 0.92 (m, 20H).

^{31}P NMR (202 MHz, C_6D_6) δ 18.67 (t, J_{PtP} = 2411 Hz, 1P).

3.3l Synthesis of (SPhos)Pt(*p*-Tol)(OTf)

A 20 mL scintillation vial was charged with (SPhos)Pt(*p*-Tol)(Cl) (23.1 mg, 0.032 mmol, 1 eq) and DCM (5 mL). To the stirring solution of (SPhos)Pt(*p*-Tol)(Cl) was added a solution of silver(I) triflate (8.9 mg, 0.035 mmol, 1.1 eq) in a MeOH/DCM mixture (3 mL, 1:1 v/v ratio). After 15 minutes of stirring at room temperature, the reaction mixture was passed

through a pad of celite with THF to remove white precipitate of AgCl. The filtrate was dried *in vacuo*. The product was recrystallized by dissolving the crude product in minimal amount of hot benzene which was then filtered through a 20 μm syringe filter into a small shell vial placed inside a 20 mL scintillation vial containing 5-10 mL of pentane. The scintillation vial was capped; vapor diffusion overnight at 0 °C afforded yellow crystals. ^{31}P NMR of the crystals showed two different peaks at roughly 60:40 ratio – likely the (SPhos)Pt(*p*-Tol)(OTf) product and one where triflate anion stays in the outer sphere. Yield: 15.4 mg, 58%.

^{31}P NMR (202 MHz, C_6D_6) δ 21.93, 19.06.

3.4 Efforts on completing the dual catalytic cycle

3.4a General procedures for transmetallation

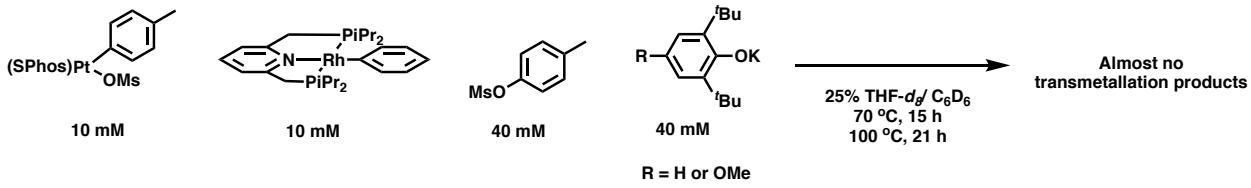

To a J.Young tube cooled to around -35 °C on cold aluminum beads were added ^{iPr}(PNP)RhPh (60 mM in C_6D_6, 100 μL, 6 μmol, 1 eq), (SPhos)Pt(*p*-Tol)(OMs) (40 mM in THF-d_8, 140 μL, 6 μmol, 1 eq), potassium phenoxide base (6.6 mg, 24 μmol, 4 eq), *p*-tolylmesylate (80 mM in C_6D_6, 300 μL, 24 μmol, 4 eq), and internal standard 1,3,5-trimethoxybenzene (10 mM in C_6D_6, 50 μL, 0.5 μmol, 0.08 eq). The J. Young tube was sealed, and the reaction was thawed right before the ^{1}H NMR of the first time point was

recorded. The reaction was heated to 70 °C for the first 15 h, followed by 100 °C for another 21 h. The reaction was monitored by ^{1}H NMR. NMR yields were measured against the internal standards. The identities of the [Pt] products (if observed) were confirmed either through comparison of NMR chemical shifts between experimental results with literature NMR spectra of the products. The yields of the biaryl products were measured on the GCMS using calibration curves of authentic biaryl products against internal standard hexamethylbenzene.

3.4b Synthesis of potassium 2,6-bis(tert-butyl)phenolate

A 100 mL flame-dried Schlenk flask was charged with 2-6-di-*tert*-butylphenol (1.4 g, 6.77 mmol, 1 eq). The flask was sealed and degassed with three cycles of evacuation and purging with N_2, after which THF (5.5 mL) was added to dissolve the phenol. The flask was then cooled to -78 °C. A suspension of potassium hydride (244 mg, 6.1 mmol, 0.9 eq) in THF (8 mL) was added to the phenol solution at -78 °C. The reaction was warmed up to room temperature and stirred for 2 h. THF was then removed *in vacuo*. Residual 2-6-di-*tert*-butylphenol was removed by washing the crude product with benzene. Yield: 3.35 g, 96%.

^{1}H NMR (500 MHz, THF) δ 6.83 (d, J = 7.6 Hz, 2H), 6.08 (br s, 1H), 1.39 (s, 18H).

3.5 Single Crystal X-ray Diffraction Details

Single crystal diffraction data for (κ^2-phosphepine)Pt(*p*-Tol)(Cl) was obtained at the Advanced Photon Source. A benzene molecule from the recrystallization solvent was co-crystallized. The structure was solved and refined by Dr. Alexander Filatov (**Figure 19**, **Table 4**).

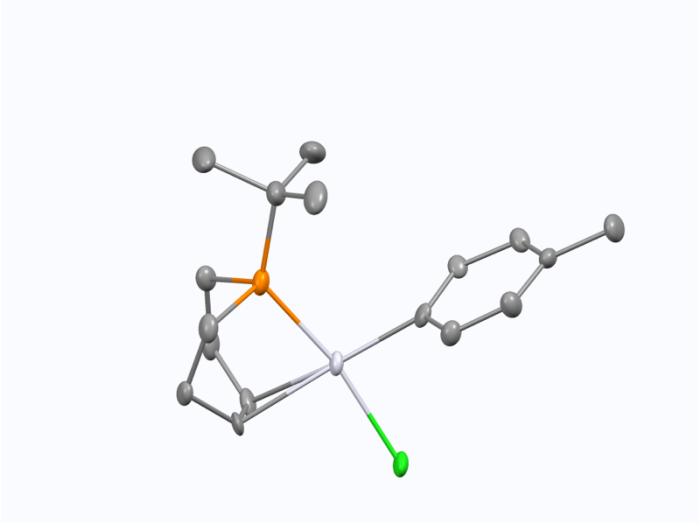

Figure 19. Crystal structure of (κ2-phosphepine)Pt(*p*-Tol)(Cl).

Bond precision: C-C = 0.0152 A Wavelength=0.41328

Cell: a=12.416(2) b=15.444(3) c=11.0958(17)
alpha=90 beta=111.183(5) gamma=90
Temperature: 100 K

	Calculated	Reported
Volume	1983.9(6)	1983.8(6)
Space group	P 21/c	P 1 21/c 1
Hall group	-P 2ybc	-P 2ybc
Moiety formula	C17 H26 Cl P Pt, 0.5(C6 H6)	C17 H26 Cl P Pt, 0.5(C6 H6)
Sum formula	C20 H29 Cl P Pt	C20 H29 Cl P Pt
Mr	530.93	530.94
Dx,g cm-3	1.778	1.778
Z	4	4
Mu (mm-1)	1.779	1.779
F000	1036.0	1036.0
F000'	1034.28	
h,k,lmax	15,19,13	15,19,13
Nref	4052	3937
Tmin,Tmax	0.958,0.965	0.586,0.744
Tmin'	0.948	

Correction method= # Reported T Limits: Tmin=0.586 Tmax=0.744
AbsCorr = MULTI-SCAN

Data completeness= 0.972 Theta(max)= 14.959

R(reflections)= 0.0445(2658) wR2(reflections)= 0.1149(3937)

S = 1.018 Npar= 212

Table 4. Single crystal X-ray diffraction details of (κ^2-phosphepine)Pt(*p*-Tol)(Cl).

Chapter 2 Studies on Fe(II) α-ketoglutarate dependent enzyme SadA and the non-native activities in its mutants

Introduction

The concept and importance off C–H functionalization were established in the previous chapter. Among the different types of C–H functionalizations, halogenation is one heavily utilized type of reactions used in the synthesis of materials that improve our modern life.[50,51] While a substantial number of halogenation transformations can be achieved via synthetic chemistry with small molecule reagents, enzymatic halogenation provides a complementary and sometimes overlapping scope of substrates for halogenation under mild conditions. There are four prominent classes of halogenases found in nature: FAD-dependent halogenases (FDH's), non-heme Fe(II) α-ketoglutarate dependent halogenase (FeDH's), haloperoxidases, and fluorinases.[52] The Lewis group is primarily interested in FDH's and FeDH's. FDH's halogenate at sp^2 carbons of substrates with arene group(s), while FeDH's do so at sp^3 carbons of aliphatic substrates.[53] In the last decade, our group has made significant contributions to understanding the halogenation mechanism in FDH's and expanding FDH's reactivity beyond their native ones.[54–60] In recent years, our group also started investigating in the chemistry of FeDH's, an effort of which I am a part. In this chapter, I shall report my findings in the FeDH project.

FeDH's are a class of enzyme within the family of non-heme Fe(II) α-ketoglutarate dependent enzymes. This family of enzymes catalyze several types of reactions, two of which are hydroxylation and halogenation of unactivated sp^3 C-H bonds in aliphatic

substrates.[61,62] These hydroxylases and halogenases have two conserved active site His residues. Hydroxylases also have a conserved Asp or Glu residue, which together with the other two His, bind to Fe(II) to form a facial triad that has been shown to be essential for carrying out the native reaction.[62,63] A similar facial triad is also formed to bind Fe(II) in halogenases, with an exogenous halide replacing the conserved Asp/Glu residue in hydoxylases.[63]

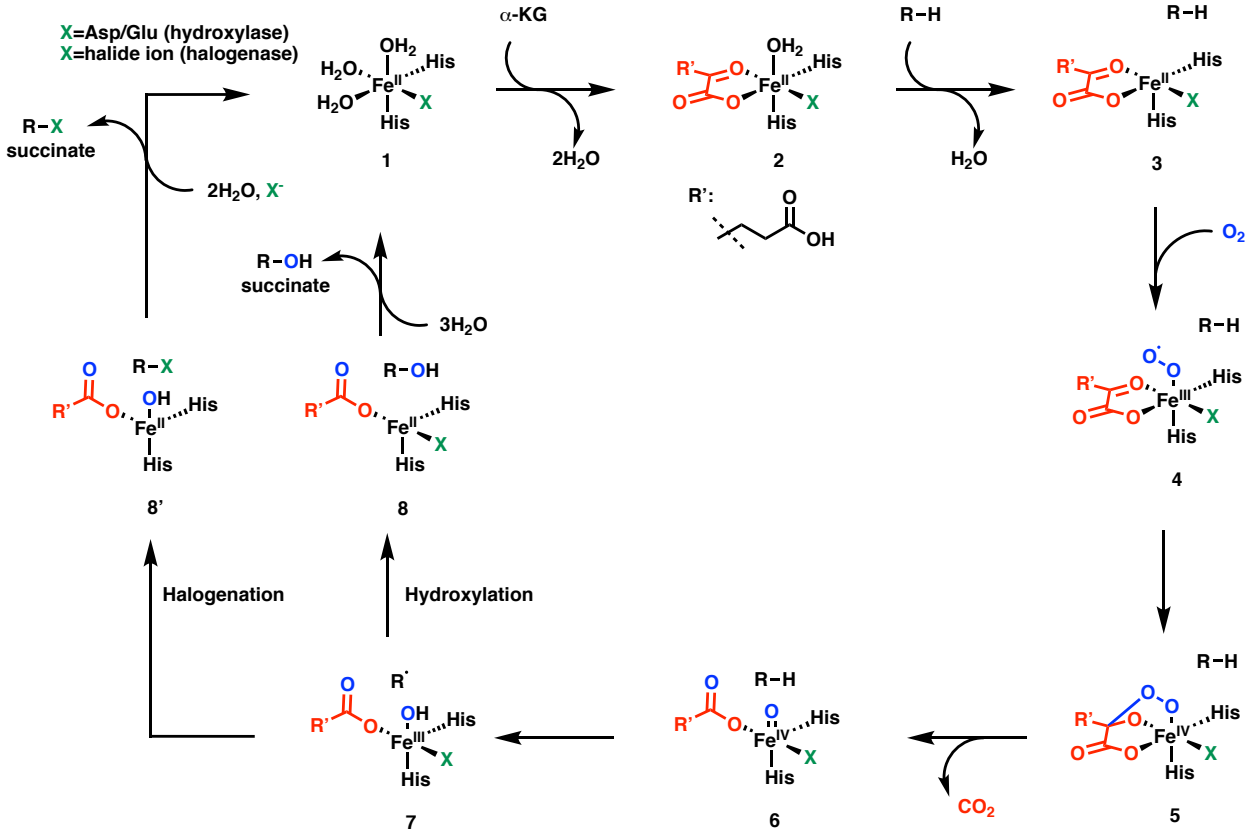

Figure 20. Established mechanisms of Fe(II) α-KG dependent hydroxylase and halogenase.

The two classes of enzymes follow similar, well-established mechanisms (**Figure 20**).[63] Catalysis in both enzyme classes initiates with Fe(II) complex **1**, which has the His_2X facial triad (where X is Asp/Glu for hydroxylase and halide for halogenase,

respectively) and three additional water molecules bound in an octahedral configuration. α-KG displaces two equatorial water molecules on Fe(II) such that α-KG binds in a bidentate configuration and opposite to the X group to form **2**. The third axial water molecule dissociates to generate **3** when substrate R–H binds in the active site of the enzyme but not to Fe(II). The binding of substrate triggers the binding of an O_2 molecule axial to Fe(II), forming a Fe(III)-superoxo intermediate **4**. The distal oxygen in the superoxo group attacks C2 of the bound α-KG, generating a peroxohemiketal bicyclic Fe(IV) intermediate **5**. Oxidative decarboxylation of α-KG results in the release of CO_2 and a highly active ferryl oxo intermediate **6**, with succinate bound in monodentate fashion. The oxo group in **6** abstracts a hydrogen atom from the active site-bound substrate to form a substrate radical and a Fe(III)-hydroxyl intermediate **7**. The major difference between the two enzyme classes lies in the next step. Whereas in a hydroxylase, rebound of the OH group on **7** yields the hydroxylated product R–OH and Fe(II) intermediate **8**, a halide rebound affords the halogenated product R–X and a different Fe(II) intermediate **8'** in a halogenase. The subsequent product release and succinate dissociation complete the catalytic cycle. Although X is usually an exogenous halide in halogenases, there have been examples of X-substitution with pseudohalides (NaN_3, $NaNO_2$) resulting in halogenases affording pseudohalide-incorporated products.[64,65] In particular, Matthews and coworkers have found that halogenase SyrB2 produced azide- and nitrite-incorporated products in the presence of NaN_3 and $NaNO_2$, respectively.[65] Targeted mutagenesis intended to carve out more space in the active site for the non-spherical

pseudohalides resulted in an estimated yield of 22% of the nitrite-incorporated product, the best result among the reported pseudohalide reactions.

Given the similarity in mechanism between Fe(II) α-KG-dependent hydroxylases and halogenases, there have been many attempts at converting a hydroxylase into a halogenase by mutating the X group from an Asp or Glu to smaller residues without coordinating side chains such as Ala or Gly. In most cases, halogenation activity with exogenous halide ions was not observed but hydroxylation activity decreases significantly.[66–68] In some cases, the hydroxylation activity can be rescued to a certain extent by the addition of anions such as halides, acetate, or formate.[67–70] Rare examples of such "halogenase" variants having partial halogenation activity in the presence of halide ions include the hydroxylases SmP4H and SadA, reported by Buller and Boal, respectively.[65,71] Hydroxylase SadA from *Burkholderia ambifaria* is known to catalyze the hydroxylation of *N*-succinylated amino acids, with *N*-suc-Leu (NsL) being the best substrate identified to date (**Figure 21A**).[72] In mutating the active site D157 to Gly, the Boal group was able to either chlorinate or hydroxylate at the C3 position of NsL in the presence of NaCl (**Figure 21B**).[73]

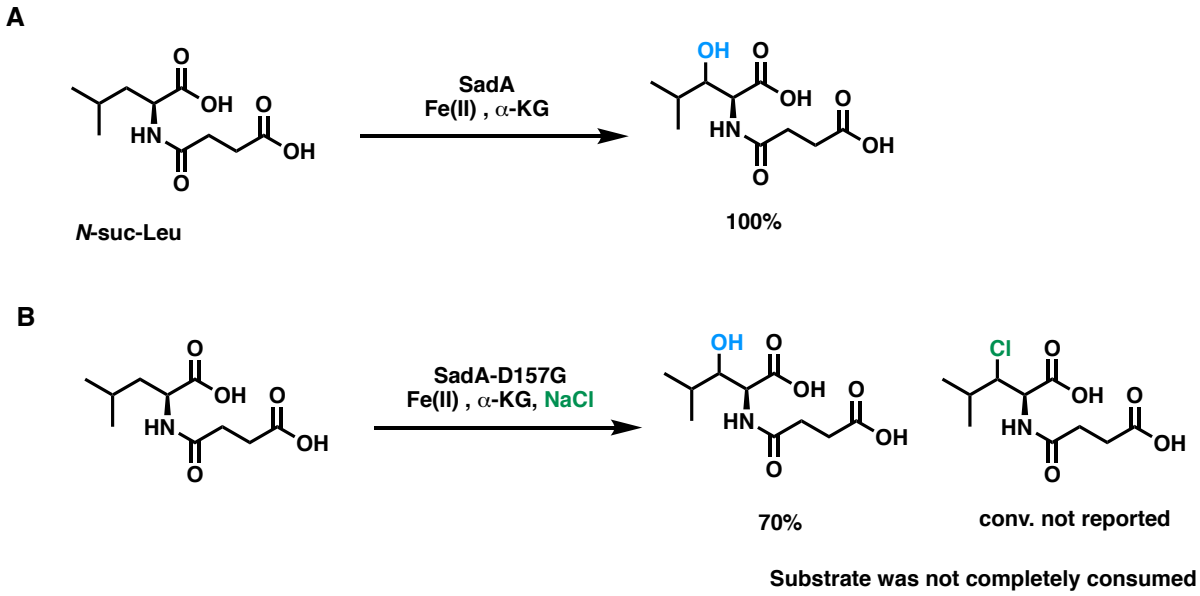

Figure 21. Reactivities of SadA and its mutant lacking the active site Asp.(A) Hydroxylation of *N*-suc-Leu was found to be the best performing reaction catalyzed by WT SadA.[72,74] (B) The "halogenase" mutant SadA D157G yielded both the C3-hydroxylated and C3-chlorinated *N*-suc-Leu products, as reported by Boal and coworkers.[73]

Upon learning of this promising result, the Lewis group further explored the chemistry of the SadA D157G mutant (hereinafter "SadH") in the presence of other anions. Prior to my involvement in this project, coworker Christian Gomez first optimized expression protocols of SadH by tethering a maltose-binding protein (MBP) to increase protein solubility during expression. Inspired by the work conducted by the Matthews and coworkers on halogenase SyrB2 to form non-native azidation and nitration products by adding the corresponding salts in lieu of chloride,[65] Mr. Gomez performed a reaction between NsL, MBP-SadH, and NaN_3. He observed a new product by LCMS, in addition to the hydroxylated product ("OH-1" hereinafter) (**Figure 22**). The new product has an m/z of 271 under negative ionization mode, which is consistent with the m/z of an azidated NsL product ("N3" hereinafter). Dr. Dibyendu Mondal isolated and characterized the N3

product by ^{1}H NMR; the azide group was assigned to the C4 tertiary position. This result suggests that not only was azide ion bound to Fe(II), the ion also rebounded with substrate radical to form the azidated product. This is an unprecedented result. The D201G mutant of α-KG dependent hydroxylase FIH, intended to imitate a halogenase, has been reported to have NaN_3 bound to its Fe(II) based on UV-vis data but had not shown any azidation activity.[70] While other native halogenases such as SyrB2 and SaDAH have been shown to form azidated products in the presence of NaN_3, as far as we know, this is the first example of an α-KG dependent hydroxylase with the active site Asp to Ala/Gly mutation that is capable of azidation.[64,65]

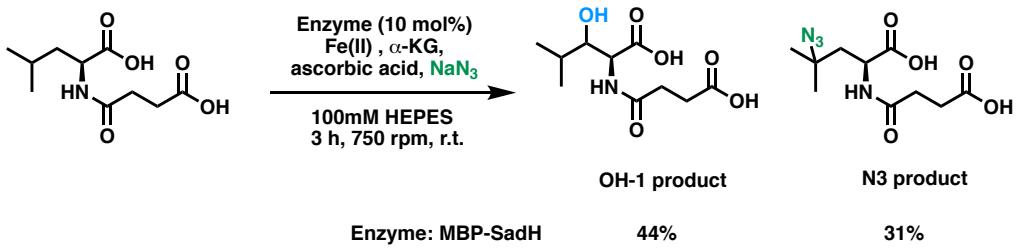

Figure 22. Preliminary results from the reaction of NsL by MBP-SadH in the presence of NaN_3.

This work has yet to be published and was conducted by Mr. Gomez and Dr. Mondal. Product conversions were calculated using relative extracted ion chromatogram peak areas of products and substrate obtained on the LCMS. Reductant ascorbic acid was added so that the reaction can be carried out in air.

With such an exciting result, Mr. Gomez embarked on an ongoing directed evolution campaign to evolve parent MBP-SadH into an azidase and to suppress its hydroxylation activity. One promising mutant in the early days of the campaign was the mutant MBP-SadH-3, with the mutations V39I and F152L. Mr. Gomez's preliminary results showed that this mutant can generate the same N3 product significantly more

selectively than the parent MBP-SadH, as judged by the percent conversion to products (**Figure 22**). When I joined this project, my main goal was investigating the binding of exogenous anions to the Fe(II) center of SadH through exploring the scope of activity of MBP-SadH in the presence of different anions, steady state kinetics, and UV-vis titrations.

Exploring the activity of MBP-SadH in the presence of exogenous anions

As part of onboarding for this project, I first attempted to reproduce results reported by Mr. Gomez (**Figure 22**) and analyzed the reactions using a different LCMS method. In this process, I discovered that MBP-SadH-3 produced a large amount of a new product, in addition to smaller amounts of the OH-1 and N3 product in the presence NaN_3 (**Figure 23A**). This new product has an m/z consistent with that of a hydroxylated product but has a much earlier retention time compared to that of the C3-hydroxylated OH-1 product on the LCMS column. This new hydroxylated product (hereinafter "OH-2") appeared to be more polar than the other products or substrate; it eluted during the solvent delay portion of the LCMS method Mr. Gomez used. The peak area of OH-2 was therefore unintentionally unaccounted for in the product conversion calculation, resulting in a misleadingly high conversion for the N3 product (87%) in the case of MBP-SadH-3. The new results in **Figure 23** revealed that the MBP-SadH-3 mutant in fact has a lower conversion to N3 but a much higher conversion to the new OH-2 product, compared to parent MBP-SadH. While the parent also produced some OH-2, the majority of its products are OH-1 and N3. A positive control with the WT SadA reaction in the presence of NaN_3 produced exclusively OH-1, consistent with reported results in literature.[73]

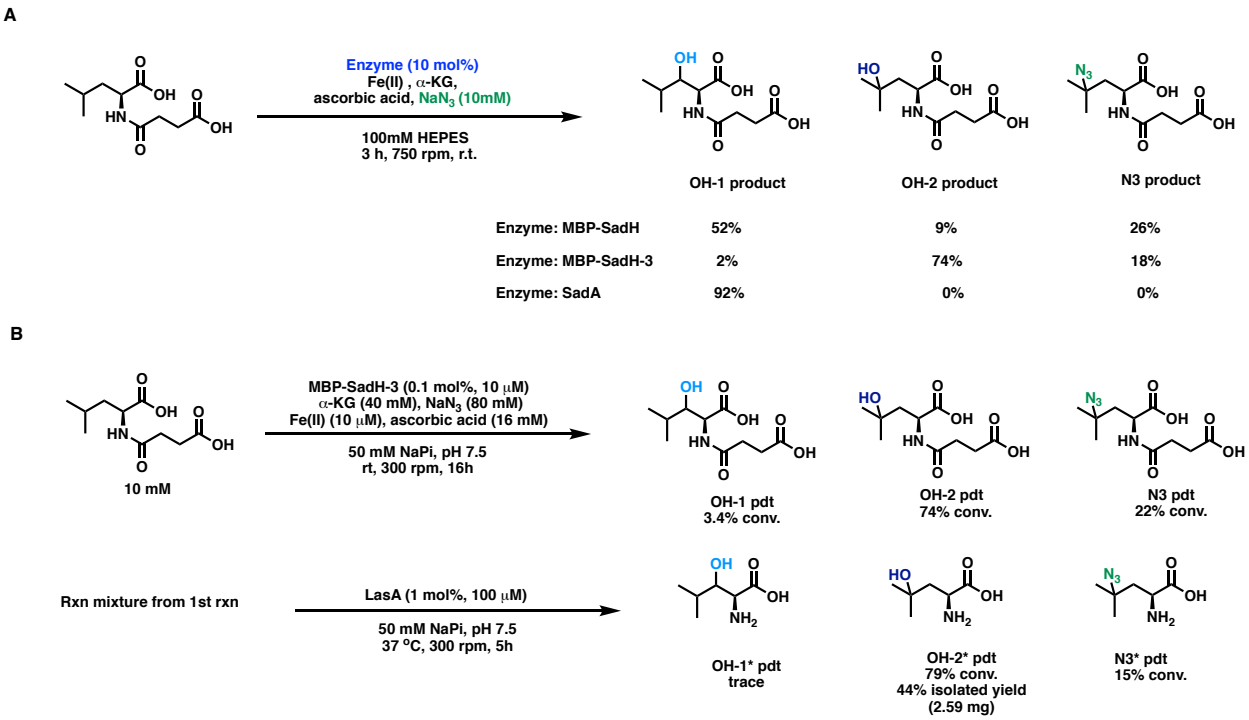

Figure 23. New results of NsL reaction with MBP-SadH(-3) in the presence of NaN_3.(A) Reproduction of results reported by Mr. Gomez revealed the presence of a new product, OH-2. (B) Assignment of hydroxylation site on OH-2 through isolation and characterization of desuccinylated product OH-2*.

I attempted but failed to isolate OH-2 from a bioconversion on a semiprep LC column due to significant overlap in retention times with the much larger amounts of other polar components of the reaction such as buffer, ascorbic acid, and succinate. I was, however, able to obtain the desuccinylated form of this product (hereinafter "OH-2*") by adding desuccinylase LasA to the completed MBP-SadH reaction with NaN_3 (**Figure 23B**). LasA has been demonstrated to in tandem desuccinylate the succinylated amino acid products of SadA reactions.[74] After isolating OH-2* on a cation exchange column followed by semiprep LC, the site of hydroxylation on OH-2* was assigned to be at the C4 tertiary position via NMR characterization. Assuming the hydroxyl group does not migrate during the desuccinylation step, OH-2 is the C4-hydroxylated product.

It is notable that the MBP-SadH-3 mutant with only two mutations switches hydroxylation site selectivity almost exclusively from the C3 secondary to C4 tertiary position of NsL. In fact, preliminary results from Mr. Gomez demonstrated that MBP-SadH only needs one of the two mutations, F152L, to switch the hydroxylation site selectivity in the presence of NaN_3. The F152 residue is part of a loop within SadA that was not resolved in its crystal structure (PDB: 3W21), presumably due to the high flexibility of the loop.[75] The flexibility of the loop may have caused the observed switch in site selectivity. To better understand the cause of this switch, Mr. Gomez is using different modeling software to predict the structure of this loop and to dock NsL into the resulting structure of SadA.

Simultaneously, I performed assays of NsL hydroxylation and anion incorporation with MBP-SadH and MBP-SadH-3 in the presence of different anions (**Figure 24**). As was the case with many other reported "halogenase" mutants of hydroxylases, there was almost no hydroxylation observed for both enzymes in the absence of exogenous anions.[67,69,70,76] The lack of the coordinating D157 residue or an exogenous anion leaves an incomplete His_2X facial triad on the iron center, hindering the enzyme's ability to undergo the hydroxylation mechanism (**Figure 20**). Control reactions with the non-coordinating salt NH_4PF_6 was included to demonstrate that increasing the ionic strength of the solution alone does not rescue the desired hydroxylation activity. Positive controls of WT SadA reactions in the presence or absence of the same panel of anions all yielded >99% conversion of OH-1 (not shown in **Figure 24**).

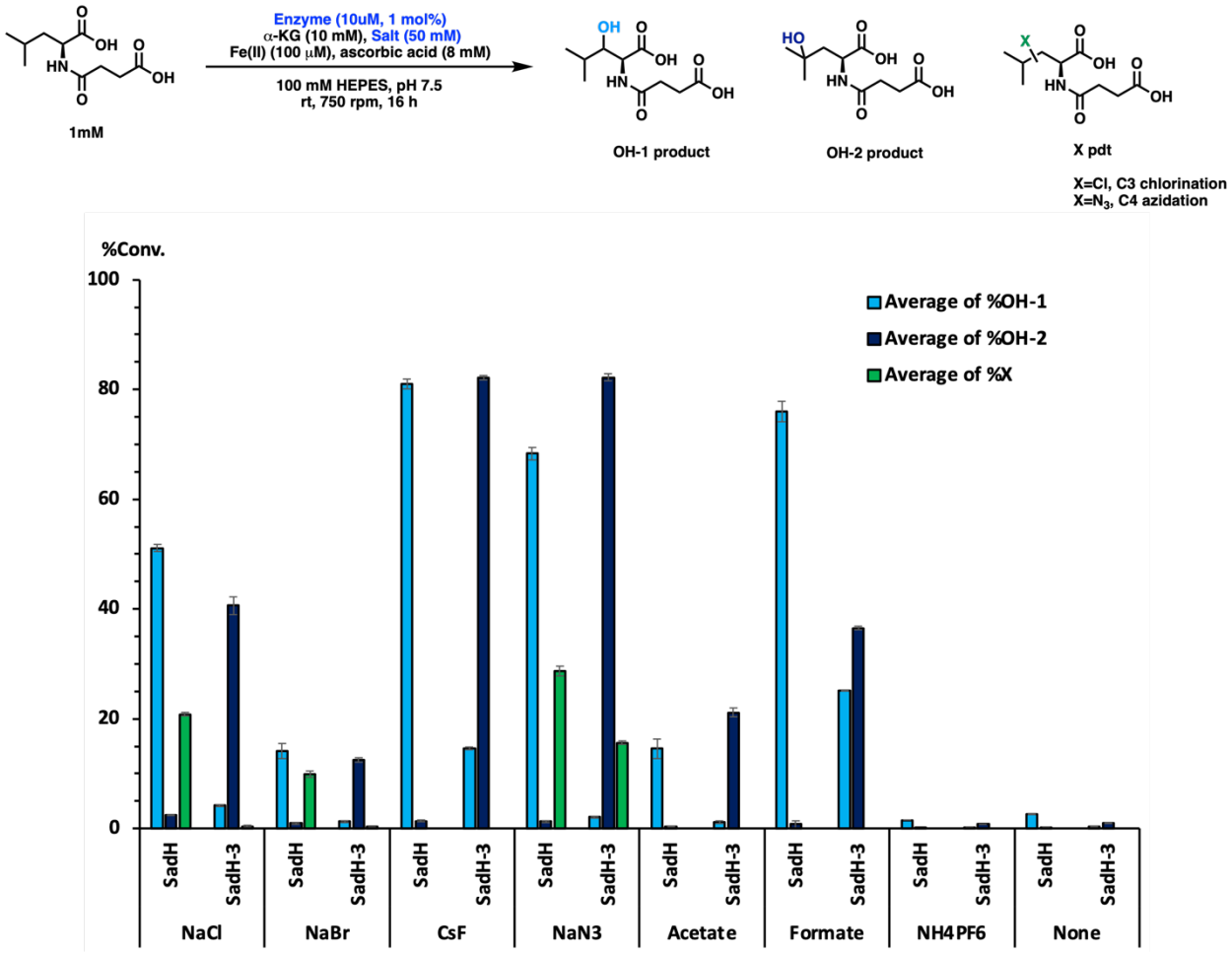

Figure 24. NsL conversions to product in the presence of different salts by MBP-SadH or MBP-SadH-3.The names of the enzymes are abbreviated to “SadH” and “SadH-3” in the chart above. Product conversions were calculated using relative extracted ion chromatogram peak areas of products and substrate obtained on the LCMS. With the exception of NH_4PF_6 (single reactions) and no anion (duplicates) sets, all reactions were performed in triplicates. Site of bromination is not assigned as the brominated product has yet to be isolated or characterized. Site of chlorination was presumed to be at C3 based on previously reported results.[73]

In general, the addition of an exogenous anion rescues the hydroxylation activity to varying extents by presumably completing the aforementioned facial triad on Fe(II). As we have suspected, for reactions that did yield hydroxylated products, parent MBP-SadH produced OH-1 almost exclusively while MBP-SadH-3 yielded mostly OH-2.

As reported in **Figure 23A**, both parent and mutant produced the N3 product and different hydroxylated products in the presence of NaN_3. Consistent with results reported by the Boal group,[73] there are low levels of conversion to the chlorinated and brominated products in the presence of NaCl and NaBr, respectively, by parent MBP-SadH. Both reactions also generated OH-1, with NaCl rescuing hydroxylation activity to a higher extent than NaBr does. Mutant MBP-SadH-3 produced even less chloride or bromide incorporated products. The same hydroxylation rescuing trend in the presence of NaCl or NaBr is observed for the mutant with the product being OH-2 instead.

The fluoride ion is included in this assay with the hopes of fluorinating the substrate as fluorination of an organic compound is a very desirable but rare reaction in the pharmaceutical industry.[77,78] Both small-molecule and enzymatic approaches to fluorinations have been studied extensively.[79,80] In my experiment, CsF was chosen over NaF as the source of fluoride due to NaF's relatively poor solubility in water. No fluorinated products were observed but fluoride appears to rescue hydroxylation activity in both parent and mutant by around 80% with regards to conversion in both the parent and mutant, compared to the near full conversion to OH-1 seen in WT SadA. In light of the NH_4PF_6 results showing that simply increasing the ionic strength does not rescue hydroxylation, the CsF results suggest that the fluoride ion was bound to the Fe center

during reaction and facilitates hydroxylation. This is in stark contrast to what was reported in literature in terms of fluoride binding. Matthews and coworkers reported the lack of fluoride binding to Fe(II) in the halogenase SyrB2 under anaerobic conditions and in the absence of substrate.[65] While the Knapp group demonstrated that NaF can rescue hydroxylation activity of FIH D201A, the hydroxylation initial rate of this mutant in the presence of NaF was only about 15% of that of the WT FIH hydroxylation. Although the metrics used for fluoride binding or hydroxylation rescue by fluoride in these studies are different from the conversions used in **Figure 24** and cannot be used for direct comparison, our results do suggest MBP-SadH and its mutant may be more capable of binding fluoride to carry out hydroxylation of NsL. Similar fluoride binding studies as ones performed by the Matthews and Knapp groups were also carried out and will be discussed later in this chapter.

Lastly, we expected anions with structures similar to the side chain of an Asp to be capable of reviving hydroxylation to some extent, presumably by mimicking the Fe intermediates in WT SadA. Despite this line of reasoning, there are not many examples of rescuing of hydroxylation activity in “halogenase” mutants of hydroxylases to significant extents in literature; most report trace to no hydroxylation in the presence of formate or acetate ions.[68,69] Gratifyingly, 72% and 62% of hydroxylated products were generated in the reactions with sodium formate for MBP-SadH and MBP-SadH-3, respectively. Reactions with sodium acetate yielded less hydroxylated products. This may suggest that formate is a better substitute for Asp than acetate, likely for steric reasons.

Seeing the general trend of the shift in hydroxylation site selectivity in MBP-SadH-3 across the panel of anions, I reverted the D157G mutation back to Asp in this mutant in the hopes that this new hydroxylase mutant would result in exclusive C4 hydroxylation. Unfortunately, this variant (MBP-SadH-3D) gave a >99% conversion to a 45:55 ratio of OH-1 and OH-2 products in the absence of anions. Addition of anions from of the same panel shown in **Figure 24** yielded similar hydroxylation site selectivity but with lower conversions overall.

Steady-state kinetics studies

To evaluate how anions affect activity in MBP-SadH, two sets of kinetics studies were carried out – initial rates of product formation were measured with varying concentrations of (i) substrate NsL or (ii) exogenous anion. In order to obtain instrument response factors for quantifying product yields, 100 to 150 mL scale bioconversions were carried out to isolate pure OH-1 and N3 products. Due to the aforementioned challenges in isolating OH-2, kinetics studies were not conducted with the mutant MBP-SadH-3, which yields OH-2 in most cases. A response factor for the chlorinated product was not measured due to our current inability to isolate large enough of an amount of it for this purpose. After extensive optimization of parameters, protocols, and LCMS methods, I obtained kinetics data for both sets in high data quality (**Figure 25** and **Figure 27**).

In the kinetics studies of OH-1 formation against substrate concentrations, the MBP-SadH reaction without exogenous anions has a k_{cat} value an order of magnitude lower than that of WT SadA, as expected (**Figure 25**, **Table 5**). CsF, NaN_3 and NaCl each

rescues hydroxylation by MBP-SadH to some extents – k_{cat} values of these three reactions are 1.2- to 3-times that of the reaction in the absence of anions (**Table 5**). A perhaps surprising finding is the presence of anions increases the enzyme's binding affinity for substrate NsL. The K_M values of the three reactions with exogenous anions are 2.5% to 60% that of WT SadA, while the absence of anions in MBP-SadH reaction brings the K_M to over three times that of WT SadA. Due to the lower K_M values, k_{cat}/K_M of the NaCl and NaN_3 reactions are at the same level of and one order of magnitude higher than that of WT SadA, respectively.

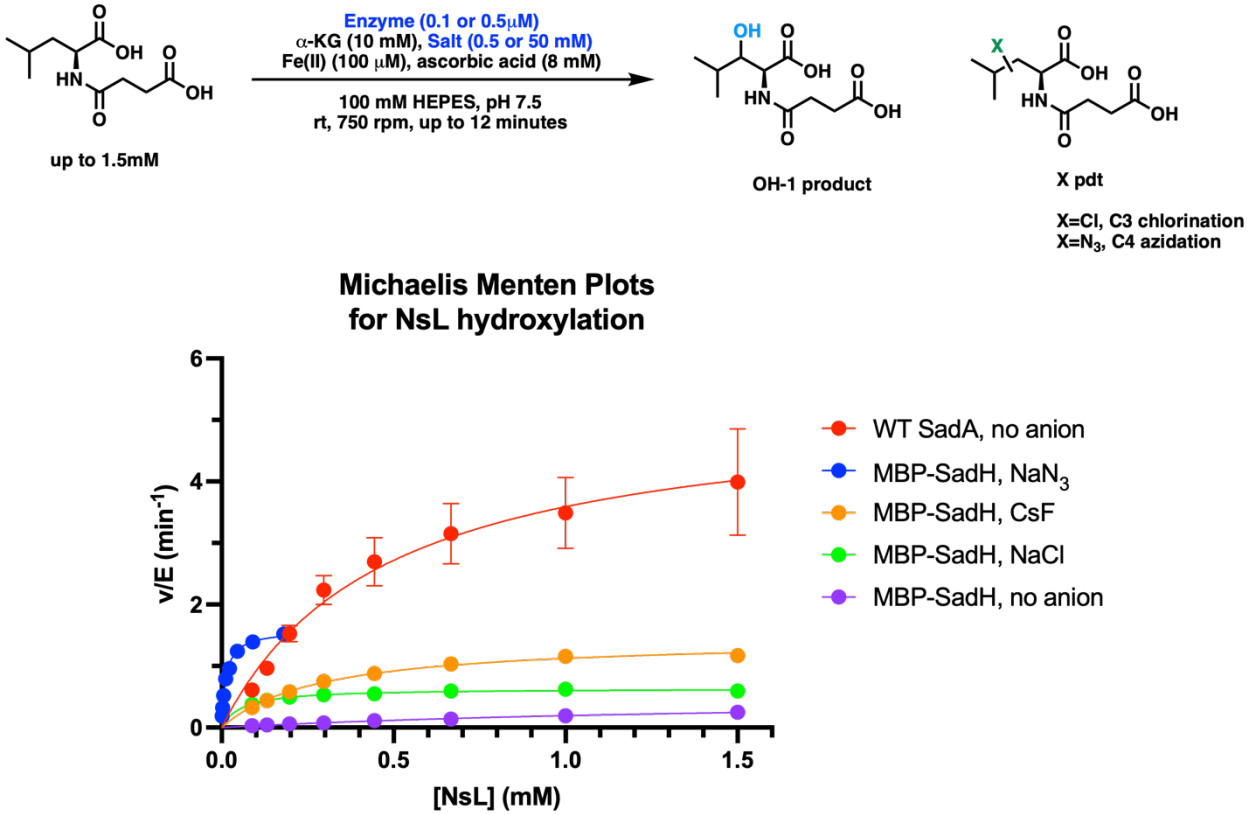

Figure 25. Initial rates of OH-1 formation in the presence of exogenous anions with MBP-SadH or WT SadA against varying substrate NsL concentrations.

Data were fitted to Michaelis Menten model.

Reaction	R^2 of fit	k_{cat} (min^{-1})	K_M (mM)	k_{cat}/K_M (M^{-1} s^{-1})
WT-SadA	0.9850	5.287(314)	0.473(066)	$1.86 \times 10^2 \pm 2.83 \times 10^1$
MBP-SadH, CsF	0.9943	1.446(036)	0.286(020)	$8.42 \times 10^1 \pm 6.16 \times 10^0$
MBP-SadH, NaN_3	0.9938	1.584(033)	0.012(001)	$2.19 \times 10^3 \pm 1.73 \times 10^2$
MBP-SadH, NaCl	0.9776	0.636(009)	0.058(005)	$1.82 \times 10^2 \pm 1.57 \times 10^1$
MBP-SadH, no anions	0.9949	0.526(048)	1.715(243)	$5.11 \times 10^0 \pm 8.63 \times 10^{-1}$

Table 5. Kinetics parameters for hydroxylation formation with varying substrate NsL concentrations using Michaelis Menten model (**Figure 25**).

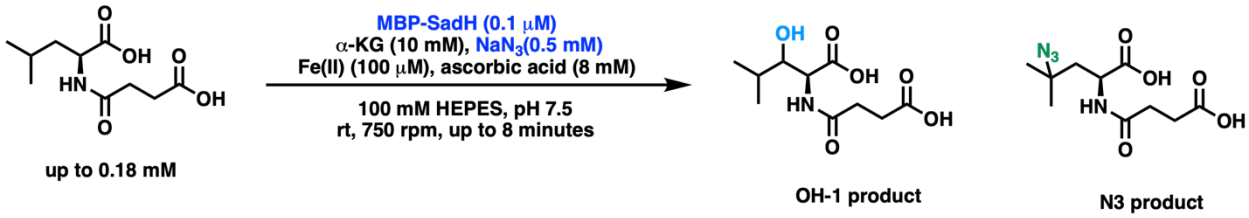

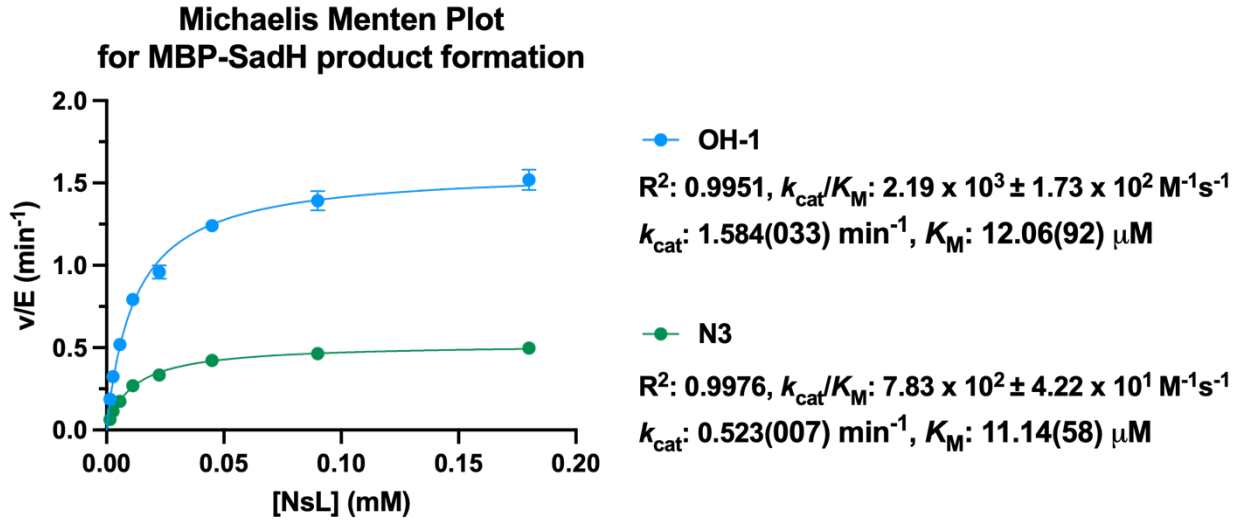

Figure 26. Initial rates of OH-1 and N3 formation with MBP-SadH in the presence of 0.5 mM NaN3 against varying substrate NsL concentrations. Data were fitted to Michaelis Menten model.

Data from the reaction with NaN_3 deviate the most from the other sets. While the other four sets in **Table 5** showed substrate inhibition behavior at around 1.75 mM NsL, the NaN_3 reaction started exhibiting such behavior at around 0.2 mM, likely due to its unusually low K_M. While optimizing conditions to obtain kinetic data in the presence of NaN_3, I discovered that NaN_3 inhibited the reaction at concentrations as low as 1mM. This inhibition was not observed for CsF or NaCl; in these cases, saturation kinetics were observed, and the initial rate of OH-1 formation plateaued after approximately 50 mM salt was added. Formation of the azidated product in the reaction containing NaN_3 also followed Michaelis Menten kinetics. The K_M value for this reaction was comparable to that associated with the formation of OH-1 in the same reaction, but the k_{cat} value is one-third that for OH-1 (**Figure 26**). The low K_M value leads to a k_{cat}/K_M value from N3 formation that is four times that of WT SadA. This is significant – not only can the "halogenase" MBP-SadH install an azide group on the substrate, it also does so with higher efficiency than the wild type hydroxylase can with hydroxylation.

Similar to N3 formation in the NaN_3 reaction (**Figure 26**), reactions conducted in the presence of NaCl also produced the C3-chlorinated product. Due to the lack of an instrument response factor for this product, a k_{cat} value cannot be calculated from the acquired initial rate data. The relative chlorinated product formation initial rates were fitted to the Michaelis Menten model with an R^2 of 0.9744. The fit provides a K_M of 0.059 mM, similar to that of OH-1 formation within the same reaction (**Table 5**).

Initial rates for reactions conducted using 1 mM substrate NsL and different salt concentrations revealed that all coordinating anions (CsF, NaCl, NaN_3) exhibit saturation

kinetics (**Figure 27**). This kinetic behavior suggests that exogenous anions bind to Fe(II) and facilitate the production of hydroxylated and anion-incorporated products. Formation of OH-1 in the presence of a non-coordinating salt NH_4PF_6 is at significantly lower levels and varying salt concentration had no effect on initial rates of product formation. This is consistent with results from **Figure 24** – simply increasing the ionic strength of the reaction does not aid the initial rate of product formation.

The NsL reaction in the presence of NaN_3 in this series of kinetics data also deviates significantly from the CsF and NaCl reactions. While saturation of initial rates is observed for both CsF and NaCl between 25 mM and 50 mM of salt added, this occurs between 0.125 mM and 0.25 mM for the reaction with NaN_3 after which azide inhibition was observed (**Figure 28**). Values of k_{cat} across the three reactions with coordinating salts are on the same order of magnitude and follow the trend of NaN_3 > NaCl > CsF (**Table 6**). MBP-SadH shows a high affinity for NaN_3 compared to NaCl and CsF; K_M of the NaN_3 set is two to three orders of magnitude lower than that of the other two reactions. This leads to a k_{cat}/K_M for the NaN_3 reaction that is three orders of magnitude higher than that of the other two reactions.

The N3 formation initial rate data for the reaction of NsL and NaN_3 set also exhibit Michaelis Menten behavior in the presence of less than 0.15 mM of NaN_3 (**Figure 28**). Similar to the NaN_3 reaction with varying substrate concentration (**Figure 26**), this set of N3 initial rate data has k_{cat} and K_M, values that are one-third and roughly the same of OH-1 data within the same reaction, respectively (**Figure 28**). The k_{cat}/K_M for the N3 formation is therefore also a third of that of OH-1 formation from the same reaction.

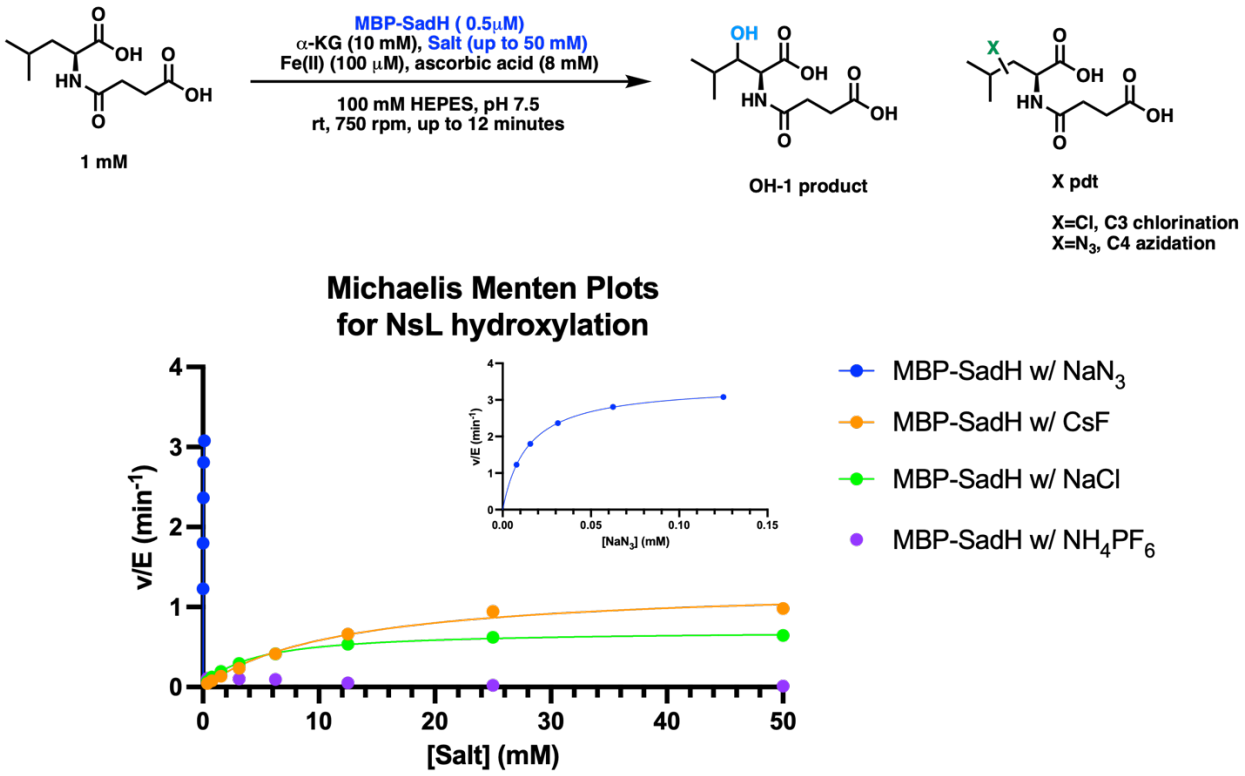

Figure 27. Initial rates of OH-1 formation in the presence of exogenous anions with MBP-SadH or WT SadA against varying salt concentrations.

Data were fitted to Michaelis Menten model, with the exception of the NH_4PF_6 set. Data points exhibiting salt inhibition in the NaN_3 reaction are not displayed. Inset shows data points from NaN_3 reaction from 0 to 0.15 mM NaN_3.

Reaction	R^2 of fit	k_{cat} (min^{-1})	K_M (mM)	k_{cat}/K_M (M^{-1} s^{-1})
MBP-SadH, NaN_3	0.9999	3.431(008)	0.014(000)	$4.06 \times 10^3 \pm 3.25 \times 10^1$
MBP-SadH, CsF	0.9949	1.281(076)	11.98(184)	$1.78 \times 10^0 \pm 2.04 \times 10^{-1}$
MBP-SadH, NaCl	0.9979	0.708(011)	4.166(217)	$2.83 \times 10^0 \pm 1.54 \times 10\text{-}^1$

Table 6. Kinetics parameters for hydroxylation formation with varying salt concentrations using Michaelis Menten model (**Figure 27**).

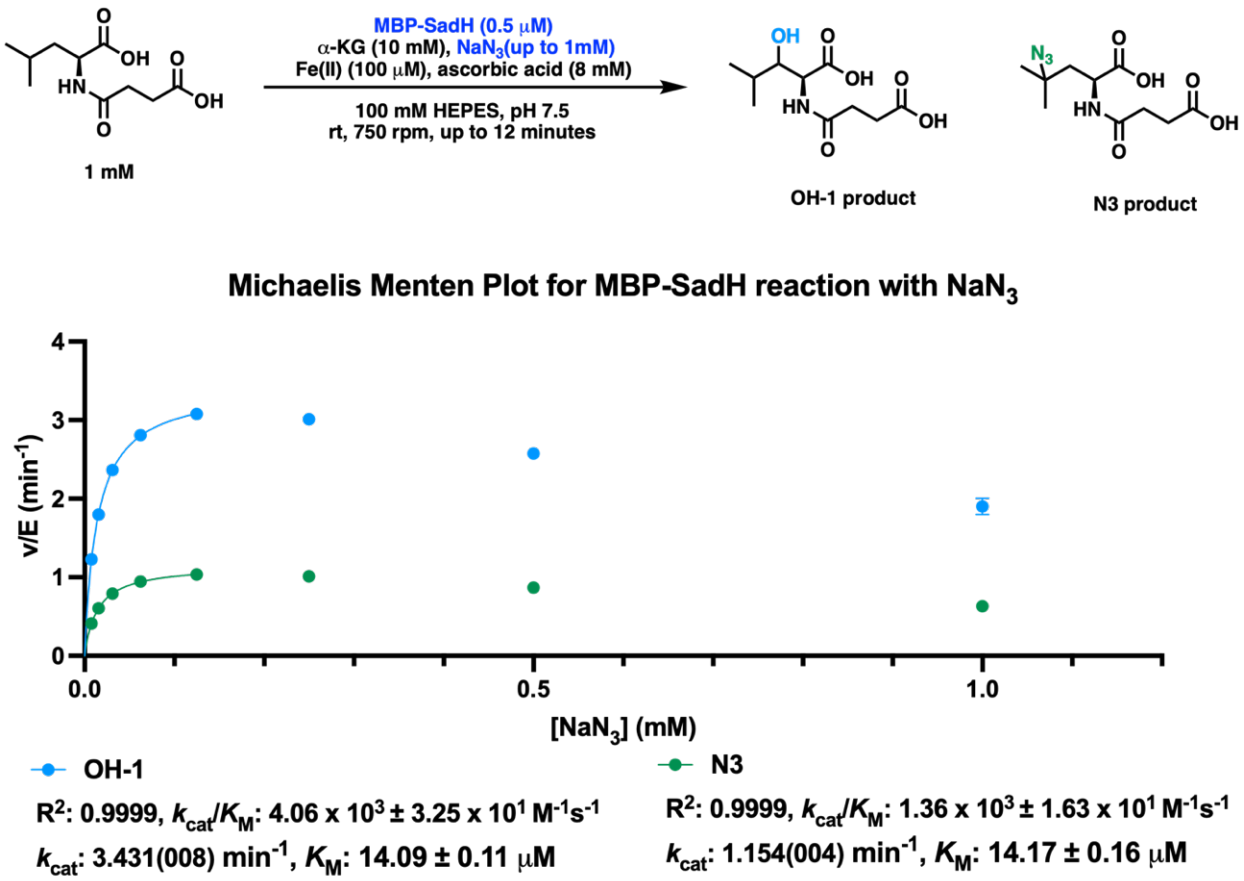

Figure 28. Initial rates of OH-1 and N3 formation with MBP-SadH against varying NaN_3 concentrations.

With the exception of data points in the salt inhibition regime, data were fitted to Michaelis Menten model.

The NaCl reaction in this series of kinetics experiments also produced kinetics data for the C3-chlorinated product, for which the instrument response factor was not measured. The relative chlorinated product formation initial rates were fitted to the Michaelis Menten model with an R^2 of 0.9984. This fit provides a K_M of 4.484 mM, similar to that of OH-1 formation within the same reaction (**Table 6**).

Fe(II) anion binding via UV-vis titration

Aside from steady state kinetics, anion binding to Fe(II) can also be probed by UV-vis spectroscopy. It is well established that members of the Fe(II) α-KG dependent enzyme family each has a Fe(II) to α-KG metal-ligand charge transfer (MLCT) transition at around 500 nm.[81,82] This transition can be observed when the enzyme is in the presence of α-KG and Fe(II) under anerobic conditions, where intermediate **2** is presumed to be the complex being formed (**Figure 20**). The Knapp group showed that when chloride, azide, or cyanate was added to a deoxygenated sample of a mutant of hydroxylase FIH lacking the active site Asp in the presence of Fe(II) and α-KG, a small shift in the Fe(II) to this MLCT band was observed.[21] Matthews and coworkers have also reported saturation behavior in similar MLCT band shifts when an exogenous anion such as azide or chloride was titrated to a deoxygenated sample containing halogenase SyrB2, a substoichiometric amount of Fe(II), and excess α-KG.[16] After each addition of the salt stock solution to the SyrB2–Fe(II)–αKG sample, an absorption spectrum was recorded. The spectrum of the starting solution of SyrB2–Fe(II)–αKG was subtracted from each spectrum acquired after an addition to generate a difference spectrum. When all difference spectra are plotted together, one can visualize the new MLCT peak (λ_{max}). Plotting the extent of spectral change at the new λ_{max} as a function of salt concentration in sample yields a binding curve from which the anion dissociation constant (K_D) can be estimated.

In the hopes of providing more evidence of anion binding to Fe(II) in MBP-SadH, I attempted this assay for MBP-SadH with three different salts: CsF, NaCl, and NaN_3. Thus

far, the MBP-SadH used in experiments contains two His-tags for ease of purification on Ni-NTA resin after expression. To ensure the substoichiometic amount of Fe(II) used in titration experiments will be bound in the active site and not to the His-tags, MBP-SadH without His-tags was expressed and purified on anion exchange resin followed by size exclusion chromatography.

Consistent with other members of the Fe(II) αKG-dependent enzyme family, the λ_{max} resulting from the MLCT band of the MBP-SadH–Fe(II)–αKG complex in the absence of exogenous anions is around 490nm. When the difference spectra were plotted, I observed two new peaks that grew in for each salt – one blue-shifted and the other red-shifted from the initial 490 nm (**Figure 29**). It is not clear which new λ_{max} corresponds to the anion-induced change in MLCT transition for the λ_{max} shifts range from 41 nm to 118nm. In the few literature examples where the anion-perturbed MLCT band was recorded, none have λ_{max} shifts exceeding 50 nm. Plotting the absorbance differences at both new λ_{max}'s against salt concentration afforded two binding curves resembling those produced in the literature for SyrB2. While the resulting K_D estimates from the two binding curves are quite similar in the case of CsF and NaCl, those from the titration of NaN_3 differ by an order of magnitude.

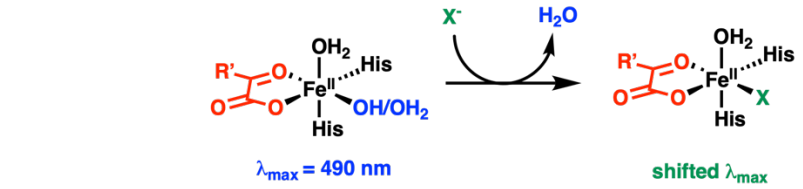

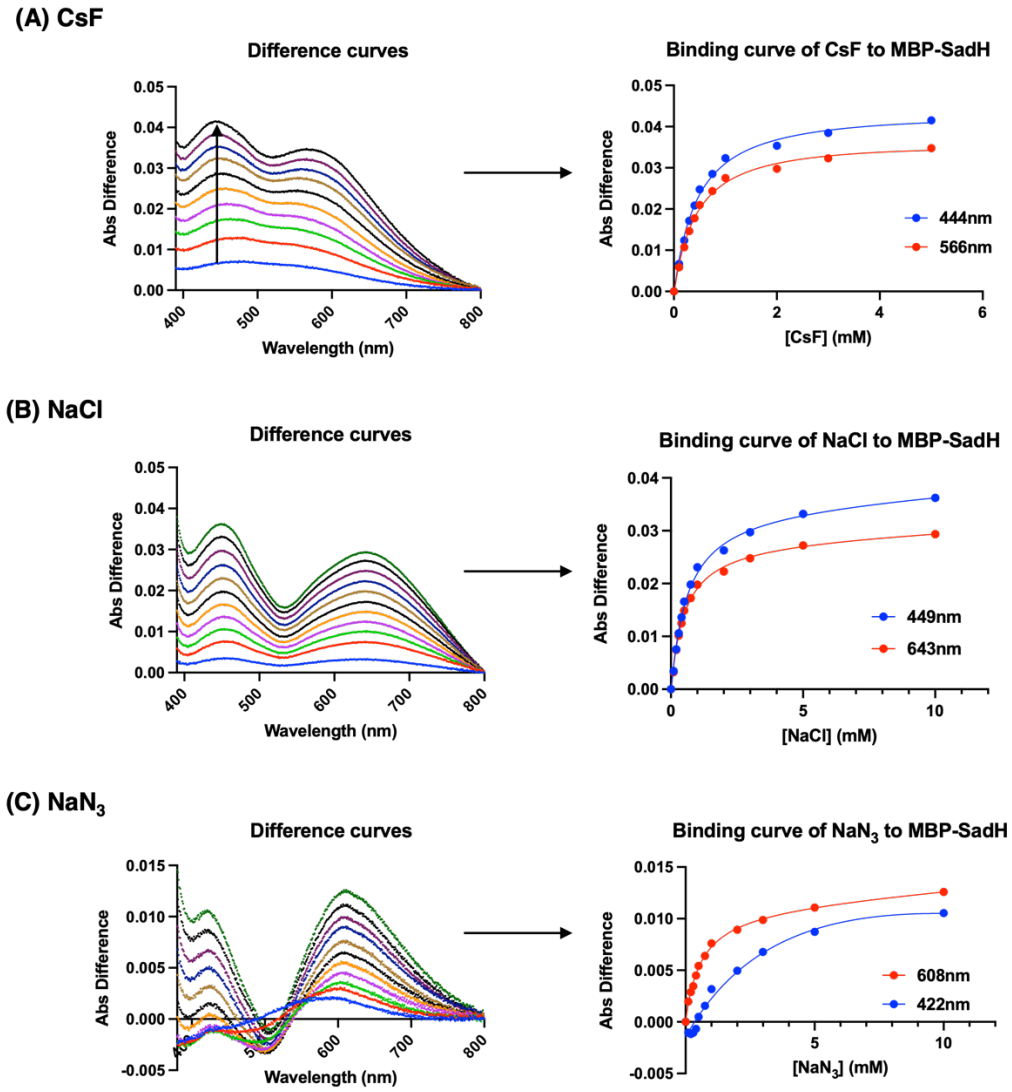

Salt	Blue-shifted λ_{max}	K_D (Blue-shifted)	Red-shifted λ_{max}	K_D (Red-shifted)
CsF	444 nm	0.457(076) mM	566 nm	0.446(074) mM
NaCl	449 nm	0.599(081) mM	643 nm	0.494(059) mM
NaN_3	422 nm	6.017(6073) mM	608 nm	0.599(070) mM

Figure 29. Binding of fluoride, chloride, and azide to MBP-SadH–Fe(II)–αKG complex monitored by perturbations to the absorption spectrum from Fe(II)–αKG MLCT transition. Difference curves are normalized by setting the absorbance difference at 800 nm to zero.

To help determine which λ_{max} represents the new MLCT transition, I am collaborating with Vyshnavi Vennelakanti of the Kulik group at MIT on the computational front. Ms. Vennelakanti is currently simulating the UV traces for intermediate **2** from **Figure 20** where X = Cl, F, N_3, and OH anions, in both gas phase and in solution. While I have yet to determine which one out of the two new bands for each experiment corresponds to the perturbed MLCT transition, both sets of data fit well to the binding model. This suggests anion binding to Fe(II) in MBP-SadH is highly likely.

Conclusion

In conclusion, the binding of exogenous anions to Fe(II) in MBP-SadH, the "halogenase" D157G mutant of the Fe(II) αKG-dependent hydroxylase SadA, was investigated. Anion activity assay, steady-state kinetics, and UV-vis titration assay of MBP-SadH in the presence of different anions provided several lines of evidence of anion binding to Fe(II) in the enzyme. This study contributes to a growing body of literature for the interconversion of hydroxylases and halogenases of the Fe(II) α-KG-dependent enzyme family. This work also lays the groundwork for several interesting future directions both experimentally and computationally, such as attempting fluorination of *N*-succinylated amino acids by MBP-SadH mutants from rational design informed by computational calculations, and exploring the causes of the change in site selectivity from OH-1 to OH-2 in NsL to inform future engineering efforts.

Experimentals

1. Materials

Unless otherwise noted, all reagents were obtained from commercial suppliers and used without further purification. SadA D157G gene was obtained as a synthetic gene from Integrated DNA Technologies. The SadA D157G gene was obtained as a synthetic gene from Integrated DNA Technologies. The Q5 HF DNA polymerase, Q5 reaction buffer, dNTPs mixture, Dpn I enzyme, and Gibson Assembly Master Mix were purchased from New England Biolabs. The oligonucleotides were obtained from Integrated DNA Technologies. The PrimeSTAR Max DNA Polymerase was purchased from Takara Bio USA. Ni-nitrilotriacetic acid (Ni-NTA) resin and Pierce® BCA Protein Assay Kits were purchased from Fisher Scientific International, Inc., and the manufacturer's instructions were followed when using both products. DOWEXTM 50WX8 strong cation exchange resin was purchased from Sigma-Aldrich. Desuccinylase LasA was expressed and purified by Christian Gomez, following published protocols.[74]

Complete analytical data have been reported in the literature for C3-chlorinated NsL and C3-hydroxylated NsL (OH-1).[73]

2. General Procedures

Measurement of protein concentration was performed either using a Tecan Infinite 200 PRO plate reader on a Tecan NanoQuant plate or with Bradford assay. Anion exchange chromatography MBP-SadH (without His tags) was performed on an ÄKTA protein

purification system (GE healthcare) with three connected HiTrap Q FF 5 mL columns (GE Life Sciences) and a Superloop Complete (150 ml, M6 fitting, GE Life Sciences) for sample injection. Size exclusion chromatography of MBP-SadH (without His tags) was performed on an ÄKTA protein purification system (GE healthcare) with a HiLoad 16/600 Superdex 200 column (GE Life Sciences). Resulting fractions from anion exchange chromatography and size exclusion chromatography were collected with an AKTA Frac-900 Fraction Collector. Preparative-scale bioconversions were purified on reverse phase using either (i) an Agilent 1100 HPLC equipped with a Supelco Discovery C18 semi-preparative column (25 cm × 10 mm, 5 µm particle size) or (ii) a Biotage Isolera One with a Biotage® Sfär C18 D - Duo 100 Å 30 μm 120 g or 60 g column (product numbers FSUD-0401-0120 and FSUD-0401-0060). NMR spectra (^{1}H, ^{13}C, and ^{31}P) were obtained using a Varian 500 MHz Inova NMR spectrometer, or a Varian 400 MHz Inova NMR Spectrometer at room temperature. Chemical shifts are reported in ppm and coupling constants are reported in Hz. LC-ESI-MS analysis was performed using an Agilent 1290 system equipped with an Agilent Eclipse Plus C18 column. Absorbance spectra were recorded on a Varian Cary 5000 UV-Vis-NIR spectrophotometer.

3. Preparation of (MBP-)SadA and mutants MBP-SadH(-3)

3.1 Cloning of (MBP-)SadA and mutants MBP-SadH(-3)

Procedures in this sub-section were performed by Christian Gomez.

3.1a Cloning of MBP-SadH fusion plasmid

The MBP tag was amplified from the pLIC-MBP/RebF plasmid[83] and the linearized vector was amplified from a pET-28a-SadH plasmid using the following oligonucleotides:

#	Name	Sequence
1	NTermMBPInsertFP	5' – GCG GCA GCC ATA TGG CTA GCA TGC ACC ATC ACC ATC ACC ATG G – 3'
2	NTermMBPInsertRP	5' – TAG GTA TGC TGC ATG GAT CCG GCT GCT CCC TGG AAA TAC AGG – 3'
3	NTermMBPVectorFP	5' – GTA TTT CCA GGG AGC AGC CGG ATC CAT GCA GCA TAC CTA TCC GG – 3'
4	NTermMBPVectorRP	5' – CCA TGG TGA TGG TGA TGG TGC ATG CTA GCC ATA TGG CTG CCG C – 3'

Table 7. Oligonucleotides used for amplication of pET-28a-SadH plasmid.

The amplification conditions were the following: 1 ng/μL template DNA, 1x Q5 reaction buffer, 0.8 mM dNTPs each, 1 μM forward primer, 1 μM reverse primer, and 0.02 U/μL Q5 HF DNA polymerase. The final PCR reaction volumes were 50 μL each and were performed using an Applied Biosystems ProFlex PCR System. The PCR program for the amplification of the MBP insert was the following: 98 °C for 2 minutes; 30 cycles of 98 °C for 30 seconds and 72 °C for 90 seconds; and ending with 72 °C for 10 minutes. The PCR program for the amplification of the vector was the following: 98 °C for 2 minutes; 30 cycles of 98 °C for 30 seconds and 72 °C for 4 minutes; and ending with 72 °C for 10

minutes. All PCR products were digested with 10 units of DpnI at 37 °C for 2 hours and purified after being run on a 1% agarose gel using Qiagen gel extraction kit.

The resulting MBP insert and pET-28a-SadH vector were joined using Gibson Assembly, incubating at 50 °C for 1 hour and using a vector: insert ratio of 1:10. The isolated plasmids were transformed by electroporation into electrocompetent *E. coli* BL-21 (DE3) using a Bio-Rad MicroPulser and plated onto LB/agar plates containing 50 μg/mL kanamycin. A glycerol stock was made from a 5 mL overnight culture in LB with 50 μg/mL kanamycin by combining 500 μL of the culture with 500 μL of 50% v/v water/glycerol. This glycerol stock was stored at -80 °C.

3.1b Cloning of SadA

The wild type enzyme SadA was obtained by reverting the D157G mutation in SadA D157G via SOE PCR. A pET-28a-SadA D157G plasmid was used to generate the desired insert and the linearized vector with the following oligonucleotides:

#	Name	Sequence
5	SadAGenFP	5' – AGC AAA TGG GTC GCG GAT CCA TGC AGC ATA CCT ATC CGG C – 3'
6	SadAG157DMutRP	5' – GTA TCA CGA CCA TAG CTA ACA TCA TCA CAA TGC GGT GCA AAG TTA AAC GGT G – 3'
7	SadAG157DMutFP	5' – GTT AGC TAT GGT CGT GAT ACC GTT AAT TGG CCT CTG AAA CGT AGC TTT CC – 3'
8	SadAGenRP	5' – TCG AGT GCG GCC GCA AGC TTT CAA TCA AAC ATA CGC CAA CC – 3'
9	SadAVectorFP	5' – GTT GGC GTA TGT TTG ATT GAA AGC TTG CGG CCG CAC TCG A – 3'
10	SadAVectorRP	5' – GCC GGA TAG GTA TGC TGC ATG GAT CCG CGA CCC ATT TGC T – 3'

Table 8. Oligonucleotides used for amplication of pET-28a-SadA D157G plasmid.

The SadA insert was obtained by a first step including two fragmentation reactions using the same template but different oligonucleotide pairs (i.e., fragment 1 with primers **5** and **6**, and fragment 2 with primers **7** and **8**). The vector was linearized using primers **9** and **10.** The amplification conditions were the following: 1 ng/μL template DNA, 1x Q5 reaction buffer, 0.8 mM dNTPs each, 1 μM forward primer, 1 μM reverse primer, and 0.02 U/μL Q5 HF DNA polymerase. The final PCR reaction volumes were 50 μL each and were performed using an Applied Biosystems ProFlex PCR System. The PCR program for the fragmentations was the following: 98 °C for 2 minutes; 24 cycles of 98 °C for 30 seconds, 56 °C for 30 seconds, and 72 °C for 45 seconds; and ending with 72 °C for 10 minutes. The PCR program for the amplification of the vector was the following: 98 °C for 2 minutes; 24 cycles of 98 °C for 30 seconds, 65 °C for 30 seconds, and 72 °C for 3.5 minutes; and ending with 72 °C for 10 minutes. All PCR products were digested with 10

units of DpnI at 37 °C for 2 hours and purified after being run on a 1% agarose gel using Qiagen gel extraction kit.

The SadA fragments were assembled via PCR using oligonucleotides **9** and **10**. The assembly PCR conditions were as follows: 2 ng/μL of each fragment, 1x Q5 reaction buffer, 0.8 mM dNTPs each, 1 μM forward primer, 1 μM reverse primer, and 0.02 U/μL Q5 HF DNA polymerase. The final PCR reaction volumes were 50 μL each. The amplification program consisted of the following: 98 °C for 2 minutes; 24 cycles of 98 °C for 30 seconds, 56 °C for 30 seconds, and 72 °C for 45 seconds; and ending with 72 °C for 10 minutes. The PCR product was digested with 10 units of DpnI at 37 °C for 2 hours and purified after being run on a 1% agarose gel using Qiagen gel extraction kit.

The resulting SadA insert and pET-28a linearized vector were joined using Gibson Assembly, incubating at 50 °C for 1 hour and using a vector: insert ratio of 1:10. The resulting product was purified and concentrated using a Zymo PCR clean and concentrator kit. The isolated SadA-pET-28a plasmid was transformed by electroporation into electrocompetent *E. coli* BL-21 (DE3) using a Bio-Rad MicroPulser and plated onto LB/agar plates containing 50 μg/mL kanamycin. A glycerol stock was made from a 5 mL overnight culture in LB with 50 μg/mL kanamycin by combining 500 μL of the culture with 500 μL of 50% v/v water/glycerol. This glycerol stock was stored at -80 °C.

3.1c MBP-SadH-3

MBP-SadH-3 is a variant of MBP-SadH obtained after three rounds of directed evolution using EP-PCR as the mutagenic step in each round. After screening, a 5 mL

overnight culture was made by inoculating LB with 50 μg/mL kanamycin with the original glycerol stock from the library plate. The MBP-SadH-3-pET-28a plasmid was extracted using a Qiagen QIAprep spin miniprep kit, sequenced, and re-transformed by electroporation into electrocompetent *E. coli* BL-21 (DE3) using a Bio-Rad MicroPulser and plated onto LB/agar plates containing 50 μg/mL kanamycin. A glycerol stock was made from a 5 mL overnight culture in LB with 50 μg/mL kanamycin by combining 500 μL of the culture with 500 μL of 50% v/v water/glycerol. This glycerol stock was stored at -80 °C.

3.1d Cloning of MBP-SadA and MBP-SadH-3D

The MBP-SadA fusion was obtained by site-directed mutagenesis of the MBP-SadH fusion previously described. MBP-SadH-3D was obtained in an analogous fashion. MBP-SadH-pET-28a and MBP-SadH-3-pET-28a plasmids were used as template for amplification using the following oligonucleotides:

#	Name	Sequence
11	MBPSadHG157DFP	5' – GTT AGC TAT GGT CGT GAT ACC GTT AAT TGG CCT CTG AAA CGT AGC TTT CC – 3'
12	MBPSadHG157DRP	5' – GTA TCA CGA CCA TAG CTA ACA TCA TCA CAA TGC GGT GCA AAG TTA AAC GGT G – 3'
13	MBPSadH3G157DFP	5' – GTT AGC TAT GGT CGT GAT ACC GTT AAT TGG CCT CTG AAA CGT AGC TTT CC – 3'
14	MBPSadH3G157DRP	5' – GTA TCA CGA CCA TAG CTA ACA TCA TCA CAA TGC GGT GCT AAG TTA AAC GGT G – 3'

Table 9. Oligonucleotides used for amplication of MBP-SadH-3-pET-28a plasmid.

The MBP-SadA fusion was obtained using primers **11** and **12**, and the MBP-SadH-3D fusion was obtained using primers **13** and **14**. The amplification conditions were the following: 2 ng/μL template DNA, 0.3 μM forward primer, 0.3 μM reverse primer, and 1x PrimeSTAR Max DNA Polymerase. The final PCR reaction volumes were 50 μL each and they were performed using an Applied Biosystems ProFlex PCR System. The PCR program for the amplifications was the following: 98 °C for 10 seconds; 30 cycles of 98 °C for 10 seconds, 55 °C for 5 seconds, and 72 °C for 45 seconds; and ending with 72 °C for 1 minute. The PCR products were digested with 10 units of DpnI at 37 °C for 1 hour and purified after being run on a 1% agarose gel using a Qiagen gel extraction kit.

The resulting MBP-SadA-pET-28a and MBP-SadH-3D-pET-28a products were transformed by electroporation into electrocompetent *E. coli* BL-21 (DE3) using a Bio-Rad MicroPulser and plated onto LB/agar plates containing 50 μg/mL kanamycin. Glycerol stocks were made from 5 mL overnight cultures in LB with 50 μg/mL kanamycin by combining 500 μL of the cultures with 500 μL of 50% v/v water/glycerol. These glycerol stocks were stored at -80 °C.

3.1e Cloning of non-His-tagged MBP-SadH

The MBP-SadH fusion lacking any histidine tags was constructed using site-targeted mutagenesis and the MBP-SadH-pET-28a plasmid as a template. The following oligonucleotides were used:

#	Name	Sequence
15	NoHisMBPSadHFP	5' – GAT ATA CCA TGA AAA TCG AAG AAG GTA AAC TGG TAA TCT GGA TTA ACG – 3'
16	NoHisMBPSadHRP	5' – CTT CGA TTT TCA TGG TAT ATC TCC TTC TTA AAG TTA AAC AAA ATT ATT TC – 3'

Table 10. Oligonucleotides used for amplication of MBP-SadH-pET-28a plasmid for the construction of non-His-tagged MBP-SadH.

The amplification conditions were the following: 2 ng/μL template DNA, 0.3 μM forward primer, 0.3 μM reverse primer, and 1x PrimeSTAR Max DNA Polymerase. The final PCR reaction volume was 50 μL and it was performed using an Applied Biosystems ProFlex PCR System. The PCR program for the amplification was the following: 98 °C for 10 seconds; 30 cycles of 98 °C for 10 seconds, 55 °C for 5 seconds, and 72 °C for 45 seconds; and ending with 72 °C for 1 minute. The PCR product was digested with 10 units of DpnI at 37 °C for 1 hour and purified after being run on a 1% agarose gel using a Qiagen gel extraction kit.

The resulting no-His-tag MBP-SadH-pET-28a product was transformed by electroporation into electrocompetent E. coli BL-21 (DE3) using a Bio-Rad MicroPulser and plated onto LB/agar plates containing 50 μg/mL kanamycin. A glycerol stock was made from a 5 mL overnight culture in LB with 50 μg/mL kanamycin by combining 500 μL of the culture with 500 μL of 50% v/v water/glycerol. This glycerol stock was stored at -80 °C.

3.2 Protein sequences

SadA

MQHTYPAQLMRFGTAARAEHMTIAAAIHALDADEADAIVMDIVPDGERDAWWDDEGFSSS
PFTKNAHHAGIVATSVTLGQLQREQGDKLVSKAAEYFGIACRVNDGLRTTRFVRLFSDALD
AKPLTIGHDYEVEFLLATRRVYEPFEAPFNFAPHCDDVSYGRDTVNWPLKRSFPRQLGGF
LTIQGADNDAGMVMWDNRPESRAALDEMHAEYRETGAIAALERAAKIMLKPQPGQLTLFQ
SKNLHAIERCTSTRRTMGLFLIHTEDGWRMFD*

MBP-SadA

MGSSHHHHHHSSGLVPRGSHMASMHHHHHHGKIEEGKLVIWINGDKGYNGLAEVGKKFE
KDTGIKVTVEHPDKLEEKFPQVAATGDGPDIIFWAHDRFGGYAQSGLLAEITPDKAFQDKL
YPFTWDAVRYNGKLIAYPIAVEALSLIYNKDLLPNPPKTWEEIPALDKELKAKGKSALMFNL
QEPYFTWPLIAADGGYAFKYENGKYDIKDVGVDNAGAKAGLTFLVDLIKNKHMNADTDYSI
AEAAFNKGETAMTINGPWAWSNIDTSKVNYGVTVLPTFKGQPSKPFVGVLSAGINAASPN
KELAKEFLENYLLTDEGLEAVNKDKPLGAVALKSYEEELAKDPRIAATMENAQKGEIMPNIP
QMSAFWYAVRTAVINAASGRQTVDEALKDAQTNSSSNNNNTSENLYFQGAAGSMQHTYP
AQLMRFGTAARAEHMTIAAAIHALDADEADAIVMDIVPDGERDAWWDDEGFSSSPFTKNA
HHAGIVATSVTLGQLQREQGDKLVSKAAEYFGIACRVNDGLRTTRFVRLFSDALDAKPLTIG
HDYEVEFLLATRRVYEPFEAPFNFAPHCDDVSYGRDTVNWPLKRSFPRQLGGFLTIQGAD
NDAGMVMWDNRPESRAALDEMHAEYRETGAIAALERAAKIMLKPQPGQLTLFQSKNLHAI
ERCTSTRRTMGLFLIHTEDGWRMFD*

MPB-SadH (with 2 His tags)

MGSSHHHHHHSSGLVPRGSHMASMHHHHHHGKIEEGKLVIWINGDKGYNGLAEVGKKFE
KDTGIKVTVEHPDKLEEKFPQVAATGDGPDIIFWAHDRFGGYAQSGLLAEITPDKAFQDKL
YPFTWDAVRYNGKLIAYPIAVEALSLIYNKDLLPNPPKTWEEIPALDKELKAKGKSALMFNL
QEPYFTWPLIAADGGYAFKYENGKYDIKDVGVDNAGAKAGLTFLVDLIKNKHMNADTDYSI
AEAAFNKGETAMTINGPWAWSNIDTSKVNYGVTVLPTFKGQPSKPFVGVLSAGINAASPN
KELAKEFLENYLLTDEGLEAVNKDKPLGAVALKSYEEELAKDPRIAATMENAQKGEIMPNIP
QMSAFWYAVRTAVINAASGRQTVDEALKDAQTNSSSNNNNTSENLYFQGAAGSMQHTYP
AQLMRFGTAARAEHMTIAAAIHALDADEADAIVMDIVPDGERDAWWDDEGFSSSPFTKNA
HHAGIVATSVTLGQLQREQGDKLVSKAAEYFGIACRVNDGLRTTRFVRLFSDALDAKPLTIG
HDYEVEFLLATRRVYEPFEAPFNFAPHCGDVSYGRDTVNWPLKRSFPRQLGGFLTIQGAD
NDAGMVMWDNRPESRAALDEMHAEYRETGAIAALERAAKIMLKPQPGQLTLFQSKNLHAI
ERCTSTRRTMGLFLIHTEDGWRMFD*

MBP-SadH (No His tags)

MKIEEGKLVIWINGDKGYNGLAEVGKKFEKDTGIKVTVEHPDKLEEKFPQVAATGDGPDIIF
WAHDRFGGYAQSGLLAEITPDKAFQDKLYPFTWDAVRYNGKLIAYPIAVEALSLIYNKDLLP
NPPKTWEEIPALDKELKAKGKSALMFNLQEPYFTWPLIAADGGYAFKYENGKYDIKDVGVD
NAGAKAGLTFLVDLIKNKHMNADTDYSIAEAAFNKGETAMTINGPWAWSNIDTSKVNYGVT
VLPTFKGQPSKPFVGVLSAGINAASPNKELAKEFLENYLLTDEGLEAVNKDKPLGAVALKSY
EEELAKDPRIAATMENAQKGEIMPNIPQMSAFWYAVRTAVINAASGRQTVDEALKDAQTNS
SSNNNNTSENLYFQGAAGSMQHTYPAQLMRFGTAARAEHMTIAAAIHALDADEADAIVMDI
VPDGERDAWWDDEGFSSSPFTKNAHHAGIVATSVTLGQLQREQGDKLVSKAAEYFGIAC
RVNDGLRTTRFVRLFSDALDAKPLTIGHDYEVEFLLATRRVYEPFEAPFNFAPHCGDVSYG

RDTVNWPLKRSFPRQLGGFLTIQGADNDAGMVMWDNRPESRAALDEMHAEYRETGAIAA
LERAAKIMLKPQPGQLTLFQSKNLHAIERCTSTRRTMGLFLIHTEDGWRMFD*

MBP-SadH-3
MGSSHHHHHHSSGLVPRGSHMASMHHHHHHGKIEEGKLVIWINGDKGYNGLAEVGKKFE
KDTGIKVTVEHPDKLEEKFPQVAATGDGPDIIFWAHDRFGGYAQSGLLAEITPDKAFQDKL
YPFTWDAVRYNGKLIAYPIAVEALSLIYNKDLLPNPPKTWEEIPALDKELKAKGKSALMFNL
QEPYFTWPLIAADGGYAFKYENGKYDIKDVGVDNAGAKAGLTFLVDLIKNKHMNADTDYSI
AEAAFNKGETAMTINGPWAWSNIDTSKVNYGVTVLPTFKGQPSKPFVGVLSAGINAASPN
KELAKEFLENYLLTDEGLEAVNKDKPLGAVALKSYEEELAKDPRIAATMENAQKGEIMPNIP
QMSAFWYAVRTAVINAASGRQTVDEALKDAQTNSSSNNNNTSENLYFQGAAGSMQHTYP
AQLMRFGTAARAEHMTIAAAIHALDADEADAIIMDIVPDGERDAWWDDEGFSSSPFTKNAH
HAGIVATSVTLGQLQREQGDKLVSKAAEYFGIACRVNDGLRTTRFVRLFSDALDAKPLTIGH
DYEVEFLLATRRVYEPFEAPFNLAPHCGDVSYGRDTVNWPLKRSFPRQLGGFLTIQGADN
DAGMVMWDNRPESRAALDEMHAEYRETGAIAALERAAKIMLKPQPGQLTLFQSKNLHAIE
RCTSTRRTMGLFLIHTEDGWRMFD*

MBP-SadH-3D
MGSSHHHHHHSSGLVPRGSHMASMHHHHHHGKIEEGKLVIWINGDKGYNGLAEVGKKFE
KDTGIKVTVEHPDKLEEKFPQVAATGDGPDIIFWAHDRFGGYAQSGLLAEITPDKAFQDKL
YPFTWDAVRYNGKLIAYPIAVEALSLIYNKDLLPNPPKTWEEIPALDKELKAKGKSALMFNL
QEPYFTWPLIAADGGYAFKYENGKYDIKDVGVDNAGAKAGLTFLVDLIKNKHMNADTDYSI
AEAAFNKGETAMTINGPWAWSNIDTSKVNYGVTVLPTFKGQPSKPFVGVLSAGINAASPN
KELAKEFLENYLLTDEGLEAVNKDKPLGAVALKSYEEELAKDPRIAATMENAQKGEIMPNIP
QMSAFWYAVRTAVINAASGRQTVDEALKDAQTNSSSNNNNTSENLYFQGAAGSMQHTYP
AQLMRFGTAARAEHMTIAAAIHALDADEADAIIMDIVPDGERDAWWDDEGFSSSPFTKNAH
HAGIVATSVTLGQLQREQGDKLVSKAAEYFGIACRVNDGLRTTRFVRLFSDALDAKPLTIGH
DYEVEFLLATRRVYEPFEAPFNLAPHCDDVSYGRDTVNWPLKRSFPRQLGGFLTIQGADN
DAGMVMWDNRPESRAALDEMHAEYRETGAIAALERAAKIMLKPQPGQLTLFQSKNLHAIE
RCTSTRRTMGLFLIHTEDGWRMFD*

3.3 General procedures for protein expression

An overnight culture was prepared by inoculating kanamycin-containing TB (7.5 mL) and shaking the culture at 250 rpm, 37 °C overnight. On the following day, the overnight culture was used to inoculate 750 mL of fresh kanamycin-containing LB media in a 3 L Erlenmeyer flask. The culture was incubated at 37 °C, 250 rpm until OD_{600} of the culture reached 0.6 – 0.8 (at ~t = 4 h), after which the culture was cooled to 18 °C without shaking. Protein expression was then induced by 1mM IPTG. The induced culture was allowed to

grow for 16 hours at 37 °C, 250 rpm. The cells were harvested afterwards by centrifugation at 4 °C, 4000 rpm for 20 minutes.

3.4 General procedures of purification of his-tagged proteins

Cell pellets were re-suspended in Ni-NTA binding buffer (100 mM HEPES, 20 mM imidazole, pH 7.5, 30 mL) and sonicated (40 amplitude, 30 second burst, 10 minute total process). Lysed culture was then clarified at 15000 rpm, 4 °C for 60 minutes. The supernatant tumbled with Ni-NTA resin (7 mL) pre-equilibrated with an equilibration buffer (20 mM sodium phosphate pH 7.4, containing 10 mM imidazole, and 50 mM NaCl) at 4 °C for 1 h. After the initial elution of sample, the resin was washed with 5CV of a wash buffer (20 mM sodium phosphate pH 7.4, containing 20 mM imidazole, and 50 mM NaCl). The desired enzyme was eluted with 5 CV of elution buffer (20 mM sodium phosphate pH 7.4, containing 500 mM imidazole, and 50 mM NaCl), with each CV of eluent collected as a separate fraction. Fraction purity was confirmed by SDS-PAGE (12% acrylamide). Pure fractions were combined, and buffer exchanged into 100 mM HEPES, 5 mM EDTA, pH 7.5 to remove any residual Fe ions. The purified protein was then buffer exchanged into 100 mM HEPES, pH 7.5 three times, concentrated to ~ 1 mM, and stored as a frozen stock at -80 °C.

3.5 Purification of MBP-SadH without His-tags

3.5a Anion exchange chromatography

Cell pellets were re-suspended in an anion exchange start buffer (50 mM Tris, pH 7.6, 30 mL) and sonicated (40 amplitude, 30 second burst, 10 minute total process). Lysed culture was then clarified at 15000 rpm, 4 °C for 60 minutes. The supernatant was filtered through a 250 mL 0.2 µm sterile filter. The resulting 32 mL of filtrate was injected into a superloop connected to the AKTA FPLC. The sample was purified by anion exchange chromatography in two to three batches. For each batch, a maximum of 12 mL of sample from the superloop was injected at 0.5 mL/min onto three connected HiTrap Q FF 5 mL columns that were pre-equilibrated with at least 2 CV of anion exchange start buffer. The low injection flow rate was required to ensure good binding of proteins to the resin. The sample was purified at 5 mL/min using a gradient of anion exchange start buffer and anion exchange elution buffer (50 mM Tris, 1 M NaCl, pH 7.6). The gradient is as follows: 5 CV of start buffer, 9 CV gradient from 0% to 45 % of elution buffer, 7.5 CV of 100% elution buffer. The eluent was tracked at 280 nm by UV and collected in fractions with a maximum volume of 22 mL each. MBP-SadH was eluted as one broad peak during the 0 to 45% gradient. Fraction purity was confirmed by SDS-PAGE. Fractions containing MBP-SadH were consolidated and concentrated to ~50 mg/mL in spin filters by centrifugation for the subsequent size-exclusion chromatography. Protein concentration was measured by Bradford assay. It is crucial to concentrate the sample to the desired concentration with minimal rounds of centrifugation to minimize aggregate formation.

3.5b Size-exclusion chromatography

Post-anion exchange MBP-SadH at ~50 mg/mL was filtered through a 0.2 µm syringe filter or 0.2 µm 50 mL falcon tube filter. A maximum of 30 mg of protein was injected into the 125 mL size-exclusion chromatography (SEC) column through a 1 mL injection loop. The sample was purified by 1.2 CV of SEC buffer (100 mM HEPES, 150 mM NaCl, pH 7.5) at 1 mL/min and 2 mL fractions were collected. MBP-SadH was eluted between 62 to 70 mL. Fraction purity was confirmed by SDS-PAGE. Pure fractions were consolidated, concentrated, and buffer exchanged into a buffer containing 100 mM HEPES and 5 mM EDTA at pH 7.5 to remove any residual Fe ions. The concentrated, purified protein was then dialyzed into 100 mM HEPES at pH 7.5 and 4 ^{o}C three times with 4 L of buffer each time. The dialysis buffer in the third time was prepared using LCMS-grade water to ensure minimal amount of NaCl remained in the protein. After dialysis, the protein was concentrated to ~70 mg/mL and stored as a frozen stock at -80 ^{o}C. Protein concentration was measured by Bradford assay.

4. Synthesis of substrate *N*-suc-Leu (NsL)

A 250 mL round bottom flask was charged with a stir bar and L-Leucine (10 g, 60.5 mmol, 1 eq). Water (50 mL) and NaOH (5 M, 12 mL) was added to leucine and the resulting suspension was stirred. Succinic anhydride (6.3 g, 63 mmol, 1.03 eq) was added as solids to the suspension. NaOH (5 M, 20 mL) was added to the suspension again. The reaction was heated to 47 ^{o}C for 2 hours, after which the reaction was cooled to room temperature. The reaction was then acidified to pH 1 with 6 M HCl, diluted with water (300 mL), and

extracted with ethyl acetate (400 mL x 2). The combined organic layers were washed with brine (300 mL x 1), dried over $MgSO_4$, and filtered. The filtrate was concentrated to wet white solids under reduced pressure. Slow evaporation of residual solvent at room temperature afforded white crystalline solids over a few days. The product was washed with hexanes and dried *in vacuo* with some heating with a heat gun. The resulting sticky solids were lyophilized to afford dry white solids. Yield: 7.4 g, 53%. ^{1}H NMR spectrum of product matched the spectrum reported in literature.[73]

5. Authentic products isolation and characterization

5.1 Isolation of OH-1 via MBP-SadA NsL hydroxylation

A 500 mL Erlenmeyer flask was charged with NsL (80 mM, 10 mL, 0.8 mmol), MBP-SadA (0.1 mol%, 1.66 mM, 482 µL, 0.8 µmol), $Fe(NH_4)_2(SO_4)_2$ (80 mM, 0.1 mL, 8 µmol), ascorbic acid (128 mM, 10 mL, 1.28 mmol), and α-KG (320 mM, 10 mL, 3.2 mmol) in 100 mM HEPES, pH 7.5. More buffer was added to make up to a 80 mL reaction volume. All stocks were made in 100 mM HEPES, and pH adjusted to pH 7.5 with 10 M NaOH prior to addition, with the exception of the stock of $Fe(NH_4)_2(SO_4)_2$ prepared in water. The flask was sealed with a breathable film and shaken at 60 rpm overnight at 30 ^{o}C. Complete consumption of NsL on the next day was confirmed by LCMS of the reaction mixture. The reaction was then lyophilized and then resuspended in MeOH (80 mL). The suspension was clarified by centrifugation at 4000 rpm for 5 minutes. The supernatant mixed with celite (27 g) and MeOH was removed under reduced pressure. One-third of the celite mixture (9 g) was loaded onto a 120 g reverse phase biotage column and OH-1 product

purified on the biotage with the following gradient: 4 CV of 100% A, 5 CV of 10% B, 5 CV from 10 to 100% B, 3 CV of 100% B, where solvent A is LCMS-grade water with 0.1% formic acid and solvent B is LCMS-grade ACN with 0.1% formic acid. Two other rounds of reverse phase purification were performed on the remaining celite mixture using the same method. Fraction purity was checked using the LCMS method NHC07095 with no solvent delay and scan MS mode. Fractions containing buffer and OH-1 were consolidated, dried, embedded with celite, and purified on the biotage with the same method again. Pure fractions from all rounds of biotage purification were combined, concentrated under reduced pressure, and lyophilized. ^{1}H NMR spectrum of the resulting OH-1 product matched the spectrum reported in literature.[73] Yield: 147.7 mg, 75%.

5.2 Isolation of N3 via MBP-SadH-3 reaction with NsL

A 1 L Erlenmeyer flask was charged with NsL (50 mM, 30 mL, 1.5 mmol), MBP-SadH-3 (0.1 mol%, 0.75 mM, 2.0 mL, 1.5 µmol), $Fe(NH_4)_2(SO_4)_2$ (100 mM, 0.15 mL, 15 µmol), ascorbic acid (80 mM, 30 mL, 2.4 mmol), and α-KG (200 mM, 30 mL, 6 mmol) in 100 mM HEPES, pH 7.5. More buffer was added to make up to a 150 mL reaction volume. All stocks were made in 100 mM HEPES, and pH adjusted to pH 7.5 with 10 M NaOH prior to addition, with the exception of the stock of $Fe(NH_4)_2(SO_4)_2$ prepared in water. The flask was sealed with a breathable film and shaken at 60 rpm overnight at 30 ^{o}C. Complete consumption of NsL on the next day was confirmed by LCMS of the reaction mixture. The reaction was then lyophilized and then resuspended in MeOH (150 mL). The suspension was clarified by centrifugation at 4000 rpm for 5 minutes. The supernatant mixed with

celite (54 g) and MeOH was removed under reduced pressure. A quarter of the celite mixture (13.5 g) was loaded onto a 60 g reverse phase biotage column and N3 product purified on the biotage with the following gradient: 4 CV of 100% A, 4 CV of 10% B, 4 CV from 10 to 60% B, 2 CV of 100% B, where solvent A is D.I. water with 0.1% formic acid and solvent B is LCMS-grade ACN with 0.1% formic acid. Two other rounds of reverse phase purification were performed on the remaining celite mixture using the same method. Fraction purity was checked using the LCMS method NHC07095 with no solvent delay and scan MS mode. Fractions containing buffer and OH-1 were consolidated, dried, embedded with celite, and purified on the biotage with the same method again. Pure fractions from all rounds of biotage purification were combined, concentrated under reduced pressure, and lyophilized. ^{1}H NMR spectrum of the resulting OH-1 product matched the spectrum reported in literature.[73] Yield: 147.7 mg, 75%.

^{1}H NMR (500 MHz, CD_3OD) δ 4.56 (dt, *J* = 9.2, 3.0 Hz, 1H), 2.69 – 2.46 (m, 4H), 2.10 (dd, *J* = 14.7, 3.4 Hz, 1H), 1.86 (dd, *J* = 14.6, 9.1 Hz, 1H), 1.34 (s, 3H), 1.32 (s, 3H).

^{13}C NMR (126 MHz, CD_3OD) δ C 176.10, C 175.30, C 174.23, C 61.57, CH 50.57, CH_2 43.37, CH_2 31.52, CH_2 30.03, CH_3 26.47, CH_3 26.24.

CH_n of ^{13}C NMR peaks were assigned based on multiplicity-edited ^{1}H-^{13}C HSQC.

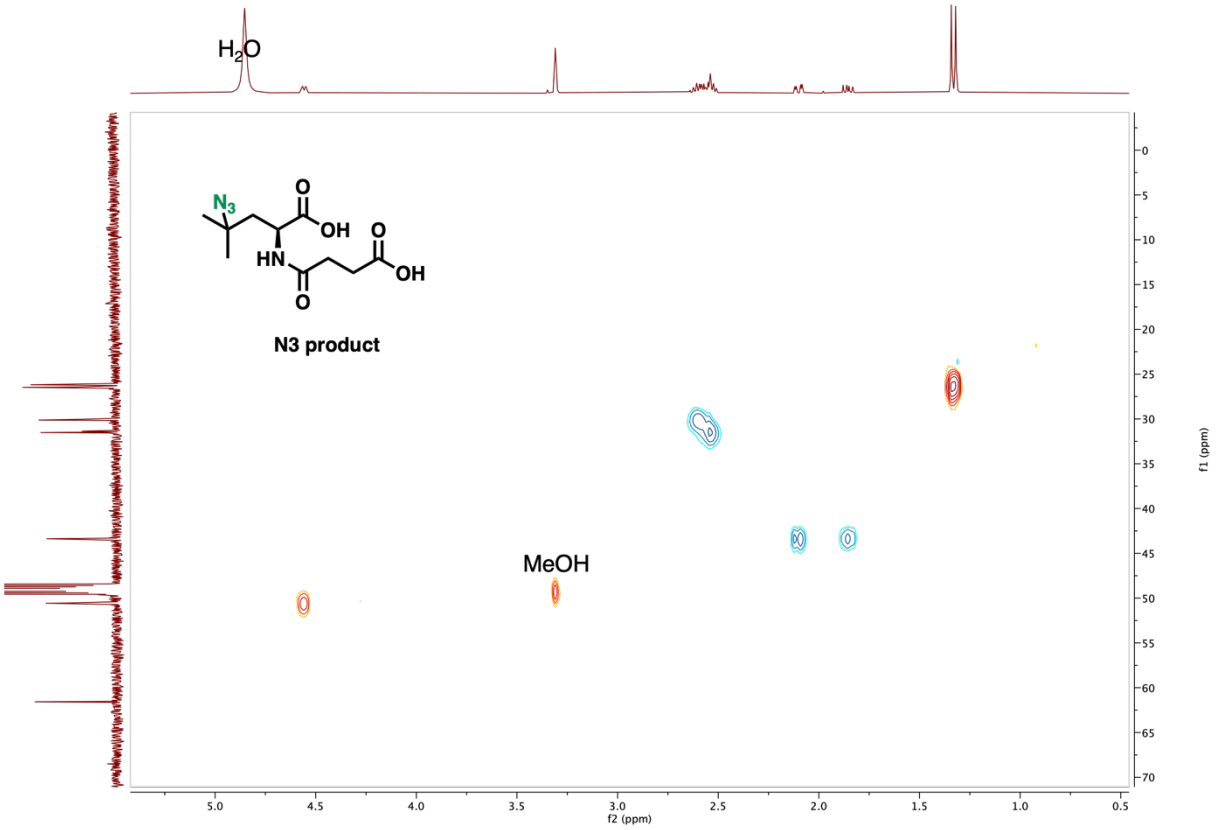

Figure 30. Multiplicity-edited 1H-13C HSQC of N3 product in CD_3OD.

5.3 Isolation of OH-2* via tandem MBP-SadH-3 and LasA reactions with NsL

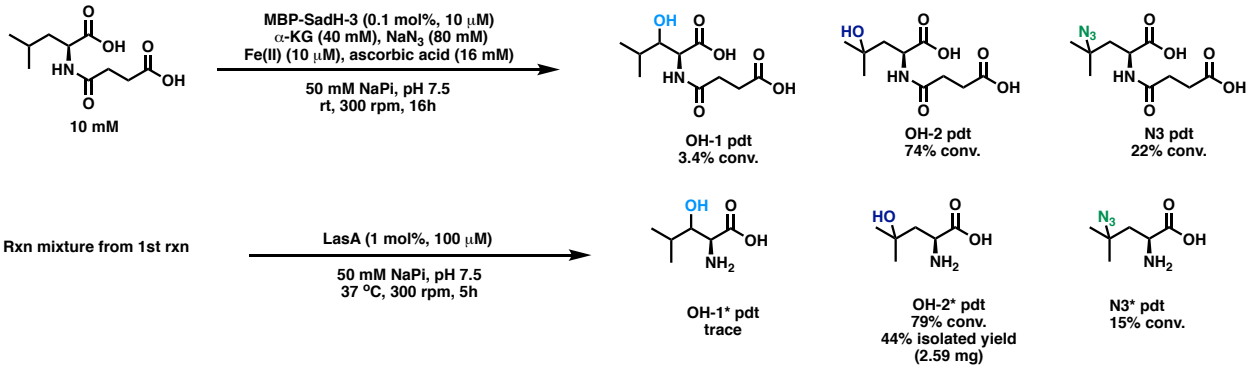

The following reaction is set up in quadruplicates. A 20 mL scintillation vial was charged with NsL (50 mM, 200 µL, 10 µmol), MBP-SadH-3 (0.1 mol%, 0.59 mM, 17 µL, 10 nmol),

$Fe(NH_4)_2(SO_4)_2$ (1 mM, 10 µL, 10 nmol), ascorbic acid (80 mM, 200 µL, 16 µmol), and α-KG (200 mM, 200 µL, 40 µmol) in 50 mM NaP_i, pH 7.5. More buffer was added to make up to a 1 mL reaction volume. All stocks were made in 50 mM NaP_i, and pH adjusted to pH 7.5 with 10 M NaOH prior to addition, with the exception of the stock of $Fe(NH_4)_2(SO_4)_2$ prepared in water and added last to avoid precipitation with phosphate ions. The vial was sealed with a breathable film and shaken at 300 rpm overnight at 23 °C. Complete consumption of NsL on the next day was confirmed by LCMS of the reaction mixture. The four reactions were transferred to four 2 mL eppendorf tubes. LasA (1.07 mM, 93.4 µL, 0.1 µmol) in 50 mM Tris/HCl at pH 7.5 was added to each reaction. Reactions were shaken at 300 rpm, 37 °C in a thermoshaker for five hours. Complete consumption of N3 and close to complete consumption of OH-2 products to their respective desuccinylated forms were observed on the LCMS. The four reactions were combined and purified on cation exchange resin following literature procedures.[58] The lyophilized post-cation exchange product (7.6 mg) was characterized by ^{1}H NMR and it contained mostly OH-2*, N3*, and amine-based buffers (Tris and HEPES) from the original protein stocks. This mixture was purified by semi-prep LC in four batches at 3 mL/min with the following method: 1% ACN in water from 0 to 7 minutes, 1 to 6% ACN from 7 to 20.7 minutes, 6 to 80% ACN from 20.7 to 25 minutes. UV of eluent was detected at 210 nm. Fractions were collected manually, and their purity confirmed by LCMS. OH-2* eluted at around 4 minutes. Pure OH-2* fractions were combined, concentrated under reduced pressure and lyophilized. Yield: 2.59 mg, 44%.

^{1}H NMR (500 MHz, D_2O) δ 3.96 (dd, *J* = 10.1, 3.3 Hz, 1H), 2.13 (dd, *J* = 15.3, 3.3 Hz, 1H), 1.95 (dd, *J* = 15.3, 10.2 Hz, 1H), 1.36 (s, 3H), 1.35 (s, 3H).

^{13}C NMR (126 MHz, D_2O) δ 174.95, 70.92, 52.46, 41.91, 29.74, 26.53.

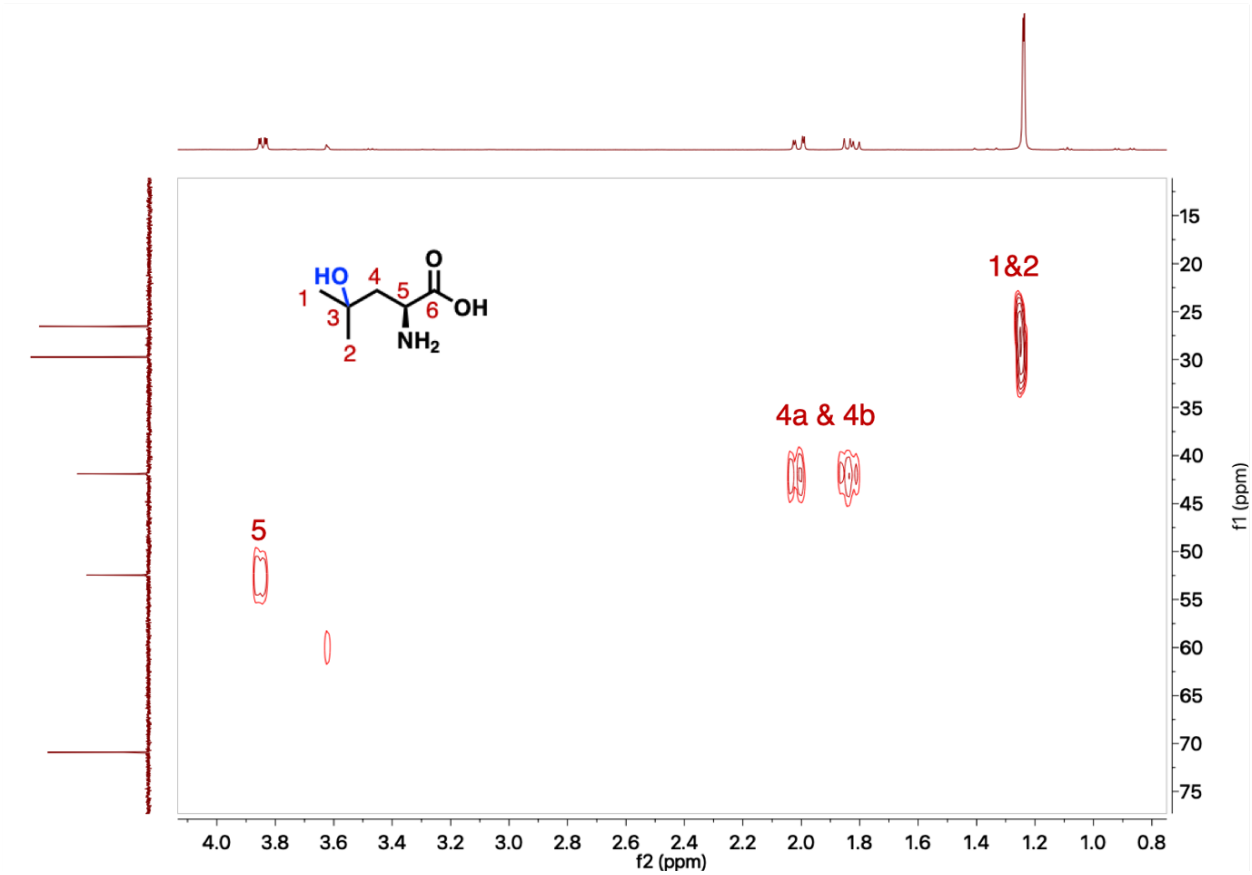

Figure 31. ^{1}H-^{13}C HSQC of OH-2* product in D_2O.

6. NsL reaction with MBP-SadH(-3) in the presence of exogenous anions

6.1 Reaction set up

To ensure accurate concentrations of exogenous anions were used, all stock solutions and buffer were prepared using LCMS-grade water. While most reagent stocks were made in buffer, stock solution of $Fe(NH_4)_2(SO_4)_2$ must be made using water and kept on ice as $Fe(NH_4)_2(SO_4)_2$ in HEPES buffer in the absence of reductant ascorbic acid quickly oxidizes in air.

Cocktail stocks containing the following were prepared: (i) NsL (3 mM), (ii) the enzyme (30 μM), (iii) $Fe(NH_4)_2(SO_4)_2$ (0.3 mM), and (iv) ascorbic acid (24 mM) in 100 mM HEPES, pH 7.5. To each well in a 96-well v-bottom plate were added an anion stock (150 mM, 30 μL, 4.5 μmol), a cocktail (30 μL), and α-KG (30 mM, 30 μL, 0.9 μmol) in 100 mM HEPES, pH 7.5. For the reactions carried out in the absence of anions, the reaction buffer (30 μL) was used in lieu of an anion stock. The final reaction volume was 90 μL with the following final concentrations: substrate (1 mM), exogenous anion (50 mM or 0 mM), the enzyme (10 μM), $Fe(NH_4)_2(SO_4)_2$ (0.1 mM), ascorbic acid (8 mM), and α-KG (10 mM). Another two 96-well v-bottom plates were set up in the same way for a triplicate set of reactions. Each plate was sealed with a breathable film and shaken at 750 rpm at room temperature overnight. The reactions were quenched the following day by the addition of methanol (90 μL). The precipitated protein was then removed by centrifugation. The supernatant (60 μL) was diluted with water (100 μL), filtered, and analyzed by the LCMS method NHC08056 with an injection volume of 0.5 μL. Products and substrate peak areas in the resulting extract ion chromatograms were integrated on the Agilent MassHunter

software. Product conversions were calculated using relative peak area ratios between product(s) and the substrate.

7. Steady-state kinetics with varying NsL concentrations

Kinetic parameters were determined for WT SadA and MBP-SadH in the presence or absence of exogenous anions at 22 °C with different concentrations of substrate NsL in triplicate. To ensure accurate concentrations of exogenous anions were used, all stock solutions and buffer were prepared using LCMS-grade water. While most reagent stocks were made in buffer, stock solution of $Fe(NH_4)_2(SO_4)_2$ must be made using water and kept on ice as $Fe(NH_4)_2(SO_4)_2$ in HEPES in the absence of reductant ascorbic acid quickly oxidizes in air. Due to relatively large fluctuations in instrument response factor on the LCMS between each experiment, freshly made calibration curve samples were analyzed on the instrument immediately before reaction samples were analyzed for each experiment.

With the exception of the NaN_3 reactions, stocks of substrate at 8 different concentrations were prepared by serial dilution of a master stock of NsL (4.5 mM) in 100 mM HEPES, pH 7.5 with a 1.5x dilution factor. The analogous 8 substrate stocks for NaN_3 reactions were prepared by serial dilution of a master stock of NsL (540 µM) in 100 mM HEPES, pH 7.5 with a 2x dilution factor. To a 96-well v-bottom plate were added the 8 substrate stocks, 5 wells each (30 µL per well). To each of these 40 wells was added a cocktail (30 µL per well) containing (i) exogenous anion (150 mM, 1.5 mM or 0 mM, see **Table 11**), (ii) the enzyme (0.3 µM or 1.5 µM, see **Table 11**), (iii) $Fe(NH_4)_2(SO_4)_2$ (0.3

mM), and (iv) ascorbic acid (24 mM) in 100 mM HEPES, pH 7.5. For wells intended for t=0 data points, extra 100 mM HEPES, pH 7.5 (30 µL per well) and methanol (90 µL per well) were added. Another two 96-well v-bottom plates were set up in the same way for a triplicate set of reactions. Each plate was activated with α-KG (30 µL per well, 30 µM) while being shaken at 750 rpm and sealed with breathable film afterwards. The final reaction volume was 90 µL with the following final concentrations: substrate (88-1500µM or 1.4-180 µM, see **Table 11**), exogenous anion (50 mM, 0.5 mM or 0 mM, see **Table 11**), the enzyme (0.1 µM or 0.5 µM, see **Table 11**), $Fe(NH_4)_2(SO_4)_2$ (0.1 mM), ascorbic acid (8 mM), and α-KG (10 mM). With the exception of the no-anion reactions, the reactions were quenched at 2-8 minutes by the addition of methanol (90 µL). The no-anion reactions were quenched at 3-12 minutes with methanol (90 µL).

Reaction	[Substrate] (uM)	[Salt] (mM)	[E] (uM)	*N*-Ac-Val
WT-SadA	88-1500	0	0.1	200 pmol
MBP-SadH, CsF	88-1500	50	0.5	200 pmol
MBP-SadH, NaN_3	1.41-180	0.5	0.1	200 pmol
MBP-SadH, NaCl	88-1500	50	0.5	200 pmol
MBP-SadH, no anions	88-1500	0	0.5	50 pmol

Table 11. Final concentration of substrate, salt, and enzyme used in each experiment and the amount of internal standard N-Ac-Val added afterwards.

A stock of internal standard *N*-Ac-Val (20 µL, 2.5 or 10 µM, 50 or 200 pmol, see **Table 11**) in water was added to each well to make up to a sample volume of 200 µL. The precipitated protein was then removed by centrifugation and the reactions were filtered. Calibration curve samples containing known pmol of the authentic products OH-1 and N3 (if using) and internal standard *N*-Ac-Val (20 µL, 2.5 or 10 µM, 50 or 200 pmol,

see **Table 11**) were first analyzed by LCMS (see **Table 12** for methods). Upon completion of analysis of calibration curve samples, reaction samples were analyzed by LCMS using the same method.

Reaction	LCMS method	Injection vol (μL)
WT-SadA	NHC07095	2
MBP-SadH, CsF	NHC07095	2
MBP-SadH, NaN_3	NHC08025	2
MBP-SadH, NaCl	NHC08012	2
MBP-SadH, no anions	NHC07095	20

Table 12. LCMS method and LCMS sample injection volume used for each experiment.

Product and internal standard peak areas in the resulting single-ion monitoring (SIM) chromatograms were integrated on the Agilent MassHunter software. Product formation was quantitated by calculating the ratio of product to internal standard and fitting that value to the calibration curve. Initial rates of product formation per unit of enzyme active site (v/E) were obtained from linear fits of product to total enzyme concentration ratios as a function of time using the software Prism 9. The kinetic parameters (K_M and k_{cat}) for each reaction were determined by fitting v/E as a function of substrate concentration to Michaelis-Menten model using the same software.

8. Steady-state kinetics with varying salt concentrations

Kinetic parameters were determined for MBP-SadH at 22 °C with substrate NsL with varying salt concentration in triplicate. To ensure accurate concentrations of exogenous anions were used, all stock solutions and buffer were prepared using LCMS-

grade water. While most reagent stocks were made in buffer, stock solution of $Fe(NH_4)_2(SO_4)_2$ must be made using water and kept on ice as $Fe(NH_4)_2(SO_4)_2$ in HEPES in the absence of reductant ascorbic acid quickly oxidizes in air. Due to relatively large fluctuations in instrument response factor on the LCMS between each experiment, freshly made calibration curve samples were analyzed on the instrument immediately before reaction samples were analyzed for each experiment.

With the exception of the NaN_3 reactions, stocks of salt at 8 different concentrations were prepared by serial dilution of a master stock of the salt (150 mM) in 100 mM HEPES, pH 7.5 with a 2x dilution factor. The analogous 8 substrate stocks for NaN_3 reactions were prepared by serial dilution of a master stock of NaN_3 (3 mM) in 100 mM HEPES, pH 7.5 with a 2x dilution factor. To a 96-well v-bottom plate were added the 8 salt stocks, 5 wells each (30 µL per well). To each of these 40 wells was added a cocktail (30 µL per well) containing (i) substrate NsL (3 mM), (ii) MBP-SadH (1.5 µM), (iii) $Fe(NH_4)_2(SO_4)_2$ (0.3 mM), and (iv) ascorbic acid (24 mM) in 100 mM HEPES, pH 7.5. For wells intended for t=0 data points, extra 100 mM HEPES, pH 7.5 (30 µL per well) and methanol (90 µL per well) were added. Another two 96-well v-bottom plates were set up in the same way for a triplicate set of reactions. Each plate was activated with α-KG (30 µL per well, 30 µM) while being shaken at 750 rpm and sealed with breathable film afterwards. The final reaction volume was 90 µL with the following final concentrations: substrate (1 mM), exogenous anion (0.39-50 mM, or 7.8-1000 µM, **Table 13**), MBP-SadH (0.5 µM), $Fe(NH_4)_2(SO_4)_2$ (0.1 mM), ascorbic acid (8 mM), and α-KG (10 mM). The reactions were quenched at 2-8 minutes by the addition of methanol (90 µL).

Reaction	[Salt]
MBP-SadH, CsF	0.39 – 50 mM
MBP-SadH, NaN_3	7.8 – 1000 µM
MBP-SadH, NaCl	0.39 – 50 mM
MBP-SadH, NH_4PF_6	0.39 – 50 mM

Table 13. Final salt concentration range for each experiment.

Reaction	LCMS method	Injection vol (µL)
MBP-SadH, CsF	NHC07095	2
MBP-SadH, NaN_3	NHC08025	2
MBP-SadH, NaCl	NHC08012	2
MBP-SadH, NH_4PF_6	NHC07095	2

Table 14. LCMS method and LCMS sample injection volume used for each experiment.

A stock of internal standard *N*-Ac-Val (20 µL, 10 µM, 200 pmol) in water was added to each well to make up to a sample volume of 200 µL. The precipitated protein was then removed by centrifugation and the reactions were filtered. Calibration curve samples containing known pmol of the authentic products OH-1 and N3 (if using) and internal standard *N*-Ac-Val (20 µL, 10 µM, 200 pmol) were first analyzed by LCMS (see **Table 14** for methods). Upon completion of analysis of calibration curve samples, reaction samples were analyzed by LCMS using the same method.

Product and internal standard peak areas in the resulting single-ion monitoring (SIM) chromatograms were integrated on the Agilent MassHunter software. Product formation was quantitated by calculating the ratio of product to internal standard and fitting

that value to the calibration curve. Initial rates of product formation per unit of enzyme active site (v/E) were obtained from linear fits of product to total enzyme concentration ratios as a function of time using the software Prism 9. The kinetic parameters (K_M and k_{cat}) for each reaction were determined by fitting v/E as a function of substrate concentration to Michaelis-Menten model using the same software.

9. LCMS methods

Four main LCMS methods were developed for this project. All four uses the same solvents (A: 0.1% formic acid in water, B: 0.1% formic acid in ACN), flow rates (0.4 mL/min), and mass spec ESI mode (negative). **Error! Reference source not found.** shows the m/z being tracked for the relevant species and their elution times in each LCMS method used. Following literature procedures, m/z value of 184 was tracked for chlorinated and brominated NsL products; m/z=184 corresponds to the dominant daughter ion that has lost the halide.[73]

Species	m/z of dominant ion	Elution time of species in each method (minutes)			
		NHC08056	NHC07095	NHC08012	NHC08025
N-Ac-Val (std)	158	-	2.6 – 2.7	2.6 – 2.7	2.6 – 2.7
NsL	230	4.3 – 4.6	-	-	-
OH-1	246	2.8 – 3.0	2.9 – 3.2	2.9 – 3.2	2.9 – 3.2
OH-2	246	0.9 – 1.4	-	-	-
N3	271	4.6 – 4.9	-	-	4.9 – 5.3
C3-chlorinated NsL	184	5.4 – 5.7	-	5.6 – 5.8	-
C3-brominated NsL	184	6.2 – 6.4	-	-	-

Table 15. Dominant m/z values tracked for each relevant species and their elution times in each LCMS method.

9.1 LCMS method NHC08056

Solvent gradient: 5% B (0-1.25 min), 5 to 15% B (1.25-3.3 min), 15% B (3.3-5 min), 15 to 95% B (5-8 min), 95% B (8-10 min), 95 to 5% B (10-12 min). Post time: 2 minutes.

ESI MS: Scan mode; turned on from 0.8 to 8 minutes only.

9.2 LCMS method NHC07095

Solvent gradient: 5% B (0-1.25 min), 5 to 15% B (1.25-4 min), 15 to 90% B (4-6 min), 90% B (6-10 min), 95 to 5% B (10-12 min). Post time: 2 minutes.

ESI MS: Single ion monitoring (SIM) mode. The detector is turned off except for: 2.3-4 minutes (m/z detected: 158, 246).

9.3 LCMS method NHC08012

Solvent gradient: 5% B (0-1.25 min), 5 to 15% B (1.25-4 min), 15 to 90% B (4-6 min), 90% B (6-10 min), 95 to 5% B (10-12 min). Post time: 2 minutes.

ESI MS: Single ion monitoring (SIM) mode. The detector is turned off except for: 2.3-3.3 minutes (m/z detected: 158, 246), and 5-6 minutes (m/z detected: 184).

9.4 LCMS method NHC08025

Solvent gradient: 5% B (0-1.25 min), 5 to 15% B (1.25-4 min), 15 to 25% B (4-6 min), 25 to 90% B (6-8 min), 95% B (8-10 min), 95 to 5% B (10-12 min). Post time: 2 minutes.

ESI MS: Single ion monitoring (SIM) mode. The detector is turned off except for: 2.3-4 minutes (m/z detected: 158, 246), and 4.9-5.5 minutes (m/z detected: 271).

10. UV-vis titration

10.1 Reaction set up

All dry reagents and frozen non-His-tagged MBP-SadH stock were prepared anaerobically using multiple cycles of evacuation and N_2 flush. Buffer was degassed inside a Schlenk bomb by bubbling N_2 through for 0.5 h beforehand. Reagent stocks were prepared inside an N2 glovebox with degassed buffer. A sample consisting of non-His-tagged MBP-SadH (0.51 mM, 985 µL, 0.5 µmol) and $FeSO_4$ (75 mM, 5 µL, 0.375 µmol) in 100 mM HEPES pH 7.50 at 23 °C was prepared in a quartz UV cuvette with a Schlenk fitting in a non-anhydrous nitrogen glovebox. The sample was carefully and thoroughly mixed with a glass pipette to avoid bubble formation. UV–vis spectra of the sample were recorded from 350 to 800 nm anaerobically on the UV–vis spectrometer until the absorption spectrum stopped changing. The cuvette was brought into the glovebox for the addition of αKG (500 mM, 10 µL, 5 µmol) in 100 mM HEPES pH 7.5; a color change of pale yellow to pale pink was observed in the sample. The sample was mixed, and its UV–vis spectra were recorded the same way. The sample had a volume of 1000 µL and contained final concentrations of 0.5 mM MBP-SadH, 0.375 mM of Fe(II), and 2.5 mM of αKG. The spectrum of the enzyme-Fe(II)-αKG sample serves as the starting spectrum for plotting difference curves later on. In the glovebox, a stock solution of salt (10/ 25/ 100/ 200 mM, 10 µL) in the same buffer was added to the sample with a 25 µL gas-tight syringe. The sample was gently tapped several times for mixing and spectra were acquired until the absorption spectrum stopped changing. The additions were repeated until saturation behavior was observed at the new MLCT band (~ 5-10 mM of salt).

10.2 Data analysis

The last spectrum of each batch of spectra collected for each addition was used for analysis. Each of the last spectrum was dilution corrected to match those of the starting sample of enzyme-Fe(II)-αKG. To obtain the initial MLCT band in the absence of anions, the dilution corrected spectrum of the enzyme-Fe(II) sample was subtracted from that of the starting spectrum. This should result in a λ_{max} of 490 nm; significant deviation from this value suggests the protein sample still contained residual salt from the SEC purification and requires additional dialysis to remove the salt for accurate measurement.

Difference curves were obtained by subtracting the starting spectrum of enzyme-Fe(II)-αKG from each dilution corrected spectra after addition of anions. Each difference curve was baseline-normalized by setting the absorbance difference at 800 nm to zero. The potential MLCT peaks can be visualized when all difference curves were plotted together as a function of wavelength. The absorbance difference at these potential MLCT wavelengths were plotted as a function of anion concentration. A single site binding saturation model was fitted to this data and K_D values were estimated using the software Prism 9.

10.3 Computational Details of UV-Vis spectra simulation

Computation work in this sub-section was conducted by Vyshnavi Vennelakanti of the Kulik lab at MIT. All iron structures were derived from the active site of nonheme iron halogenase WelO5 (PDB 5IQS). The equatorial anion ligand has then been replaced with fluoride and azide. The structures were then optimized with hybrid density functional

PBE0 with def2-tZVP basis set using ORCA v4.0.1.2. UV-VIS spectra were computed using the optimized geometries at the same level of theory, i.e., PBE0/def2-tZVP. Computation for fluoride and azide are ongoing. For chloride, a strong peak for Fe(II)(H_2O)(Cl^-)(His)(His)(α-KG) was observed at 617 nm. Ms. Vennelakanti then checked the natural transition orbital (NTO) corresponding to the peak at 617 nm, and the transition electron density. She observed a depletion of electron density on the Fe metal and an increase in electron density on the αKG ligand, confirming that this peak corresponds to an MLCT.

Chapter 3 Toward artificial metalloenzymes based on Ni salicylaldiminato complexes

Introduction

From food packaging to photovoltaic devices, polymers are ubiquitous in the modern life. Olefin polymerization, the process of forming polymers from olefin monomers, is essential in the production of commonly used polymers such as polyethylene and polypropylene. This process can be performed in organic solvents or aqueous medium. The advantages of aqueous polymerization include (i) the use of a harmless solvent, water, (ii) the resulting heterogenous polymer-solvent mixture tends to be less viscous than ones with organic solvent, allowing for easier transfer in the manufacturing process, and (iii) removal of water from monomer feed for anhydrous organic solvent systems is not required.[84] There are two main pathways through which aqueous polymerization can be achieved: free radical polymerization and transition metal catalyzed polymerization. While the former typically offers higher rates and yields, the latter offers more control over the microstructure and composition of the resulting polymer, e.g., in the extent of branching, level of co-polymerization, or molecular weight of the final product.[84] Transition metal catalysts used in aqueous polymerization tend to possess late transition metal centers as they are less oxophilic and more tolerant toward water and functional groups on monomers. Several of such catalysts have been developed in the last few decades using late transition metals such as Ni, Pd, and Rh.[85–87]

One interesting example of a transition metal catalyst used in aqueous polymerization is the Ni(II) salicylaldiminato type of polymerization catalyst. First developed by Grubbs for polymerization conducted in non-polar organic solvents, these complexes offer many possibilities for fine-tuning the electronic and steric profile of the catalyst to produce polymers with specific microstructures and compositions (**Figure 32**).[88–90] The water tolerance of this class of complexes was demonstrated by Mecking, who showed that Ni salicylaldimine complexes could polymerize ethylene in water with or without surfactant.[91,92] However, this aqueous system faces challenges in expanding beyond the scope of polymerizing ethylene, for the use of a continuous flow of ethylene gas is vastly different from using single batch liquid monomers or monomer solutions in laboratory settings. Owing to this, aqueous copolymerization of ethylene and norbornene or 1-butylene resulted in co-polymers with at most 14% and 3.5% incorporation of norbornene or 1-butylene, respectively, rendering co-polymers with higher incorporation of norbornene much less accessible.[92,93] Aqueous polymerization of 1-propylene and 1-butylene, monomers containing more than two carbons, with Ni salicylaldimine catalysts yielded polymers with poor regio- and/ or stereoregularity due to the multiple possible pathways through which chain growth could occur.[94]

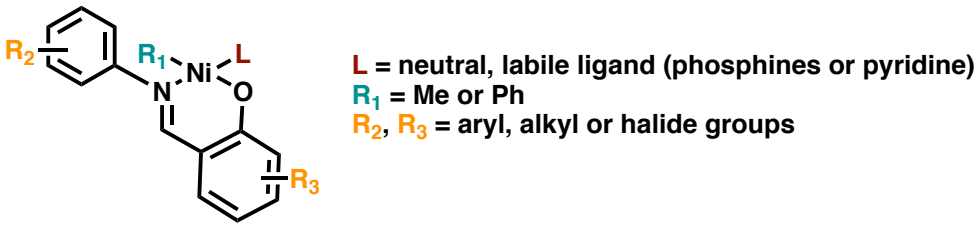

Figure 32. Highly tunable Ni Salicylaldiminato polymerization catalyst.

These challenges are not unique to this type of polymerization catalyst or even to aqueous polymerization. The Lewis group proposed to develop an artificial metalloenzyme (ArM) system to address some of these challenges. ArMs are comprised of two components: a metal catalyst ensconced in a protein scaffold. The metal catalyst provides the desired reactivity while the evolvable protein scaffold serves as the secondary sphere that imparts molecular recognition for the binding and orientation of the substrate to impart selectivity to a transformation of interest.[95] By embedding a polymerization catalyst inside a protein scaffold, we envisioned that the protein could be evolved to address common polymerization challenges, including controlling the extent of branching (**Figure 33A**, **B**), the level of co-monomer incorporation in copolymerization (**Figure 33C**), and protecting the metal center of the catalyst from functional groups in monomers and the growing chain (**Figure 33D**). Another potential benefit of the ArM system is the protection of the metal center from hydrolysis by the hydrophobic environment inside the protein scaffold. In recent years, a few ArM polymerization systems have been reported to demonstrate improved polydispersity index (PDI) or complementary selectivity relative to the metal catalyst in the absence of the scaffold.[96,97]

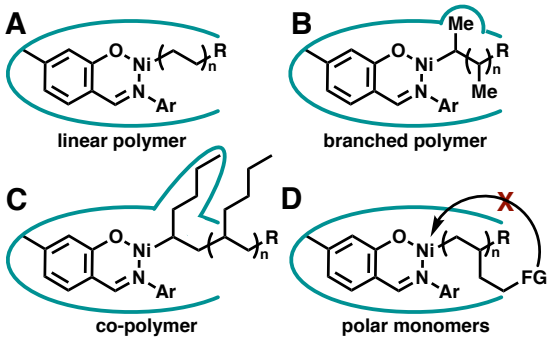

Figure 33. How an ArM could facilitate different types of polymerizations.

Previous work

The development of a polymerization ArM in our group was pioneered by former member Dr. Yifan Gu.[98] The Ni salicylaldiminato type of complexes was chosen as the metal catalyst for the ArM system for its tunability and water tolerance (**Figure 32**). To embed a metal catalyst inside a protein scaffold, there are four commonly used strategies in the bioconjugation toolkit: covalent bioconjugation, supramolecular binding, non-covalent anchoring, and metal substitution.[95] Examples of covalent bioconjugation include Michael addition of a cysteine residue on the scaffold to a maleimide linker on the catalyst (**Figure 33A**), and the phosphonation of a serine residue with a phosphonate-substituted catalyst (**Figure 33B**). An example of non-covalent anchoring is the well-established strong non-covalent binding by the protein streptavidin of a biontinyl group tethered to the catalyst (**Figure 33C**).[95] Dr. Gu synthesized and tested several Ni salicylaldimine complexes derived from Grubbs' polymerization catalysts with different linkers to exploit these three bioconjugation strategies with thermophilic enzymes, tHisF or serine hydrolase *Pfu* POP (**Figure 33**).[98] Complexes **1** and **2** with maleimide linkers were synthesized with the goal of reacting with a cysteine introduced by mutagenesis into tHisF for bioconjugation (**Figure 31A**). Unfortunately, the highly active Ni center reacted with the thiol of the cysteine sidechain and inhibited bioconjugation. Dr. Gu also synthesized the phosphonate-substituted complex **3**; no bioconjugation to the active site serine in *Pfu* POP was observed (**Figure 31B**). His last attempt was to synthesize a biotinylated Ni complex **4** in the hopes that the tethered biotinyl group will bind to

streptavidin (**Figure 33C**). Dr. Gu was unable to isolate pure complex **4** or express and purify streptavidin before graduating and embarking on his next endeavor.

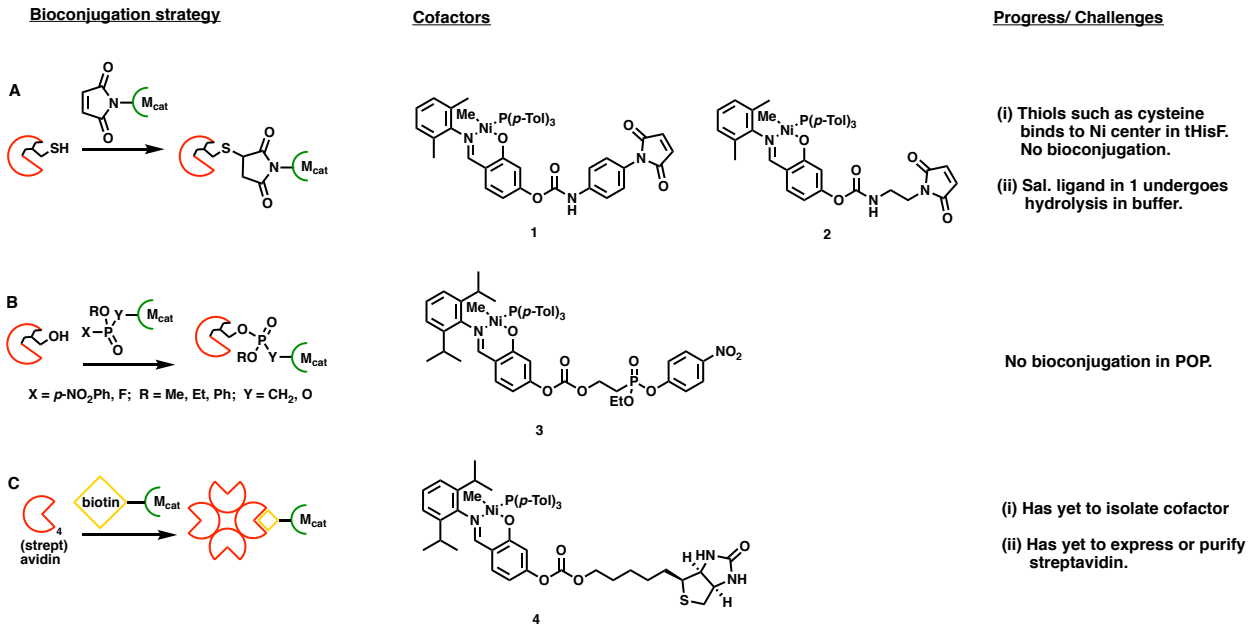

Figure 34. Dr. Gu's efforts and progress in identifying a suitable cofactor and bioconjugation strategy for building an ArM.

In parallel with the synthesis of cofactor **4**, Dr. Gu tested the reactivity non-biotinylated Ni catalysts. Polymerization of norbornene by catalyst **5**, the precursor of cofactor **4**, was observed in the presence of the phosphine scavenger $B(C_6F_5)_3$ in toluene solution (**Figure 35A**). The same reaction carried out in a THF-water mixture was unsuccessful, likely due to poor substrate solubility and water binding to the phosphine scavenger. In addition to polymerization, Dr. Gu also explored the aqueous olefin hydrosilylation by this class of Ni catalysts as a recent report demonstrated hydrosilylation of norbornene and 1-octene by **6** and similar catalysts in acetonitrile.[99] He reproduced literature results with norbornene in acetonitrile (ACN) but also observed hydrosilylation

from reactions conducted in ACN/water mixtures with **6**, albeit with lower conversions (**Figure 35B**). The hydrosilylation of 5-norbornene-2-methanol, a more water-soluble substrate, resulted in higher conversion than that of the norbornene reaction in 20% ACN.

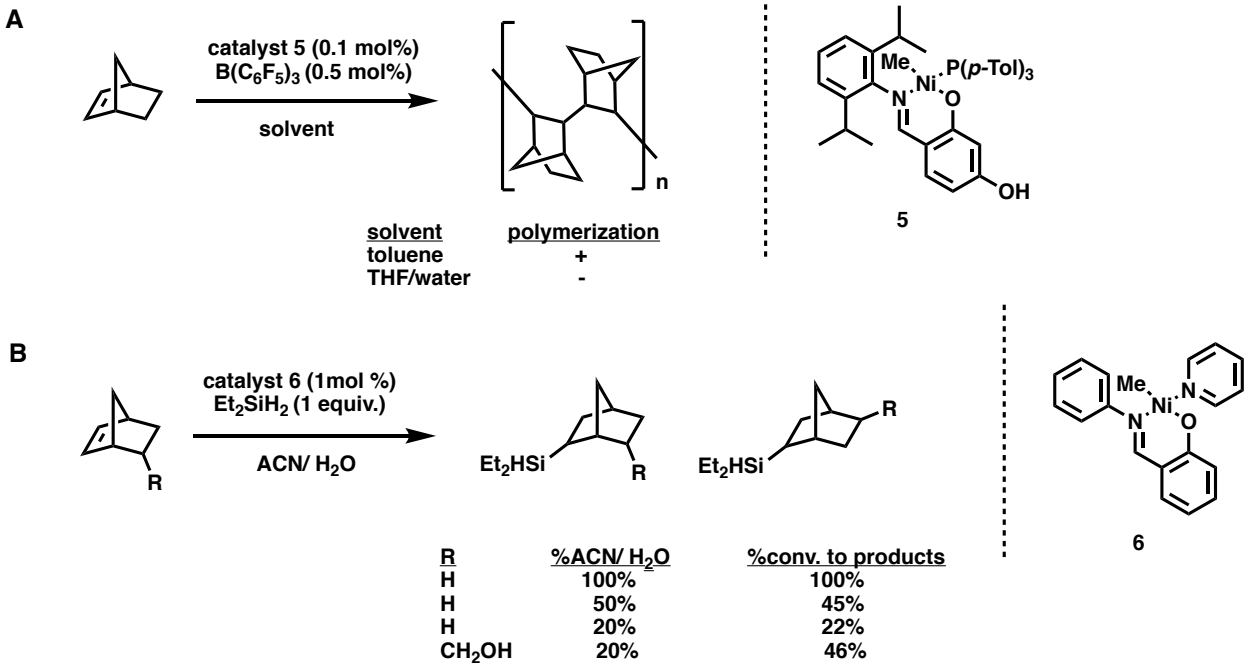

Figure 35. Dr. Gu's work on exploring polymerization and hydrosilylation activity of Ni catalysts without bioconjugation linkers.(A) Norbornene polymerization by Ni catalyst **5** in the presence of phosphine scavenger $B(C_6F_5)_3$ in toluene or aqueous medium. (B) Hydrosilylation of norbornene and its methanol derivative by Ni catalyst **6**.

At this stage, we decided to focus on developing an ArM for olefin hydrosilylation before attempting to achieve ArM polymerization due to the relative simplicity of hydrosilylation compared to polymerization. This was the promising premise from which I took over this project. My goals are (i) to synthesize and purify a biotinylated Ni cofactor that could hydrosilylate olefins in water, (ii) express and purify streptavidin (SAV), and (iii) to use the bioconjugated Ni ArM for hydrosilylation.

Synthesis, bioconjugation, and activity of cofactor **4**

Cofactor **4** was initially chosen as an ArM cofactor for the following reasons: (i) R_1=Me in general raises activity of Ni, (ii) L=P(*p*-Tol)$_3$ lowers the activity of Ni due to its low lability but affords a more stable and more easily isolable complex, and (iii) the bulkier 2,6-diisopropyl groups on N–Ar help prevent the formation of an inactive bis-salicylaldimine Ni complex (**Figure 32**, **Figure 34C**).[6,7] Dr. Gu showed that a crude mixture containing cofactor **4** was capable of hydrosilylation of 5-norbornene-2-methanol with diethylsilane. Given this preliminary result and the aforementioned benefits of the components in **4**, I decided to isolate **4** and test its hydrosilylation activity despite our shift in focus away from polymerization and the lack of literature precedent of hydrosilylation by Ni salicylaldimine complexes with L=phosphine.

I optimized the 9-step synthesis of cofactor **4** and was able to isolate purer batches of precursor **5** and cofactor **4** after column chromatography on silica gel under anaerobic (but not anhydrous) conditions (**Figure 36A**). It is crucial that the silica gel must not be dried rigorously and that the purification be conducted in a non-anhydrous glovebox. Using rigorously dried silica causes THF in the mobile phase to bind tightly to silica and results in diffusion of products in the stationary phase. The biotinylated cofactor **4** was thoroughly characterized by 1D and 2D NMR spectroscopy. A crystal structure of precursor **5** was also obtained at the Advanced Photon Source. Simultaneously, I successfully expressed and purified SAV.

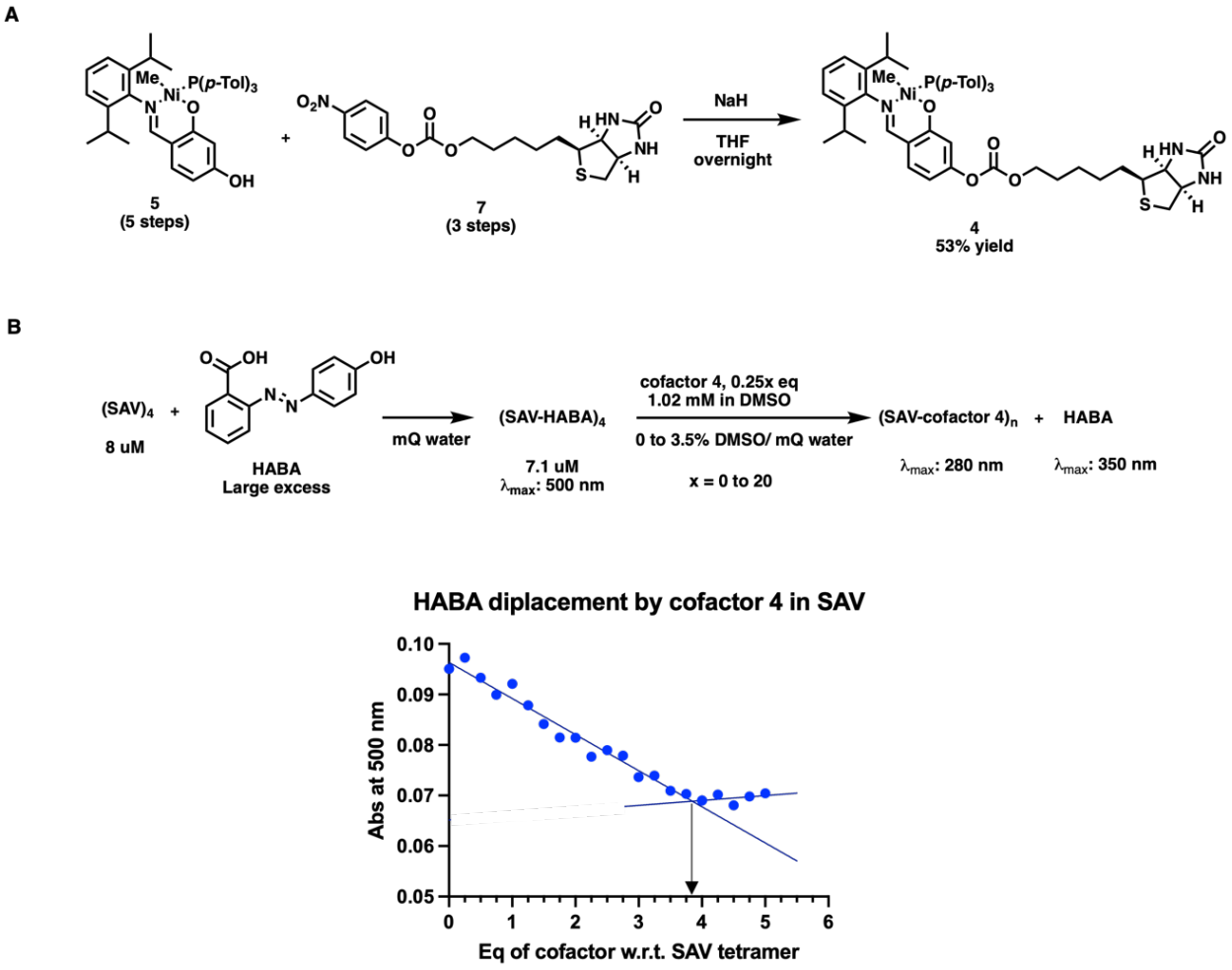

Figure 36. Synthesis and bioconjugation of Ni cofactor **4**.(A) Successful synthesis and isolation of cofactor **4**. (B) Proof of bioconjugation of **4** to SAV via an HABA displacement assay.

To confirm whether cofactor **4** can be anchored to SAV, a 2-(4'-hydroxyazobenzene) benzoic acid (HABA) displacement assay was performed (**Figure 36B**). The HABA displacement assay is a well-established experiment for measuring the number of equivalents of biotin or a biotin derivative, binds to the biotin-binding site of the tetrameric SAV.[100,101] In this assay, SAV is initially flooded by an excess of HABA that

loosely binds to the binding site of each of the four monomers of SAV. This (SAV-HABA) adduct has an absorbance at 500 nm. Owing to SAV's strong affinity for the biotinyl group, HABA in the binding site is displaced by biotinylated compounds. The resulting adduct does not absorb at 500 nm, so the absorbance at 500 nm decreases until the biotinylated compound is bound at all four SAV binding sites. When the absorbance at 500 nm is plotted as a function of the number of equivalents of biotin added with respect to SAV tetramer, one would expect a linear downward sloping curve from 0 to ~4 equivalents of cofactor. In the current case, fitting the data from the anaerobic titration of cofactor **4** to a sample of (SAV-HABA) indicates that saturation of the SAV binding sites occurs after ~3.8 equivalents of **4** was added (**Figure 36B**). This provides evidence for anchoring of cofactor **4** to SAV.

Hydrosilylation of 5-norbornene-2-methanol was tested with cofactor **4** in different solvent mixtures in the presence or absence of the phosphine scavenger $B(C_6F_5)_3$ (**Figure 37A**). Unfortunately, no or trace hydrosilylation product was observed. When the same reactions were repeated with phosphine-containing, non-biotinylated catalyst **5** or **8**, no hydrosilylation was observed either. While there are several examples of Ni polymerization catalyst with L=phosphine, the only examples of olefin hydrosilylation were catalyzed by Ni complexes bearing a pyridine ligand instead of phosphine ligand.[5,6,16] Hydrosilylation by Ni salicylaldimine catalysts was proposed to follow a modified Cossee-Arlman mechanism (**Figure 37B**).[99,102] It is likely that while a phosphine ligand on the Ni catalyst enables polymerization, my hydrosilylation results suggest that it may not labile enough for the ligand displacement step in hydrosilylation.

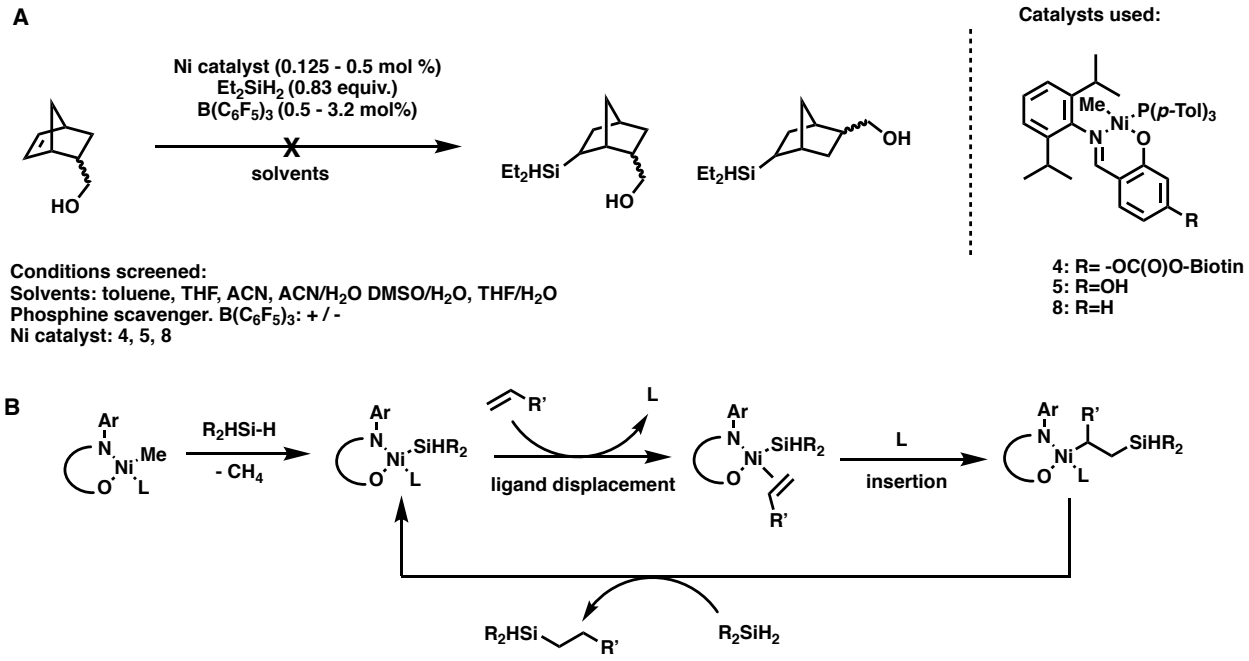

Figure 37. Lack of hydrosilylation activity by cofactor **4**.(A) 5-norbornene-2-methanol hydrosilylation attempt with cofactor **4** and non-biotinylated catalysts **5** and **8**. (B) Hydrosilylation was proposed to follow a modified Cossee-Arlman mechanism.[99]

Pyridyl-containing Ni catalysts and cofactor

There are two main avenues reported in literature that raise polymerization activity of Ni salicylaldimine catalysts in organic solvent or aqueous medium: a more labile neutral L ligand and a more electron-deficient Ni center.[88,103–105] Although our goal is an active hydrosilylation catalyst, these trends for polymerization may still hold true for a hydrosilylation catalyst due to the similarity of their proposed mechanisms. Given the literature precedent for using pyridine ligands on Ni for hydrosilylation, I synthesized non-biotinylated pyridine-containing complexes **9** and **10** to test for hydrosilylation activity before attempting to obtain the more synthetically challenging biotinylated cofactors (**Figure 38A**). Catalyst **9** is one of the most active hydrosilylation catalysts reported while

the novel catalyst **10** bears a nitro group in the salicylaldimine ligand to lower the electron density on the Ni center. Neither catalyst contains the hydroxyl group on the phenol ring in the salicylaldimine ligand that would be required for subsequent biotinylation; preliminary results showed that the hydroxyl group somehow destabilizes pyridyl-containing Ni complexes substantially to yield black Ni(0) during syntheses.

Hydrosilylation of four water-soluble olefins with diphenylsilane or diethyl silane was tested for both catalysts **9** and **10** in acetonitrile (**Figure 38B**). Catalyst **10** with the nitro group had no or trace hydrosilylation activity. Catalyst **10** was less stable for handling during its synthesis and isolation compared to catalyst **9**; it may be the case that **10** decomposed in the more polar ACN before any reaction occurred. While trace or no hydrosilylation occurred with diethylsilane with **9**, the catalyst demonstrated high hydrosilylation activity on all four substrates tested in the presence of diphenylsilane. Hydrosilylation of substrate **14** with diphenylsilane was chosen as the model reaction going forward, for it is the only reaction that gives the highest conversion to mostly one hydrosilylation product (alongside a small amount of hydrogenation product) in our preliminary tests across all four substrates with catalyst **9** in 10% ACN/H_2O. Confident with the performance of non-biotinylated catalyst **9**, I set out to synthesize its biotinylated analogue.

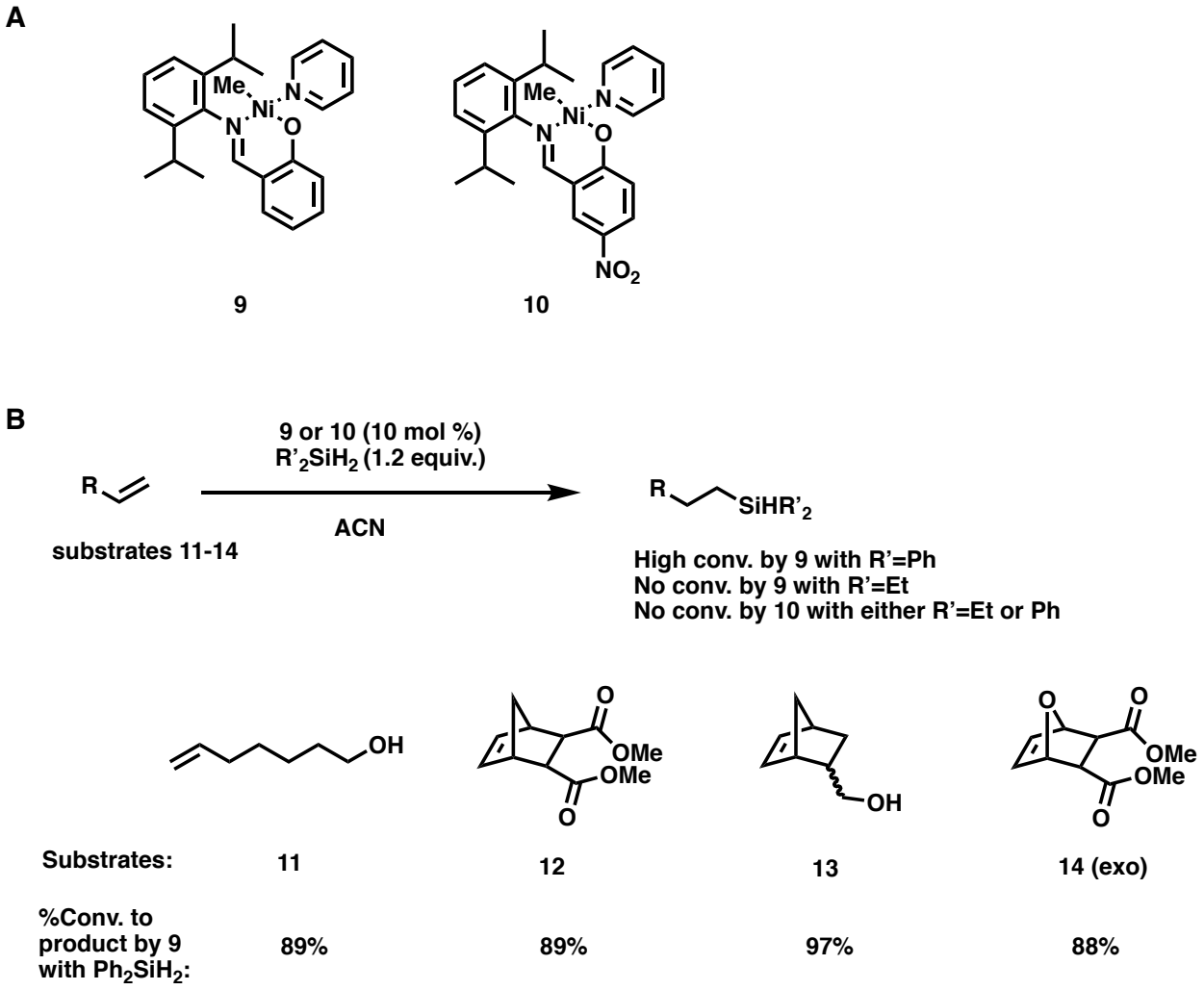

Figure 38. Hydrosilylation activities of pyridyl-containing Ni catalysts **9** and **10**.(A) Non-biotinylated pyridyl-containing Ni complexes **9** and **10** were synthesized. (B) Hydrosilylation of water-soluble substrates in ACN by **9** or **10**.

Synthesis, bioconjugation, and activity of cofactor **16**

To obtain cofactor **16**, the biotinylated analogue of **9**, I initially attempted to synthesize and isolate the hydroxyl-containing precursor **15** based on my experience with cofactor **4** (**Figure 39A**). Despite attempted optimization of this protocol, precursor **15** was only observed by ^{1}H NMR in the reaction; any attempts at isolating **15** via column chromatography resulted in degradation to 4-coordinate bis(salicylaldimine)Ni complex.

Similar bis-ligated Ni complexes have been reported to form during syntheses of certain Ni catalysts with labile L ligands and less bulky salicylaldimine ligands; such complexes are inactive polymerization catalysts.[90] Instead of isolating **15** after complete conversion of the limiting salicylaldimine ligand by ^{1}H NMR, sodium hydride and the biotin fragment **7** were added directly to the crude reaction mixture of **15** (**Figure 39A**). A pure sample of cofactor **16** was obtained after careful column chromatography on silica under anaerobic (but not anhydrous) conditions of the final reaction mixture.

A HABA displacement assay was carried out with **16** and SAV under anaerobic conditions (**Figure 39B**). The saturation in the decline of absorbance at 506 nm occurs at ~4.8 equivalents of cofactor which exceeds the expected 4 equivalents, perhaps due to low purity of the sample of **16** used in the assay (**Figure 35**). Nonetheless, the expected trend of falling absorbance at 506 nm corresponding to the (SAV-HABA) adduct followed by saturation of this decline suggested that cofactor binding was occurring as expected.

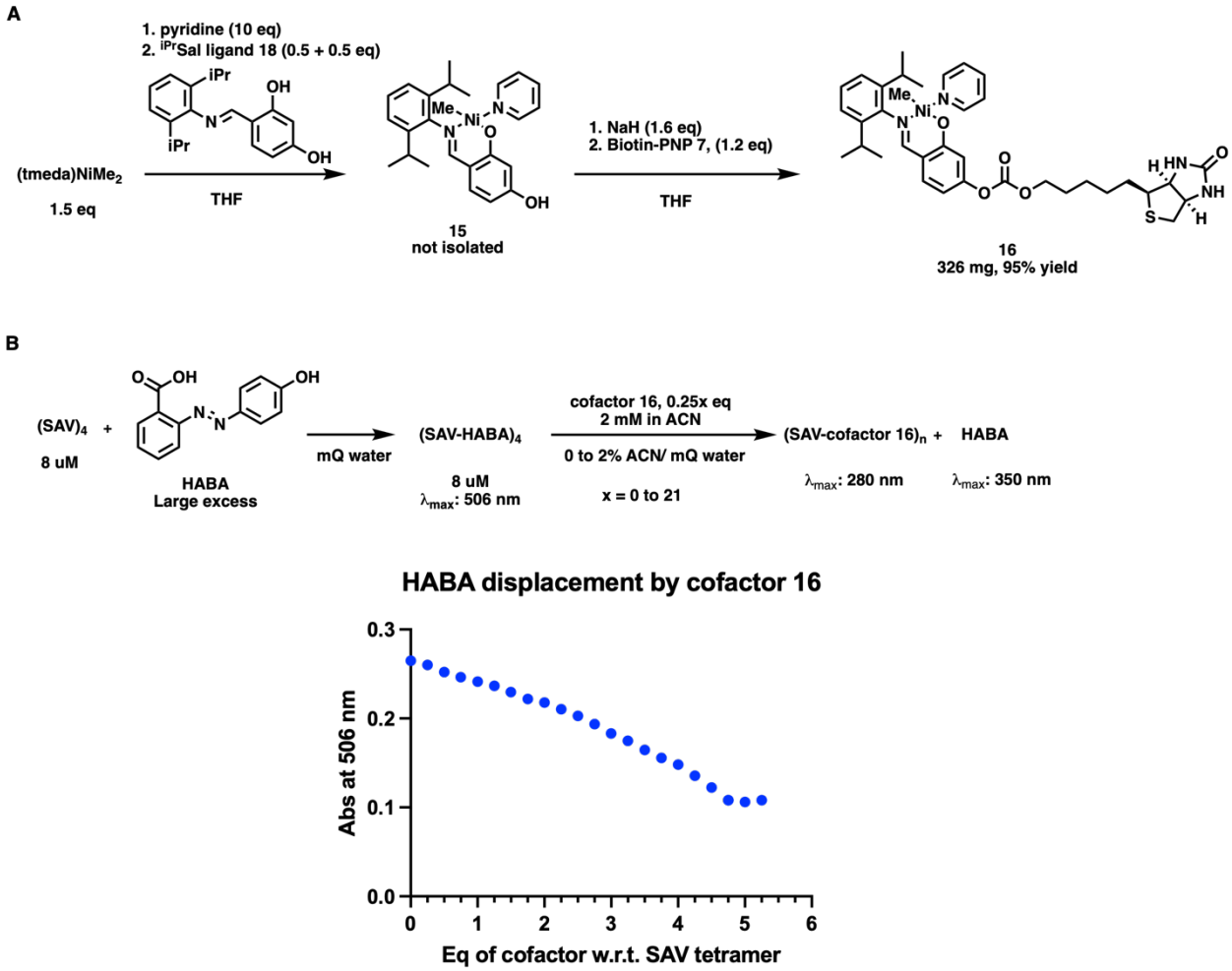

Figure 39. Synthesis and bioconjugation of biotinylated Ni cofactor **16**.(A) Synthesis of cofactor **16**. (B) Proof of bioconjugation of **16** to SAV via a HABA displacement assay.

The same set of 8 hydrosilylation reactions in ACN shown in **Figure 38** was repeated using cofactor **16**. Surprisingly, none of the reactions afforded any hydrosilylation products. The model reaction with substrate **14**, phenylsilane, and **16** in 10% ACN/water did not yield any desired product either. There are two reasons that could explain the activity difference between non-biotinylated catalyst **9** and cofactor **16**: (i) the carbonate linker in **16** contributes more electron density to Ni through the conjugated system and reduces the electrophilicity of Ni for hydrosilylation, (ii) components in the

biotinyl fragment in **16**, such the thioether, could coordinate to Ni inter- and/or intra-molecularly and affect hydrosilylation activity of the Ni center.

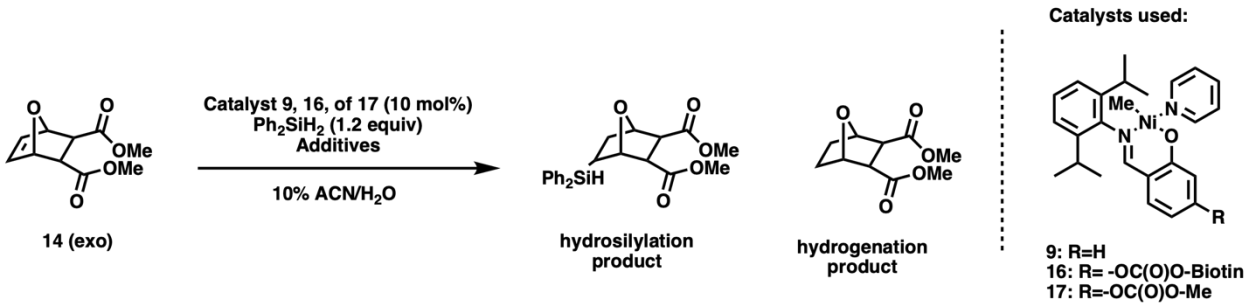

Entry	Catalyst	Additives	Hydrosilylation product conv.	Hydrogenation product conv.
a	**9**	-	87%	13%
b	**9**	Biotinol (10 mol%)	84%	13%
c	**9**	SAV(5 mol%)	37%	27%
d	**9**	BSA (5 mol%)	23%	11%
e	**16**	-	0%	0%
f	**16**	SAV (5 mol%)	0%	0%
g	**17**	-	88%	13%
h	**17**	Biotinol (10 mol%)	79%	11%

Table 16. Model hydrosilylation reaction with controls for troubleshooting.

5 mol% of tetrameric SAV, i.e., 20 mol% of SAV monomer was used.

A set of model reactions were conducted to help identify what features in cofactor **16** causes the difference in its hydrosilylation activity relative to catalyst **9** (**Table 16**). The benchmark hydrosilylation with non-biotinylated catalyst **9** afforded 87% and 13% conversion to the hydrosilylated and hydrogenated products, respectively (**Table 16a**). As mentioned previously, reaction in the presence of cofactor **16** did not afford any products (**Table 16e**). To test whether the electronic effects of the carbonate linker in **16** lowers the activity of Ni, catalyst **17** with a methyl carbonate ester was synthesized and isolated. Hydrosilylation with catalyst **17** gave similarly high conversions to the

hydrosilylated product as catalyst **9** (**Table 16g** and **7a**). The hypothesis of intermolecular interaction between the Ni center and biotinyl fragment causing low hydrosilylation activity was tested by adding biotinol to reactions using catalysts **9** and **17** (**Table 16b**, **7h**). Biotinol did not appear to change hydrosilylation activity significantly. To test for whether intramolecular interactions between the biotinyl group and Ni are detrimental for catalysis, SAV was added to cofactor **16** such that the biotinyl group is concealed within the binding pocket of SAV to protect the Ni center. This ArM reaction did not afford any products (**Table 16f**). Concerned that the presence of protein in general may shut down the entire reaction, SAV or bovine serum albumin (BSA), a protein of similar molecular weight as SAV, was added to reactions using catalyst **9** (**Table 16c**, **7d**). While the presence of protein did reduce the final conversion to the hydrosilylated product, the reaction was not completely ceased by either SAV or BSA.

Based on these data, it was concluded that: (i) cofactor **16** did not work well potentially due to intramolecular interactions between its biotinyl fragment and Ni, (ii) while the ArM, SAV-**16**, protects the Ni center from its own biotinyl group, certain residues in the SAV binding pocket was interacting with the Ni center in such a way that deters hydrosilylation, either by coordinating to Ni and/ or protonating the methyl group on **16**.

Outlook and Obstacles

According to the hypothesis outlined above, it may be possible to create a functional ArM by mutating potentially Ni-binding residues in SAV to non-coordinating residues. My lab mate Yasmine Zubi conducted docking studies with Rosetta Ligand

using a model of cofactor **16** and a crystal structure of SAV. K109 in the binding pocket of SAV was identified as a potentially problematic residue that could either coordinate to Ni or protonate the methyl group of **16**. Mutagenesis to generate the K109A SAV mutant is currently in progress. If the K109A variant improves hydrosilylation, subsequent active site engineering will be pursued to further optimized ArM activity.

In conclusion, hydrosilylation of olefins in acetonitrile or aqueous medium can be achieved by the non-biotinylated Ni catalyst **9**. Cofactor **16**, the biotinylated analogue of **9**, was successfully isolated and was shown to bioconjugate to SAV to create a potential ArM for hydrosilylation. Unfortunately, SAV-**16** was unable to hydrosilylate substrate **14**, likely due to interactions between residues in SAV binding pocket and cofactor **16**. Further investigation to identify and mutate these residues could result in a functioning hydrosilylation ArM. This lays the groundwork for modifying the hydrosilylation ArM into one capable of catalyzing aqueous polymerization in the future.

Experimental

1. Materials

Unless otherwise noted, all reagents were obtained from commercial suppliers and used without further purification. Tetrahydrofuran (THF), diethyl ether, methylene chloride (DCM), toluene (PhMe), and pentane were obtained from an Innovative Technologies solvent purification system (solvent deoxygenated by N_2 sparge and dried over alumina). Benzene-d_6, $CDCl_2$, THF-d_8 were degassed by three freeze-pump-thaw cycles in a glass tube sealed with a Kontes stopper and stored under N_2. Pyridine was degassed by three

freeze-pump-thaw cycles in a glass tube sealed with a Kontes stopper, dried over 3Å molecular sieves, and stored in an anhydrous nitrogen glovebox. Anhydrous, nitrogen-flushed *N,N,N′,N′*-tetramethylethylenediamine (tmeda) was purchased from Sigma Aldrich and stored in an anhydrous nitrogen glovebox. Trimethylaluminum solution (2.0 M in hexanes) was purchased from Sigma Aldrich, stored inside an anhydrous nitrogen glovebox, and used with the assumption that the concentration provided by the vendor was accurate. Diphenylsilane and diethylsilane were distilled. Sodium hydride (60 % dispersion in mineral oil) was purchased from Sigma Aldrich; the mineral oil was removed with pentane washes and NaH was dried *in vacuo* prior to being used in reactions. Molecular sieves were activated in a Schlenk flask under vacuum (<0.05mmHg) in a heating mantle set to 250°C for at least 12 hours. Silica used inside the nitrogen glovebox was degassed at room temperature with three cycles of evacuation and nitrogen purge, and stored in a nitrogen glovebox.

Complete analytical data and preparations have been reported for salicylaldimine ligands (^{iPr}Sal-R),[106] and substrate **14**.[107]

Plasmid pET-24a/SAV BL-21 DE3 *E. coli* was provided by the Ward group of University of Basel, Basel, Switzerland. *E. coli* cells were purchased from Invitrogen. Luria broth (LB) media was purchased from Research Products International (Mt. Prospect, IL). Qiagen Miniprep Kits were purchased from QIAGEN Inc. and used according to the manufacturer's instructions. Protein ladder (PageRuler™ Prestained Protein Ladder, 10

to 180 kDa; product number 26616) was purchased from Thermo Fisher Scientific. Kanamycin was purchased from Chem-Impex International Inc. and was prepared as 1000x stock solutions at 50 mg/mL. Pierce® BCA Protein Assay Kits were purchased from Fisher Scientific International, Inc., and the manufacturer's instructions were followed. Iminobiotin resin (Pierce™ Iminobiotin Agarose; product number 20221) was purchased from Thermo Fisher Scientific. Chemically-competent BL21(DE3) *E. coli* cells for transformation were provided by colleague Harrison Snodgrass and was prepared according to published procedures.[60]

2. General Procedures

Unless otherwise noted, all reactions and manipulations were performed under a circulating nitrogen atmosphere in a non-anhydrous Inert glove box, or using standard Schlenk technique. Certain catalyst syntheses were conducted inside an anhydrous Innovative Technology glovebox and will be noted. Flash column chromatography was carried out using Silicycle 230-400 mesh silica gel. NMR spectra (^{1}H, ^{13}C, and ^{31}P) were obtained using a Bruker 500 MHz spectrometer, a Varian 500 MHz Inova NMR spectrometer, or a Varian 400 MHz Inova NMR Spectrometer at room temperature. Chemical shifts are reported in ppm and coupling constants are reported in Hz. Absorbance spectra of HABA-displacement assays were recorded on a Varian Cary 5000 UV-Vis-NIR spectrophotometer. Measurement of protein concentration was performed using a Tecan Infinite 200 PRO plate reader on a Tecan NanoQuant plate.

3. Preparation of Streptavidin (SAV)

3.1 Transformation of pET24a/SAV

Transformation was conducted with help from Harrison Snodgrass. Chemically-competent BL21(DE3) *E. coli* cells were transformed with pET24a containing SAV insert. Aliquots of competent cells were transferred to 5 mL polypropylene culture tubes on ice, to which approximately 10 ng of plasmid was added. Competent cells were incubated with plasmid on ice for 30 min, and the cells were heat shocked at 42 °C in water bath for 45 seconds. The culture tubes were afterward incubated on ice for 2 minutes, then 350 µL SOC medium was added. The culture tubes were transferred to an incubator at 37 °C shaking at 250 rpm for 1 h to recover. After recovery, 100 µL cells were added to agar plates (with 50 µg/mL kanamycin) and spread using 3 mm glass beads. After drying, the agar plates were transferred to a 37 °C incubator and grown overnight. Single colonies were picked, cultured in LB, and stored as glycerol stocks at -80 °C.

3.2 SAV sequence

MASMTGGQQMGRDQAGITGTWYNQLGSTFIVTAGADGALTGTYESAVGNAESRYVL
TGRYDSAPATDGSGTALGWTVAWKNNYRNAHSATTWSGQYVGGAEARINTQWLLTS
GTTEANAWKSTLVGHDTFTKVKPSAASIDAAKKAGVNNGNPLDAVQQ

3.3 Expression of SAV

This autoinduction protocol is based on one given to our group by the Ward group at University of Basel. An overnight culture of inoculated LB (7.5 mL) and kanamycin (7.5

µL, 50 µg/mL) was shaken at 250 rpm, 37 °C for 16 h. Normal ZYP-5052 medium (800 mL) in a 3L Erlenmeyer flask was prepared according to literature procedures.[108] The next day, kanamycin (800 µL, 50 µg/mL) and the overnight culture (200 µL) were added to the normal ZYP-5052 medium. The culture was shaken for 24 h at 30 °C. After 24 h, cells were harvested by centrifugation at 4 °C, 4000 rpm for 20 minutes.

3.4 Purification of SAV

This purification protocol is modified based on one given to our group by the Ward group at University of Basel. Cell pellets were resuspended in a lysis buffer containing lysozyme (50 mg), DNaseI (tip of small spatula), RNase (tip of small spatula) in 20 mM Tris/HCl, pH 7.4 (60 mL). The suspension was shaken at 250 rpm, 37 °C for 1.5 h, after which the resuspended pellets were frozen at -20 °C for 2 h. The frozen lysate was then thawed at room temperature. More lysozyme and DNaseI were added to the thaw lysate, which was then shaken at 250 rpm, 20 °C for another 0.5 h. The lysate was clarified by centrifugation at 4 °C, 15000 rpm for 20 minutes. The clarified lysate (supernatant) was dialyzed into 6 M guanidinium HCl, pH 1.5 (2 L) at room temperature overnight. The lysate containing denatured proteins was then dialyzed into 20 mM Tris/HCl pH 7.4 (800 mL) at 4 °C for 8 hours, after which it was dialyzed into an iminobiotin binding buffer (50 mM $NaHCO_3$, 0.5 M NaCl, pH 10.8, 1 L) overnight at 4 °C. The lysate was clarified again by centrifugation the next day at 4 °C, 15000 rpm for 50 minutes. The supernatant was filtered through a 250 mL 0.2 µm sterile filter. The total amount of proteins (48 mg) in the filtrate was measured using Bradford assay. At 4 °C, iminobiotin resin (50 mL, 1 mg/mL binding

capacity) was equilibrated with 2 column volumes (CV) of water followed by 5 CV of iminobiotin binding buffer. The filtrate was incubated with the equilibrated resin for 0.5 h at 4 °C with slow rotation. After the initial elution of sample, the resin was washed with 5CV of iminobiotin binding buffer. SAV was eluted with 3 CV of elution buffer (1% acetic acid in water), with each CV of eluent collected as a separate fraction. The three eluted fractions were immediately dialyzed into 10 mM Tris/HCl pH 7.4 (4 L) at 4 °C overnight for neutralization. Samples of eluted fractions were analyzed on an SDS-page protein gel (15% acrylamide) to determine which fractions contained SAV. Neutralized fraction(s) containing SAV were dialyzed into milliQ water (4 L each) at 4 °C three times over three days. SAV was obtained after lyophilization. Yield: 47 mg. Titer: 58.8 mg/L.

4. HABA-displacement assay

The sample was prepared in a non-anhydrous nitrogen glovebox. All dry reagents and frozen SAV stock were prepared anaerobically using multiple cycles of evacuation and N_2 flush. Solvents were degassed by bubbling N_2 through for 0.5 h beforehand. Reagent stocks were prepared inside an N_2 glovebox with degassed solvents. A solution of streptavidin (8 µM of tetramer, 400 µL, 3.2 nmol) was prepared in milliQ water. Then, HABA solution (1.78 mM, 3.6 mL, 6.4 mmol) in water was added in order to saturate the tetrameric streptavidin. The solution was transferred to a Schlenk cuvette with 5 mL capacity. Aliquots of cofactor (0.25 eq with respect to SAV tetramer, 2 mM in ACN, 4 µL, 8 nmol per aliquot) were sequentially added up to 5.0 equivalents using a p10 pipette. The cuvette was gently tapped several times for mixing. The UV/Vis absorbance was

recorded between 400-500 nm for ten times for each addition of the cofactor solution. The absorbance at 500 nm of each of the 10th absorbance spectrum was dilution correct, and plotted against the equivalence of cofactor added with respect to SAV tetramer.

5. General procedures for hydrosilylation

The reactions were set up in a non-anhydrous nitrogen glovebox. Lyophilized BSA and frozen SAV stock were prepared anaerobically using multiple cycles of evacuation and N_2 flush. Solvents were degassed by bubbling N_2 through for 0.5 h beforehand. Reagent stocks were prepared inside an N_2 glovebox with degassed solvents. To an eppendorf was added the following (in order): (i) water (450 µL) or protein solution (0.139 mM, 450 µL, 0.0625 µmol), (ii) Ni catalyst or cofactor (8.33 mM, 30 µL, 0.25 µmol) in ACN, (iii) pre-mixed substrate (125 mM, 2.5 µmol) and silane (150 mM, 3 µmol) stock in ACN (20 µL) to reach a final reaction volume of 500 µL. If biotinol was used, the water (450 µL) was substituted with water (400 µL) and a biotinol stock (5 mM, 50 µL, 0.25 µmol) in water. The eppendorf was shaken at 750 rpm for 6 h at 22 ^{o}C in a thermoshaker in a non-anhydrous nitrogen glovebox.

After 6 h of shaking, the reaction was brought out of the glovebox for working up. The eppendorf was first spun down by centrifugation. An internal standard stock of hexamethylbenzene in benzene (5 mM, 100 µL, 0.5 µmol) and ethyl acetate (500 µL) were added to the reaction. After vortexing the eppendorf tube for thorough mixing, the tube was spun down by centrifugation again. The top organic layer was extracted with a 1 mL syringe and needle, and diluted to 1.5 mL. 0.3 mL of the diluted sample was filtered

through a 0.2 μm syringe filter for GCMS analysis. Product conversions were calculated using relative peak area ratios between product(s) and the substrate.

6. Synthesis and characterization of compounds

All glassware used in this sub-section were oven-dried at 180 ^{o}C. Unless otherwise noted, all procedures in this sub-section were conducted in an anhydrous nitrogen glovebox or using standard Schlenk techniques. Silica used inside the non-anhydrous nitrogen glovebox was degassed at room temperature with three cycles of evacuation and nitrogen purge, and stored in a nitrogen glovebox. It is crucial that this silica retains most of its water content after being degassed, or else coordinating solvents such as THF or MeOH would bind to silicon atoms too tightly to cause slow elution and diffusion of product and side product bands on silica. The non-anhydrous nitrogen glovebox was fitted with an inlet tube that allows nitrogen from an external cylinder to flow into the glovebox for flash chromatography on silica gel in an airtight fashion.

6.1 Synthesis of (tmeda)Ni(acac)$_2$

A 250 mL round bottom flask was charged with Ni(acac)$_2$ (12.8 g, 50 mmol, 1 eq), pentane (100 mL), and a stir bar in an anhydrous nitrogen glovebox. Tmeda (15 mL, 100 mmol, 2 eq) was added to the suspension of Ni(acac)$_2$. The reaction was stirred for 1 h at room temperature, during which the suspension turned into a dark blue solution. The reaction was then filtered through a 150 mL medium porosity frit. The filtrate was transferred to a 250 mL Schlenk flask. Pentane in the blue filtrate was partially removed

in vacuo such that there remained a minimal amount of pentane to keep the filtrate homogeneous at room temperature. The Schlenk flask was sealed, brought out of the glovebox, and cooled to -78 ^{o}C. Once blue crystals were formed in the cooled flask, this mixture was filtered into a second 250 mL Schlenk flask with a Schlenk-frit under N_2. The whole set up (2 Schlenk flasks and 1 Schlenk frit) was pumped down *in vacuo* and then brought into the glovebox. Blue crystals deposited on the frit were collected. Product was stored at -35 ^{o}C in an anhydrous nitrogen glovebox. Yield: 13 g, 70%. Product is paramagnetic and its ^{1}H NMR was not recorded. HR-MS spectrum of product was consistent with the formula $C_{16}H_{30}N_2NiO_4$.

Additional product can be isolated from the residual blue solids in the second Schlenk flask. To do so, the residual solids were redissolved in a minimal amount of pentane. The solution was stored in 20 mL scintillation vials which were loosely capped and stored at -35 ^{o}C in the glovebox. Over the course of months, more blue crystals were formed in these vials.

6.2 Synthesis of (tmeda)Al_2Me_6

To a 250 mL round bottom flask were added tmeda (6 mL, 40 mmol, 0.5 eq), pentane (60 mL) and a stir bar. $AlMe_3$ (2.0 M in hexanes, 40 mL, 80 mmol, 1 eq) was added dropwise to the tmeda solution. The reaction was stirred for 15 minutes and then filtered through a 150 mL course porosity frit. The white crystalline solids were washed with a small amount

of pentane. Residual pentane was removed *in vacuo*. Product was stored at -35 °C in an anhydrous nitrogen glovebox. Yield: 20 g, 96%.

^{1}H NMR (500 MHz, C_6D_6) δ 2.48 (s, 4H), 1.71 (s, 12H), -0.54 (s, 18H).

6.3 Synthesis of (tmeda)$NiMe_2$

In an anhydrous nitrogen glovebox, a 100 mL Schlenk flask was charged with (tmeda)$Ni(acac)_2$ (4.15 g, 11.1 mmol, 1 eq) and diethyl ether (20 mL). A 250 mL Schlenk was charged with a stir bar, (tmeda)Al_2Me_6 (1.45 g, 5.5 mmol, 0.5 eq), and diethyl ether (20 mL). Both flasks were sealed, brought out of the glovebox, and cooled to -30 °C. (tmeda)$Ni(acac)_2$ solution in the 100 mL Schlenk flask was cannulated to (tmeda)Al_2Me_6 solution in the 250 mL Schlenk flask under N_2. The reaction was stirred at -30 °C for 0.5 h and 1.5 h at room temperature, after which diethyl ether was removed *in vacuo*. The 250 mL Schlenk containing the pumped down reaction mixture was brought into the glovebox. The crude product was suspended in cold pentane and filtered through a 60 mL medium porosity frit. The yellow solids deposited on the frit was washed with cold pentane (40 mL x 3) and dried *in vacuo*. Product was stored at -35 °C in an anhydrous nitrogen glovebox. Yield: 655 mg, 58%.

^{1}H NMR (400 MHz, C_{6D6}) δ 1.92 (s, 12H), 1.37 (s, 4H), -0.44 (s, 3H).

6.4 Synthesis of (^{iPr}Sal-Biot.)Ni[P(*p*-Tol)$_3$](Me), cofactor **4**

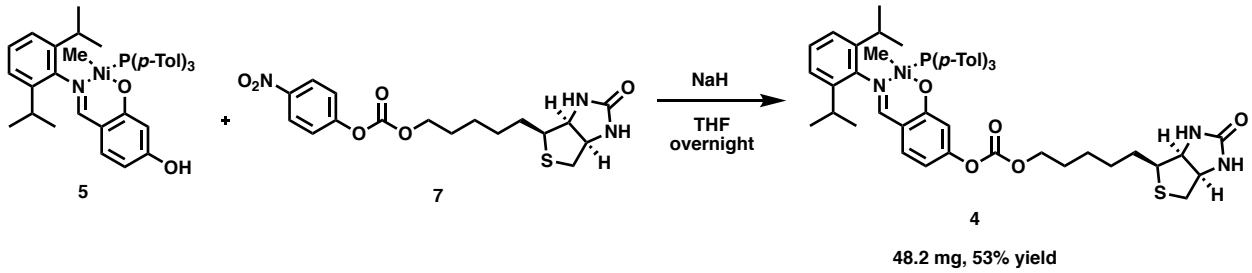

In an anhydrous nitrogen glovebox, a 100 mL bomb was charged with a stir bar and precursor **5** (92.6 mg, 0.137 mmol, 1.4 eq) dissolved in THF. Sodium hydride (3.3 mg, 0.137 mmol, 1.4 eq) was suspended THF and added to the stirring solution **5**. The deprotonation of 5 was monitored by ^{31}P NMR and completed in 0.5 h. Biotin fragment **7** (36.2 mg, 0.1 mmol, 1 eq) was suspended in THF and added to the solution of deprotonated **5**. The bomb was sealed, transferred to a non-anhydrous nitrogen glovebox and stirred at room temperature overnight. The complete consumption of deprotonated **5** was confirmed by ^{31}P NMR the next day. The crude mixture was embedded in celite and purified by column chromatography on a 2" tall pad of silica equilibrated with THF. The desired product eluted at between 1-2% MeOH in THF. After removing solvents *in vacuo*, the brownish yellow product was transferred back to the anhydrous nitrogen glovebox for storage at -35 ^{o}C. Yield: 48.2 mg, 53%.

^{31}P NMR (162 MHz, CD_2Cl_2) δ 31.56.

^{1}H NMR (400 MHz, CD_2Cl_2) δ 7.90 (d, *J* = 8.4 Hz, 1H, N=C<u>H</u>), 7.60 (dd, *J* = 10.2, 7.9 Hz, 6H, *o*-Tol-C<u>H</u>), 7.20 (d, *J* = 7.8 Hz, 6H, *m*-Tol-C<u>H</u>), 7.15 (br s, 3H, *m*-, *p*-C<u>H</u> of Ar-N), 7.07

(d, *J* = 8.7 Hz, 1H, *m*-phenol C<u>H</u>), 6.24 (dd, *J* = 8.7, 2.4 Hz, 1H, *p*-phenol C<u>H</u>), 5.85 (d, *J* = 2.3 Hz, 1H, *o*-phenol C<u>H</u>), 4.68 (br s, 1H, N<u>H</u>), 4.55 (br s, 1H, N<u>H</u>), 4.50 – 4.47 (m, 1H, β-C<u>H</u> to thioether), 4.31 – 4.27 (m, 1H, β-C<u>H</u> to thioether), 4.19 (t, *J* = 6.7 Hz, 2H, C<u>H</u>$_2$-OC(O)O-), 3.86 (p, *J* = 6.9 Hz, 2H, iPr<u>H</u>), 3.20 – 3.15 (m, 1H, α-C<u>H</u> to thioether), 2.92 (dd, *J* = 12.7, 5.0 Hz, 1H, α-C<u>H</u>$_2$ to thioether), 2.70 (d, *J* = 12.8 Hz, 1H, α-C<u>H</u>$_2$ to thioether), 2.36 (s, 9H, P-Ph-C<u>H</u>$_3$), 1.77 – 1.62 (m, 4H, β- to ε-C<u>H</u>$_2$ to carbonate), 1.49 – 1.43 (m, 4H, β- to ε-C<u>H</u>$_2$ to carbonate), 1.39 (d, *J* = 6.8 Hz, 6H, CH(C<u>H</u>$_3$)$_2$), 1.13 (d, *J* = 6.8 Hz, 6H, CH(C<u>H</u>$_3$)$_2$), -1.59 (d, *J* = 6.3 Hz, 3H, Ni-C<u>H</u>$_3$).

^{13}C NMR (126 MHz, CD_2Cl_2, DEPT) δ C 167.87 (d, J_{CP} =1.91 Hz, 3C), CH 164.83 (s, 1C, N=<u>C</u>H), C 155.81, C 153.55, C 148.86, C 142.75, C 142.37, C 141.51, C 140.60 (d, *J* = 2.3 Hz, 3C), CH 135.23 (s, 1C, *m*-phenol <u>C</u>H), CH 134.84 (d, *J* = 10.7 Hz, 6C, *o*-Tol-<u>C</u>H), 129.07 (d, *J* = 10.2 Hz, 6C, *m*-Tol-<u>C</u>H), CH 126.42 (s, 1C *p*-<u>C</u>H of Ar-N), CH 123.62 (s, 2C, *m*-<u>C</u>H of Ar-N), C 117.93, CH 113.29 (s, 1C, *o*-phenol <u>C</u>H), CH 107.91 (s, 1C, *p*-phenol <u>C</u>H), CH_2 69.08 (s, 1C, <u>C</u>H_2-OC(O)O-), CH 56.05 (s, 1C, α-<u>C</u>H to thioether), CH_2 40.99 (s, 1C, α-<u>C</u>H_2 to thioether), CH_2 29.05 (s, 1C, β- to ε-<u>C</u>H_2 to carbonate), CH_2 28.79 (s, 2C, β- to ε-<u>C</u>H_2 to carbonate), CH 28.74 (s, 2C, iPr<u>C</u>H), CH_2 26.09 (s, 1C, β- to ε-<u>C</u>H_2 to carbonate), CH_3 25.27 (s, 2C, CH(<u>C</u>H_3)$_2$), CH_3 22.96 (s, 2C, CH(<u>C</u>H_3)$_2$), CH_3 21.54 (d, J_{CP} = 1.3 Hz, 3C, P-Ph-<u>C</u>H_3), CH_3 -8.65 (d, *J* = 40.6 Hz, 1C, Ni-<u>C</u>H_3).

Quaternary ^{13}C peaks could not be assigned using characterization results from ^{1}H-^{13}C HMQC and DEPT.

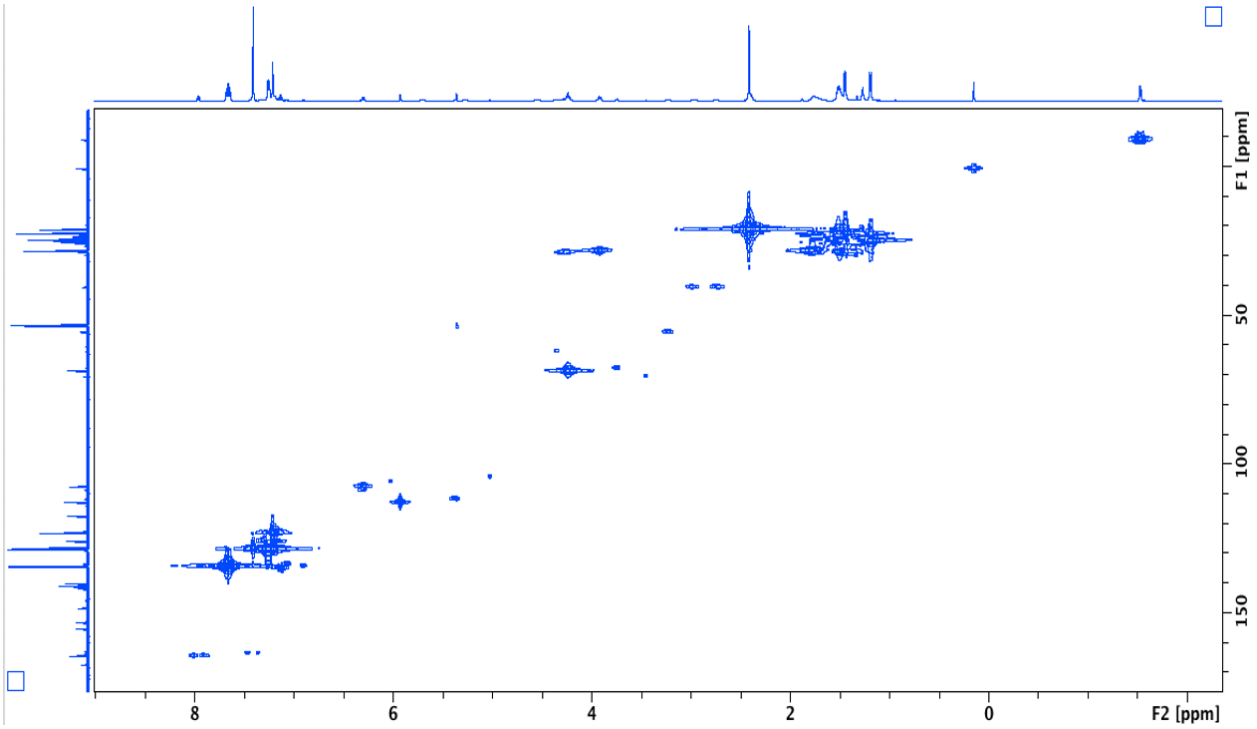

Figure 40. ^{1}H-^{13}C HMQC of cofactor **4** in CD_2Cl_2.

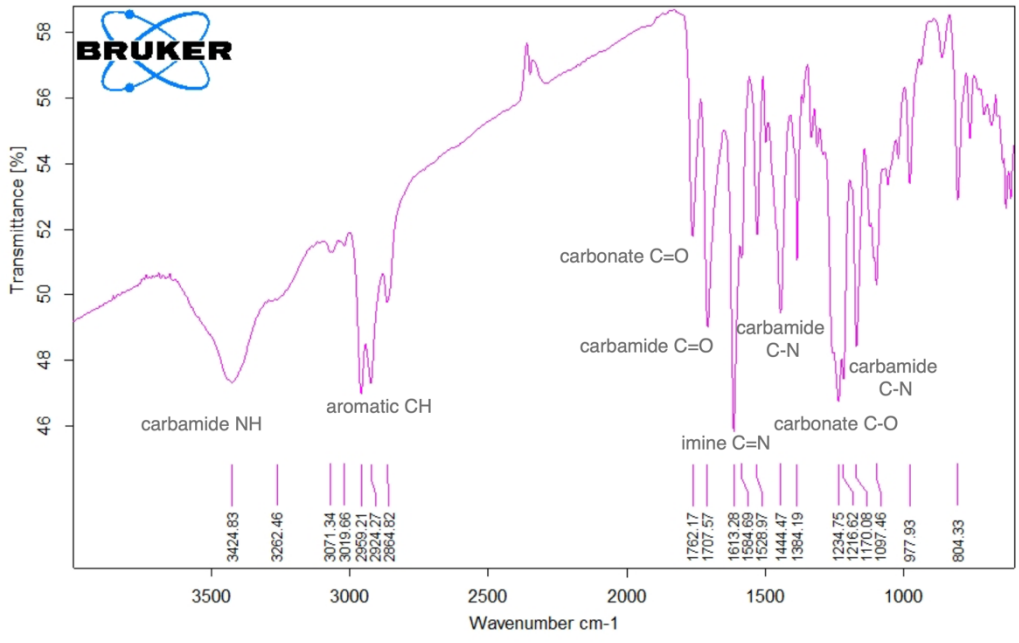

Figure 41. IR spectrum of cofactor **4**.

6.5 Synthesis of (^{iPr}Sal-OH)Ni[P(*p*-Tol)$_3$](Me), precursor **5**

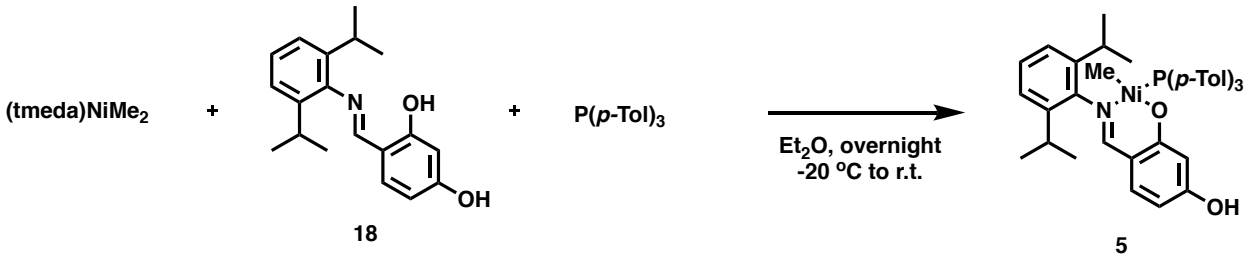

18 **5**

93.4 mg, 13%

In an anhydrous nitrogen glovebox, a 50 mL bomb cooled to -20 °C was charged with a stir bar and (tmeda)Ni(Me)$_2$ (247 mg, 1.21 mmol, 1.1 eq) dissolved in diethyl ether (10 mL). Salicylaldimine ligand **18** and P(*p*-Tol)$_3$ were dissolved in diethyl ether (10 mL) and added dropwise to the stirring solution of (tmeda)Ni(Me)$_2$. The bomb was sealed, transferred to a non-anhydrous nitrogen glovebox, and stirred overnight at room temperature. The crude mixture was embedded in celite and purified by column chromatography on a 2" tall pad of silica equilibrated with pentane. The desired product eluted at 20% Et$_2$O in pentane. After removing solvents *in vacuo*, the yellow product was transferred back to the anhydrous nitrogen glovebox for storage at -35 °C. Single crystals suitable for crystallography were obtained by slow evaporation of solvent from a saturated solution of product in benzene, followed by vapor diffusion of pentane. Yield: 93.4 mg, 13%.

^{1}H NMR (400 MHz, C_6D_6) δ 7.89 (dd, *J* = 10.0, 7.9 Hz, 6H), 7.81 (d, *J* = 8.6 Hz, 1H), 7.12 (d, *J* = 8.5 Hz, 2H), 6.97 (d, *J* = 6.9 Hz, 7H), 6.81 (d, *J* = 8.6 Hz, 1H), 5.96 (dd, *J* = 8.6, 2.4 Hz, 1H), 5.86 (d, *J* = 2.4 Hz, 1H), 4.15 (q, *J* = 7.0 Hz, 2H), 3.74 (s, 1H), 2.00 (s, 9H), 1.44 (d, *J* = 6.9 Hz, 6H), 1.10 (d, *J* = 6.8 Hz, 6H), -0.99 (d, *J* = 6.5 Hz, 3H).

^{31}P NMR (162 MHz, C_6D_6) δ 31.68.

6.6 Synthesis of biotin methyl ester

In air, *D*-Biotin (1g, 4.09 mmol) was suspended in methanol (25 mL) in a 100 mL round bottom flask. The flask was capped with a rubber septum and the suspension was stirred. Thionyl chloride (0.97 mL, 3.25 eq, 13.3 mmol) was added to the suspension slowly with a syringe and needle. The suspension turned clear upon completion of the addition. The reaction was stirred at room temperature overnight, after which it was transferred to a 250 mL round bottom flask and concentrated under reduced pressure. The white solids were further dried *in vacuo* and used in the next step without further purification. Product was stored at 4 ^{o}C in air. Yield: 1.05 g, >99%. ^{1}H NMR chemical shifts of the product matched those reported in literature.[109]

6.7 Synthesis of biotinol

A reflux condenser was fitted onto the round bottom flask containing biotin methyl ester (1.05 g, 4.09 mmol) from the previous step. The system was degassed by three cycles of evacuation and N_2 purge. THF (20 mL) was added to the starting material under N_2. The flask was cooled to 0 ^{o}C. In an anhydrous nitrogen glovebox, lithium aluminum hydride (465.6 mg, 12.27 mmol, 3 equiv.) was suspended in anhydrous THF (25 mL). The suspension was added to the starting material dropwise using three sets of 12 mL syringes and long needles under N_2. Reaction was warmed to room temperature and then refluxed overnight. The next day, the reaction was diluted with some diethyl ether and

then cooled to 0 °C. Water (0.5 mL), NaOH (2M, 0.5 mL), and a second addition of water (1.5 mL) were added to the reaction. Reaction was warmed to room temperature and stirred for 15 minutes. The suspension was transferred to a 500 mL Erlenmeyer flask, dried over anhydrous $MgSO_4$, and stirred for 15 minutes. The suspension was then filtered through a pad of celite on a course porosity frit with some methanol. The filtrate was concentrated under reduced pressure with celite. The celite-embedded product was purified on a 30 g reverse phase column on Biotage with the following method: 3CV of 0% B, 15CV gradient from 0 to 15% B, 3CV gradient of 15 to 100% B (solvent A: water; solvent B: acetonitrile.) Fractions were checked by the LCMS. Those containing the product were combined and concentrated under reduced pressure. Product was stored at 4 °C in air. Yield: 800 mg, 85% over two steps. ^{1}H NMR chemical shifts of the product matched those reported in literature.[110]

6.8 Synthesis of biotin-OC(O)O-(*p*-NO_2-C_6H_4), **7**

A 250 mL round bottom flask was charged with a stir bar, biotinol (206.5 mg, 0.90 mmol, 1 eq), pyridine (435 μL, 5.4 mmol, 6 eq), and THF (50 mL) inside an anhydrous nitrogen glovebox. *p*-nitrophenyl chloroformate (542.1 mg, 2.7 mmol, 3 eq) was added to the stirring reaction as solids. The reaction was stirred overnight at room temperature, after which THF and pyridine were removed under reduced pressure. In air, the crude mixture was purified on silica gel. The product eluted at 3% MeOH in DCM. Product can be recrystallized in DCM to form white feather-like crystals. Yield: 280 mg, 79%.

^{1}H NMR (500 MHz, $CDCl_3$) δ 8.27 (d, *J* = 9.1 Hz, 2H), 7.42 – 7.35 (d, *J* = 9.1 Hz, 2H), 5.76 (br s, 1H), 5.26 (br s, 1H), 4.51 (dd, *J* = 7.8, 5.0 Hz, 1H), 4.32 (d, *J* = 5.1 Hz, 1H), 4.29 (t, *J* = 6.6 Hz, 2H), 3.16 (ddd, *J* = 8.5, 6.2, 4.6 Hz, 1H), 2.92 (dd, *J* = 12.8, 5.0 Hz, 1H), 2.73 (d, *J* = 12.8 Hz, 1H), 1.78 (m, 2H), 1.70 (dq, *J* = 14.3, 7.0 Hz, 2H), 1.48 (p, *J* = 4.1 Hz, 4H).

A note on ^{1}H NMR: chemical shifts reported above were obtained using anhydrous $CDCl_3$; using non-anhydrous $CDCl_3$ results in small shifts in the chemical shift of aliphatic protons and the absence of the urea NH peaks at 5.76 and 5.26 ppm.

6.9 Synthesis of (^{iPr}Sal)Ni[P(*p*-Tol)$_3$](Me), **8**

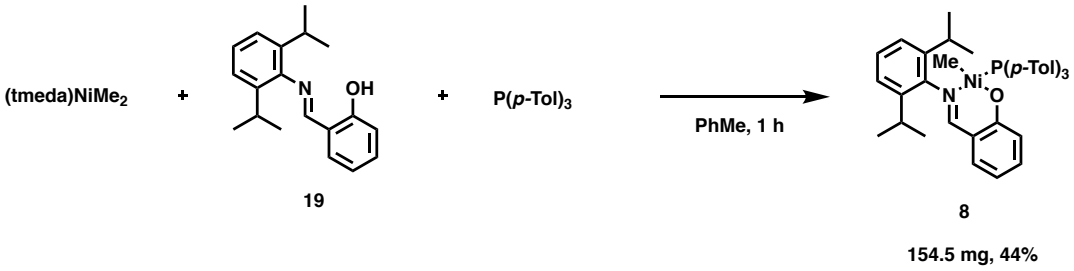

A 20 mL scintillation vial was charged with a stir bar, (tmeda)$NiMe_2$ (120 mg, 0.587 mmol, 1.1 eq), P(*p*-Tol)$_3$ (162.4 mg, 0.534 mmol, 1 eq), ligand **19** (150.3 mg, 0.534 mmol, 1 eq), and toluene (10 mL). The reaction was stirred at room temperature and monitored by ^{31}P NMR for complete consumption of free phosphine (~ t =1 h). The reaction was dried *in vacuo* and purified by flash chromatography on silica gel. The product eluted at 0.75 to 2% diethyl ether in pentane. Yellow solids were obtained after solvents were removed from the fractions *in vacuo*. Yield: 154.5 mg, 44%.

^{31}P NMR (162 MHz, C_6D_6) δ 32.13.

^{1}H NMR (400 MHz, C_6D_6) δ 7.96 (d, *J* = 8.0 Hz, 1H), 7.89 (t, *J* = 9.1 Hz, 6H), 7.14 – 6.97 (m, 11H), 6.61 (d, *J* = 8.6 Hz, 1H), 6.47 (t, *J* = 7.3 Hz, 1H), 4.11 (h, *J* = 6.3, 5.9 Hz, 2H), 2.01 (s, 9H), 1.44 (d, *J* = 6.9 Hz, 6H), 1.08 (d, *J* = 6.9 Hz, 6H), -0.98 (d, *J* = 5.6 Hz, 3H).

6.10 Synthesis of (^{iPr}Sal)Ni(py)(Me), catalyst **9**

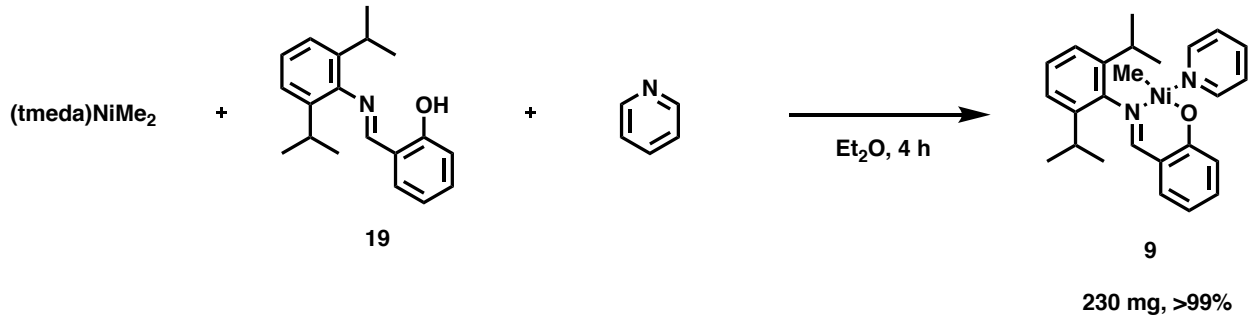

19 **9**

230 mg, >99%

A 20 mL scintillation vial was charged with a stir bar, (tmeda)$NiMe_2$ (117.7 mg, 0.577 mmol, 1.1 eq) in Et_2O (4 mL), and pyridine (0.42 mL, 5.2 mmol, 10 eq). The reaction as stirred for a minute and the brown suspension quickly turned a dark red. Ligand **19** (149.4 mg, 0.53 mmol, 1 eq) in Et_2O (2.5 mL) was added to the reaction. The reaction was stirred at room temperature for 4 h. The reaction was filtered through a 0.2 μm syringe filter and the filtrate was dried *in vacuo*. Red solids were obtained. Consistent with literature procedures, product was deemed pure enough for use without further purification.[99] Yield: 230 mg, >99%.

^{1}H NMR (500 MHz, c_6d_6) δ 8.71 (d, *J* = 5.1 Hz, 2H), 7.58 (s, 1H), 7.14 – 7.11 (m, 3H), 6.99 (d, *J* = 8.7 Hz, 1H), 6.96 (dd, *J* = 7.9, 1.9 Hz, 1H), 6.68 (br s, 1H), 6.58 (dd, *J* = 8.7,

6.5 Hz, 1H), 6.47 (ddd, *J* = 7.9, 6.8, 1.1 Hz, 1H), 6.23 (t, *J* = 6.9 Hz, 2H), 4.23 (hept, *J* = 6.9 Hz, 2H), 1.53 (d, *J* = 6.9 Hz, 6H), 1.08 (d, *J* = 6.8 Hz, 6H), -0.68 (s, 3H).

6.11 Synthesis of (^{iPr}Sal-NO_2)Ni(py)(Me), catalyst **10**

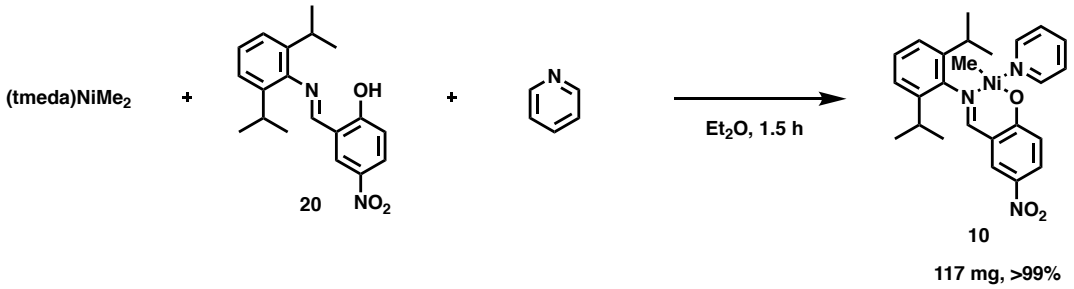

A 20 mL scintillation vial was charged with a stir bar, (tmeda)$NiMe_2$ (50 mg, 0.245 mmol, 1.05 eq) in Et_2O (3 mL), and pyridine (0.1 mL, 1.1 mmol, 5 eq). The reaction as stirred for a minute and the brown suspension quickly turned a dark red. Ligand **20** (76.1 mg, 0.233 mmol, 1 eq) in Et_2O (3 mL) was added to the reaction. The reaction was stirred at room temperature for 1.5 h. The reaction was filtered through a 0.2 μm syringe filter and the filtrate was dried *in vacuo*. Reddish orange solids were obtained. Consistent with literature procedures, product was deemed pure enough for use without further purification.[88] Yield: 117 mg, >99% (due to a small amount of residual tmeda).

^{1}H NMR (500 MHz, c_6d_6) δ 8.46 (d, *J* = 5.2 Hz, 2H), 8.04 – 7.98 (m, 2H), 7.21 (s, 1H), 7.11 (m, 1H), 7.07 (br s, 1H), 7.06 (d, *J* = 1.4 Hz, 1H), 6.57 (t, *J* = 7.7 Hz, 1H), 6.47 (d, *J* = 10.2 Hz, 1H), 6.21 (t, *J* = 6.8 Hz, 2H), 4.02 (p, *J* = 6.9 Hz, 2H), 1.49 (d, *J* = 6.9 Hz, 6H), 1.03 (d, *J* = 6.9 Hz, 6H), -0.67 (s, 3H).

6.12 Synthesis of (^{iPr}Sal-Biot.)Ni(py)(Me), cofactor **16**

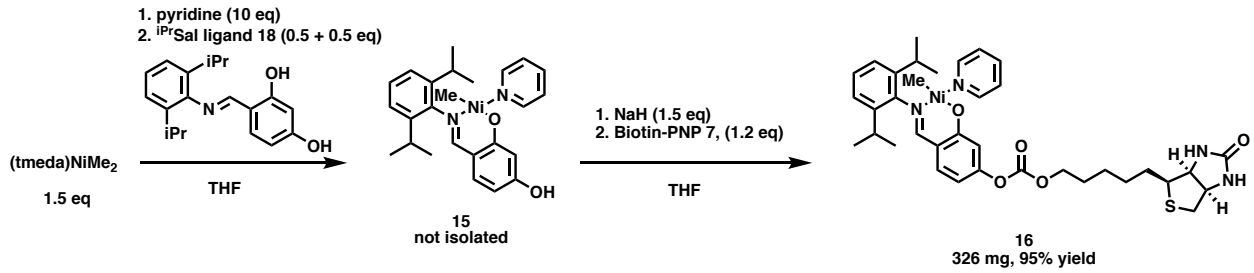

In an anhydrous nitrogen glovebox, a 100 mL round bottom flask was charged with a stir bar and (tmeda)Ni(Me)$_2$ (148.7 mg, 0.73 mmol, 1.5 eq) dissolved in THF (6 mL). Pyridine (0.4 mL, 4.85 mmol, 10 eq) was added to the stirring solution of (tmeda)Ni(Me)$_2$, turning the brown solution dark red. After a few minutes of stirring, ligand **18** (144.4mg, 0.485 mmol, 1 eq) dissolved in THF (5 mL) was added dropwise to the solution in two rounds, spaced 15 minutes apart. The reaction was monitored by 1H NMR for the complete consumption of ligand **18**, about 1.5 hours. Sodium hydride (18.6 mg, 0.78 mmol, 1.6 eq) suspended in THF (2.5 mL) was then added to the reaction. After 10 minutes of stirring, biotin fragment **7** (230 mg, 0.58 mmol, 1.2 eq) suspended in a mixture of DCM and THF (20 mL, 1:1 v/v ratio) was added to the reaction. The reaction was stirred for 1.5 h and monitored by ^{1}H NMR for the complete consumption of the diagnostic upfield Ni-C<u>H</u>$_3$ peak of intermediate **15**. Upon completion, the reaction was filtered through a 0.2 μm syringe filter under vacuum. The filtrate was dried *in vacuo* and then transferred to a non-anhydrous nitrogen glovebox for purification by flash chromatography. The crude mixture was dissolved in minimal amount of THF (~2 mL) and loaded onto a 2-inch silica column equilibrated with THF. The desired product eluted at 100% THF as the second band. TLC of the crude mixture and fractions were performed with 1%-10% MeOH/THF to visualize

the desired product and two UV-active impurities. Fractions containing the desired product (R_f: 0.5 with 10% MeOH/THF) were dried *in vacuo* to afford orange solids. Product was stored at -35 °C in an anhydrous nitrogen glovebox. Yield: 326.3 mg, 95%.

^{1}H NMR (400 MHz, CD_2Cl_2) δ 8.86 (d, *J* = 5.5 Hz, 2H), 8.27 (d, *J* = 9.2 Hz, 2H), 7.70 (t, *J* = 7.7 Hz, 1H), 7.55 (s, 1H), 7.40 (d, *J* = 9.2 Hz, 2H), 7.24 (t, *J* = 6.8 Hz, 2H), 7.19 – 7.12 (m, 3H), 7.06 (d, *J* = 8.6 Hz, 1H), 6.33 (d, *J* = 2.3 Hz, 1H), 6.26 (dd, *J* = 8.5, 2.3 Hz, 1H), 4.85 (br s, 1H), 4.67 (br s, 1H), 4.51 (br s, 1H), 4.31 (br s, 1H), 4.28 (t, *J* = 6.6 Hz, 2H), 4.20 (t, *J* = 6.5 Hz, 2H), 3.99 (p, *J* = 6.8 Hz, 2H), 3.18 (s, 1H), 2.94 (d, *J* = 12.8 Hz, 1H), 2.70 (dd, *J* = 12.9, 5.3 Hz, 1H), 1.77 – 1.67 (m, 4H), 1.46 (m, *J* = 6.9 Hz, 10H), 1.13 (d, *J* = 6.8 Hz, 6H), -1.19 (s, 3H).

6.13 Synthesis of [^{iPr}Sal-OC(O)OMe]Ni(py)(Me), cofactor **17**

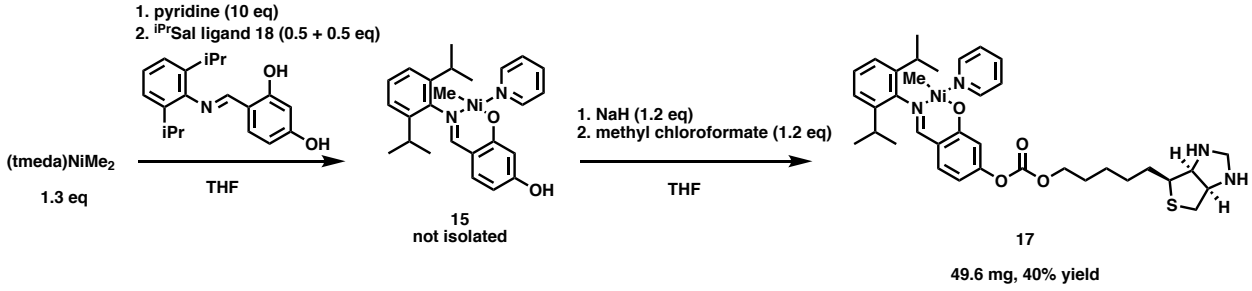

In an anhydrous nitrogen glovebox, a 20 mL scintillation vial was charged with a stir bar and (tmeda)Ni(Me)$_2$ (53.1 mg, 0.26 mmol, 1.3 eq) dissolved in THF (1.2 mL). Pyridine (0.16 mL, 2 mmol, 10 eq) was added to the stirring solution of (tmeda)Ni(Me)$_2$, turning the brown solution dark red. After a few minutes of stirring, ligand **18** (71.4 mg, 0.24 mmol, 1.2 eq) dissolved in THF (2.5 mL) was added dropwise to the solution in two rounds,

spaced 15 minutes apart. The reaction was stirred for 2 hours. Sodium hydride (5.8 mg, 0.24 mmol, 1.2 eq) suspended in THF (2 mL) was then added to the reaction. After 10 minutes of stirring, methyl chloroformate (15.5 μL, 0.2 mmol, 1 eq) was added to the reaction dropwise. The reaction was stirred for 2 h and monitored by ^{1}H NMR. Another two additional equivalence of methyl chloroformate were added to the reaction such that only one upfield Ni-Me peak was observed by ^{1}H NMR. The orange cloudy reaction was filtered through a 0.2 μm syringe filter. The filtrate was dried *in vacuo* and then transferred to a non-anhydrous nitrogen glovebox for purification by flash chromatography. The crude mixture was dissolved in minimal amount of diethyl ether (~2 mL) and loaded onto a 2-inch silica column equilibrated with pentane. The desired product eluted at 15% THF in pentane as the second band. TLC of the crude mixture and fractions were performed with 20% THF in pentane to visualize the desired product and three UV-active impurities. Fractions containing the desired product (R_f: 0.2) were dried *in vacuo* to afford orange solids. Product was stored at -35 °C in an anhydrous nitrogen glovebox. Yield: 49.6 mg, 40%.

^{1}H NMR (500 MHz, cd_2cl_2) δ 8.86 (d, *J* = 4.5 Hz, 1H), 7.70 (tt, *J* = 7.5, 1.7 Hz, 1H), 7.56 (s, 1H), 7.24 (t, *J* = 6.9 Hz, 2H), 7.16 (m, 3H), 7.07 (d, *J* = 8.6 Hz, 1H), 6.34 (d, *J* = 2.3 Hz, 1H), 6.27 (dd, *J* = 8.6, 2.4 Hz, 1H), 4.00 (hept, *J* = 6.8 Hz, 2H), 3.84 (s, 3H), 1.47 (d, *J* = 6.9 Hz, 7H), 1.14 (d, *J* = 6.8 Hz, 6H), -1.17 (s, 3H).

6.14 Single Crystal X-ray Diffraction Details

Single crystal diffraction data for precursor **5**, (^{iPr}Sal-OH)Ni[P(*p*-Tol)$_3$](Me), was obtained at the Advanced Photon Source. The single crystal was yellow and football-shaped. A benzene molecule from the recrystallization solvent was co-crystallized. The structure was solved and refined by Dr. Alexander Filatov.

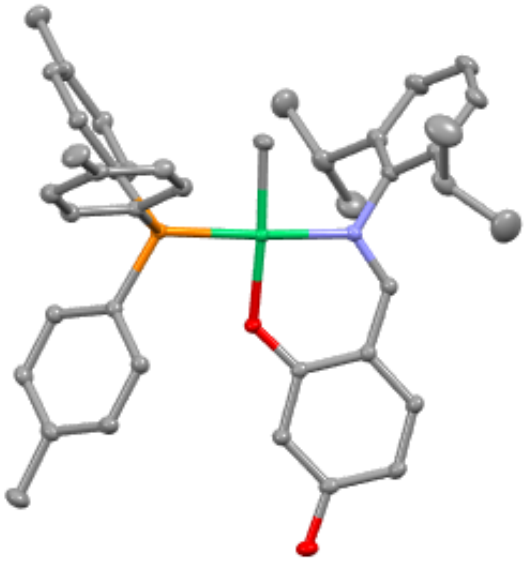

Figure 42. Crystal structure of (^{iPr}Sal-OH)Ni[P(*p*-Tol)$_3$](Me), precursor **5**.

Crystal data and structure refinement for 437_Ni_APS.

Identification code	437_Ni_APS
Empirical formula	$C_{44}H_{49}NNiO_2P$
Formula weight	713.52
Temperature/K	100(2)
Crystal system	monoclinic
Space group	$P2_1/c$
a/Å	12.8947(5)
b/Å	10.4275(4)
c/Å	28.3995(11)
α/°	90
β/°	95.7880(10)
γ/°	90
Volume/Å^3	3799.1(3)
Z	4
ρ_{calc}g/cm^3	1.247
μ/mm^{-1}	0.145
F(000)	1516.0
Crystal size/mm^3	0.04 × 0.025 × 0.02
Radiation	synchrotron (λ = 0.41328)
2Θ range for data collection/°	1.846 to 34.442
Index ranges	$-18 \leq h \leq 18$, $-14 \leq k \leq 14$, $-40 \leq l \leq 40$
Reflections collected	120981
Independent reflections	11517 [R_{int} = 0.0723, R_{sigma} = 0.0333]
Data/restraints/parameters	11517/0/454
Goodness-of-fit on F^2	1.098
Final R indexes [I>=2σ (I)]	R_1 = 0.0369, wR_2 = 0.1003
Final R indexes [all data]	R_1 = 0.0377, wR_2 = 0.1012
Largest diff. peak/hole / e Å^{-3}	0.44/-1.15

$R_{int} = \Sigma \mid F_o^2 - \langle F_o^2 \rangle \mid / \Sigma \mid F_o^2 \mid$

$R1 = \Sigma \mid \mid F_o \mid - \mid F_c \mid \mid / \Sigma \mid F_o \mid$

$wR2 = [\Sigma [w (F_o^2 - F_c^2)^2] / \Sigma [w (F_o^2)^2]]^{1/2}$

$\text{Goodness-of-fit} = [\Sigma [w (F_o^2 - F_c^2)^2] / (n-p)]^{1/2}$

n: number of independent reflections; p: number of refined parameters

Figure 43. Crystal data and structure refinement for (^{iPr}Sal-OH)Ni[P(*p*-Tol)$_3$](Me), precursor **5**.

References

(1) Bergman, R. G. C–H Activation. *Nature* 2007, *446* (7134), 391–393. https://doi.org/10.1038/446391a.

(2) Hartwig, J. F. Evolution of C–H Bond Functionalization from Methane to Methodology. *J Am Chem Soc* 2016, *138* (1), 2–24. https://doi.org/10.1021/jacs.5b08707.

(3) Dams, M.; Vos, D. E. D.; Celen, S.; Jacobs, P. A. Toward Waste-Free Production of Heck Products with a Catalytic Palladium System under Oxygen. *Angewandte Chemie Int Ed* 2003, *42* (30), 3512–3515. https://doi.org/10.1002/anie.200351524.

(4) Zhang, Y.-H.; Shi, B.-F.; Yu, J.-Q. Pd(II)-Catalyzed Olefination of Electron-Deficient Arenes Using 2,6-Dialkylpyridine Ligands. *J Am Chem Soc* 2009, *131* (14), 5072–5074. https://doi.org/10.1021/ja900327e.

(5) Lapointe, D.; Markiewicz, T.; Whipp, C. J.; Toderian, A.; Fagnou, K. Predictable and Site-Selective Functionalization of Poly(Hetero)Arene Compounds by Palladium Catalysis. *J Org Chem* 2011, *76* (3), 749–759. https://doi.org/10.1021/jo102081a.

(6) Liégault, B.; Lapointe, D.; Caron, L.; Vlassova, A.; Fagnou, K. Establishment of Broadly Applicable Reaction Conditions for the Palladium-Catalyzed Direct Arylation of Heteroatom-Containing Aromatic Compounds. *J Org Chem* 2009, *74* (5), 1826–1834. https://doi.org/10.1021/jo8026565.

(7) Shabashov, D.; Daugulis, O. Auxiliary-Assisted Palladium-Catalyzed Arylation and Alkylation of Sp2 and Sp3 Carbon–Hydrogen Bonds. *J Am Chem Soc* 2010, *132* (11), 3965–3972. https://doi.org/10.1021/ja910900p.

(8) Chan, K. S. L.; Fu, H.-Y.; Yu, J.-Q. Palladium(II)-Catalyzed Highly Enantioselective C–H Arylation of Cyclopropylmethylamines. *J Am Chem Soc* 2015, *137* (5), 2042–2046. https://doi.org/10.1021/ja512529e.

(9) Kuhl, N.; Hopkinson, M. N.; Wencel-Delord, J.; Glorius, F. Beyond Directing Groups: Transition-Metal-Catalyzed C-H Activation of Simple Arenes. *Angewandte Chemie Int Ed* 2012, *51* (41), 10236–10254. https://doi.org/10.1002/anie.201203269.

(10) Ishiyama, T.; Takagi, J.; Ishida, K.; Miyaura, N.; Anastasi, N. R.; Hartwig, J. F. Mild Iridium-Catalyzed Borylation of Arenes. High Turnover Numbers, Room Temperature Reactions, and Isolation of a Potential Intermediate. *J Am Chem Soc* 2002, *124* (3), 390–391. https://doi.org/10.1021/ja0173019.

(11) Cho, J.-Y.; Tse, M. K.; Holmes, D.; Jr., R. E. M.; III, M. R. S. Remarkably Selective Iridium Catalysts for the Elaboration of Aromatic C-H Bonds. *Science* 2002, *295* (5553), 305–308. https://doi.org/10.1126/science.1067074.

(12) Pamplin, C. B.; Legzdins, P. Thermal Activation of Hydrocarbon C–H Bonds by Cp*M(NO) Complexes of Molybdenum and Tungsten. *Accounts Chem Res* 2003, *36* (4), 223–233. https://doi.org/10.1021/ar0202215.

(13) Schwartsburd, L.; Iron, M. A.; Konstantinovski, L.; Ben-Ari, E.; Milstein, D. A Dearomatized Anionic PNP Pincer Rhodium Complex: C–H and H–H Bond Activation by Metal–Ligand Cooperation and Inhibition by Dinitrogen. *Organometallics* 2011, *30* (10), 2721–2729. https://doi.org/10.1021/om200104b.

(14) Janowicz, A. H.; Bergman, R. G. Activation of Carbon-Hydrogen Bonds in Saturated Hydrocarbons on Photolysis of (.Eta.5-C5Me5)(PMe3)IrH2. Relative Rates of Reaction of the Intermediate with Different Types of Carbon-Hydrogen Bonds and Functionalization of the Metal-Bound Alkyl Groups. *J Am Chem Soc* 1983, *105* (12), 3929–3939. https://doi.org/10.1021/ja00350a031.

(15) Friis, S. D.; Pirnot, M. T.; Buchwald, S. L. Asymmetric Hydroarylation of Vinylarenes Using a Synergistic Combination of CuH and Pd Catalysis. *J Am Chem Soc* 2016, *138* (27), 8372–8375. https://doi.org/10.1021/jacs.6b04566.

(16) Ackerman, L. K. G.; Lovell, M. M.; Weix, D. J. Multimetallic Catalysed Cross-Coupling of Aryl Bromides with Aryl Triflates. *Nature* 2015, *524* (7566), 454–457. https://doi.org/10.1038/nature14676.

(17) Lee, S. Y.; Hartwig, J. F. Palladium-Catalyzed, Site-Selective Direct Allylation of Aryl C–H Bonds by Silver-Mediated C–H Activation: A Synthetic and Mechanistic Investigation. *J Am Chem Soc* 2016, *138* (46), 15278–15284. https://doi.org/10.1021/jacs.6b10220.

(18) Wang, D.; Izawa, Y.; Stahl, S. S. Pd-Catalyzed Aerobic Oxidative Coupling of Arenes: Evidence for Transmetalation between Two Pd(II)-Aryl Intermediates. *J Am Chem Soc* 2014, *136* (28), 9914–9917. https://doi.org/10.1021/ja505405u.

(19) Durak, L. J.; Lewis, J. C. Transmetalation of Alkyl Ligands from Cp*(PMe 3)IrR1R2 to (Cod)PtR3X. *Organometallics* 2013, *32* (11), 3153–3156. https://doi.org/10.1021/om400289s.

(20) Low, J. J.; Goddard, W. A. Theoretical Studies of Oxidative Addition and Reductive Elimination: Hydrogen + Diphosphineplatinum -> Dihydridodiphosphineplatinum. *J Am Chem Soc* 1984, *106* (23), 6928–6937. https://doi.org/10.1021/ja00335a010.

(21) Partyka, D. V. Transmetalation of Unsaturated Carbon Nucleophiles from Boron-Containing Species to the Mid to Late d-Block Metals of Relevance to Catalytic C–X

Coupling Reactions (X = C, F, N, O, Pb, S, Se, Te). *Chem Rev* 2011, *111* (3), 1529–1595. https://doi.org/10.1021/cr1002276.

(22) Durak, L. J.; Lewis, J. C. Iridium-Promoted, Palladium-Catalyzed Direct Arylation of Unactivated Arenes. *Organometallics* 2014, *33* (3), 620–623. https://doi.org/10.1021/om401221v.

(23) Klei, S. R.; Golden, J. T.; Burger, P.; Bergman, R. G. Cationic Ir(III) Alkyl and Hydride Complexes: Stoichiometric and Catalytic C□H Activation by Cp∗(PMe3)Ir(R)(X) in Homogeneous Solution. *J Mol Catal Chem* 2002, *189* (1), 79–94. https://doi.org/10.1016/s1381-1169(02)00192-9.

(24) Klei, S. R.; Golden, J. T.; Tilley, T. D.; Bergman, R. G. Iridium-Catalyzed H/D Exchange into Organic Compounds in Water. *J Am Chem Soc* 2002, *124* (10), 2092–2093. https://doi.org/10.1021/ja017219d.

(25) Arndtsen, B. A.; Bergman, R. G. Unusually Mild and Selective Hydrocarbon C-H Bond Activation with Positively Charged Iridium(III) Complexes. *Science* 1995, *270* (5244), 1970–1973. https://doi.org/10.1126/science.270.5244.1970.

(26) Chan, N. H.; Gair, J. J.; Roy, M.; Qiu, Y.; Wang, D.-S.; Durak, L. J.; Chen, L.; Filatov, A. S.; Lewis, J. C. Insight into the Scope and Mechanism for Transmetalation of Hydrocarbyl Ligands on Complexes Relevant to C–H Activation. *Organometallics* 2020. https://doi.org/10.1021/acs.organomet.0c00628.

(27) Gair, J. J. Transition Metal Mediated Non-Directed C-H Functionalization. Ph.D. Thesis, The University of Chicago, Chicago, U.S.A., 2018.

(28) Widenhoefer, R. A.; Buchwald, S. L. Electronic Dependence of C–O Reductive Elimination from Palladium (Aryl)Neopentoxide Complexes. *J Am Chem Soc* 1998, *120* (26), 6504–6511. https://doi.org/10.1021/ja9806581.

(29) Laurent, P.; Veyre, L.; Thieuleux, C.; Donet, S.; Copéret, C. From Well-Defined Pt(Ii) Surface Species to the Controlled Growth of Silica Supported Pt Nanoparticles. *Dalton T* 2012, *42* (1), 238–248. https://doi.org/10.1039/c2dt31639k.

(30) Peterson, T. H.; Golden, J. T.; Bergman, R. G. Deprotonation of the Transition Metal Hydride (η 5 -C 5 Me 5)(PMe 3)IrH 2 . Synthesis and Chemistry of the Strongly Basic Lithium Iridate (η 5 -C 5 Me 5)(PMe 3)Ir(H)(Li). *Organometallics* 1999, *18* (10), 2005–2020. https://doi.org/10.1021/om980945d.

(31) Durak, L. J. Organometallic And Chemoenzymatic Approaches To Arene Arylation Via C-H Bond Cleavage. Ph.D. Thesis, The University of Chicago, Chicago, U.S.A., 2015.

(32) Bergbreiter, D. E.; Rainville, D. P. Electrophilic Substitution of Primary Alkylboranes. *J Organomet Chem* 1976, *121* (1), 19–23. https://doi.org/10.1016/s0022-328x(00)85504-7.

(33) Obligacion, J. V.; Semproni, S. P.; Pappas, I.; Chirik, P. J. Cobalt-Catalyzed C(Sp2)-H Borylation: Mechanistic Insights Inspire Catalyst Design. *J Am Chem Soc* 2016, *138* (33), 10645–10653. https://doi.org/10.1021/jacs.6b06144.

(34) Brunker, T. J.; Blank, N. F.; Moncarz, J. R.; Scriban, C.; Anderson, B. J.; Glueck, D. S.; Zakharov, L. N.; Golen, J. A.; Sommer, R. D.; Incarvito, C. D.; Rheingold, A. L. Chiral Palladium(0) Trans-Stilbene Complexes: Synthesis, Structure, and Oxidative Addition of Phenyl Iodide. *Organometallics* 2005, *24* (11), 2730–2746. https://doi.org/10.1021/om050115h.

(35) Oh, C. H.; Lim, Y. M.; You, C. H. Platinum-Catalyzed Cross-Couplings of Organoboronic Acids with Aryl Iodides. *Tetrahedron Lett* 2002, *43* (26), 4645–4647. https://doi.org/10.1016/s0040-4039(02)00863-8.

(36) Oh, C. H.; Reddy, V. R. Pt(0)-Catalyzed Alkynylation of Aryl Iodides with Lithium Alkynyltriisopropoxy Borates. *Synlett* 2004, No. 12, 2091–2094. https://doi.org/10.1055/s-2004-832819.

(37) Chen, L.; Sanchez, D. R.; Zhang, B.; Carrow, B. P. “Cationic” Suzuki–Miyaura Coupling with Acutely Base-Sensitive Boronic Acids. *J Am Chem Soc* 2017, *139* (36), 12418–12421. https://doi.org/10.1021/jacs.7b07687.

(38) Isobe, K.; Bailey, P. M.; Maitlis, P. M. Pentamethylcyclopentadienyl-Rhodium and -Iridium Complexes. Part 30. Trimethylphosphine-Chloro-, -Acetato-, and -Hydrido-Complexes and Related Compounds of (Hexamethylbenzene)Ruthenium. *J Chem Soc Dalton Transactions* 1981, *0* (9), 2003–2008. https://doi.org/10.1039/dt9810002003.

(39) Clark, H. C.; Manzer, L. E. Reactions of (π-1,5-Cyclooctadiene) Organoplatinum(II) Compounds and the Synthesis of Perfluoroalkylplatinum Complexes. *J Organomet Chem* 1973, *59*, 411–428. https://doi.org/10.1016/s0022-328x(00)95058-7.

(40) Shekhar, S.; Hartwig, J. F. Distinct Electronic Effects on Reductive Eliminations of Symmetrical and Unsymmetrical Bis-Aryl Platinum Complexes. *J Am Chem Soc* 2004, *126* (40), 13016–13027. https://doi.org/10.1021/ja0480365.

(41) Lewis, J. C.; Berman, A. M.; Bergman, R. G.; Ellman, J. A. Rh(I)-Catalyzed Arylation of Heterocycles via C–H Bond Activation: Expanded Scope through Mechanistic Insight. *J Am Chem Soc* 2008, *130* (8), 2493–2500. https://doi.org/10.1021/ja0748985.

(42) Ent, A. V. D.; Onderdelinden, A. L.; Schunn, R. A. Chlorobis(Cyclooctene)Rhodium(I) and–Iridium(I) Complexes. In *Inorganic Syntheses*; Angelici, R. J., Ed.; John Wiley & Sons, Inc.: Hoboken, NJ, USA, 1990; Vol. 28, pp 90–91.

(43) Gair, J. J.; Qiu, Y.; Chan, N. H.; Filatov, A. S.; Lewis, J. C. Rhodium Complexes of 2,6-Bis(Dialkylphosphinomethyl)Pyridines: Improved C–H Activation, Expanded Reaction Scope, and Catalytic Direct Arylation. *Organometallics* 2017, *36* (24), 4699–4706. https://doi.org/10.1021/acs.organomet.7b00532.

(44) Feller, M.; Diskin-Posner, Y.; Leitus, G.; Shimon, L. J. W.; Milstein, D. Direct Observation of Reductive Elimination of MeX (X = Cl, Br, I) from Rh III Complexes: Mechanistic Insight and the Importance of Sterics. *J Am Chem Soc* 2013, *135* (30), 11040–11047. https://doi.org/10.1021/ja401852c.

(45) Gair, J. J.; Qiu, Y.; Khade, R. L.; Chan, N. H.; Filatov, A. S.; Zhang, Y.; Lewis, J. C. Synthesis, Characterization, and Theoretical Investigation of a Transition State Analogue for Proton Transfer during C–H Activation by a Rhodium-Pincer Complex. *Organometallics* 2019, *38* (7), 1407–1412. https://doi.org/10.1021/acs.organomet.8b00887.

(46) Kubota, Y.; Hanaoka, T.-A.; Takeuchi, K.; Sugi, Y. An Efficient Synthesis of 2,6-Di-Tert -Butylphenyl Esters by Palladium-Catalysed Carbonylation of 4-Bromobiphenyl. *J Chem Soc Chem Commun* 1994, *0* (13), 1553–1554. https://doi.org/10.1039/c39940001553.

(47) Love, B. E.; Jones, E. G. The Use of Salicylaldehyde Phenylhydrazone as an Indicator for the Titration of Organometallic Reagents. *J Org Chem* 1999, *64* (10), 3755–3756. https://doi.org/10.1021/jo982433e.

(48) Fang, G. Y.; Aggarwal, V. K. Asymmetric Synthesis of A-Substituted Allyl Boranes and Their Application in the Synthesis of Iso-agatharesinol. *Angewandte Chemie Int Ed* 2007, *46* (3), 359–362. https://doi.org/10.1002/anie.200603659.

(49) Rashidi, M.; Nabavizadeh, S. M.; Akbari, A.; Habibzadeh, S. Secondary Kinetic Deuterium Isotope Effects in the Reaction of MeI with Organoplatinum(II) Complexes. *Organometallics* 2005, *24* (10), 2528–2532. https://doi.org/10.1021/om0500016.

(50) Roughley, S. D.; Jordan, A. M. The Medicinal Chemist's Toolbox: An Analysis of Reactions Used in the Pursuit of Drug Candidates. *J Med Chem* 2011, *54* (10), 3451–3479. https://doi.org/10.1021/jm200187y.

(51) Jeschke, P. The Unique Role of Halogen Substituents in the Design of Modern Agrochemicals. *Pest Manag Sci* 2010, *66* (1), 10–27. https://doi.org/10.1002/ps.1829.

(52) Vaillancourt, F. H.; Yeh, E.; Vosburg, D. A.; Garneau-Tsodikova, S.; Walsh, C. T. Nature's Inventory of Halogenation Catalysts: Oxidative Strategies Predominate. *Chem Rev* 2006, *106* (8), 3364–3378. https://doi.org/10.1021/cr050313i.

(53) Chen, X.; Pée, K. V. Catalytic Mechanisms, Basic Roles, and Biotechnological and Environmental Significance of Halogenating Enzymes. *Acta Bioch Bioph Sin* 2008, *40* (3), 183–193. https://doi.org/10.1111/j.1745-7270.2008.00390.x.

(54) Payne, J. T.; Andorfer, M. C.; Lewis, J. C. Regioselective Arene Halogenation Using the FAD-Dependent Halogenase RebH . *Angew Chem-ger Edit* 2013, *125* (20), 5379–5382. https://doi.org/10.1002/ange.201300762.

(55) Poor, C. B.; Andorfer, M. C.; Lewis, J. C. Improving the Stability and Catalyst Lifetime of the Halogenase RebH By Directed Evolution. *Chembiochem* 2014, *15* (9), 1286–1289. https://doi.org/10.1002/cbic.201300780.

(56) Payne, J. T.; Poor, C. B.; Lewis, J. C. Directed Evolution of RebH for Site-Selective Halogenation of Large Biologically Active Molecules. *Angewandte Chemie Int Ed* 2015, *54* (14), 4226–4230. https://doi.org/10.1002/anie.201411901.

(57) Andorfer, M. C.; Park, H. J.; Vergara-Coll, J.; Lewis, J. C. Directed Evolution of RebH for Catalyst-Controlled Halogenation of Indole C–H Bonds† †Electronic Supplementary Information (ESI) Available: Complete Experimental Procedures and Characterization Are Supplied as Supporting Information. See DOI: 10.1039/C5sc04680g. *Chem Sci* 2016, *7* (6), 3720–3729. https://doi.org/10.1039/c5sc04680g.

(58) Andorfer, M. C.; Belsare, K. D.; Girlich, A. M.; Lewis, J. C. Aromatic Halogenation by Using Bifunctional Flavin Reductase–Halogenase Fusion Enzymes. *Chembiochem* 2017, *18* (21), 2099–2103. https://doi.org/10.1002/cbic.201700391.

(59) Payne, J. T.; Butkovich, P. H.; Gu, Y.; Kunze, K. N.; Park, H. J.; Wang, D.-S.; Lewis, J. C. Enantioselective Desymmetrization of Methylenedianilines via Enzyme-Catalyzed Remote Halogenation. *J Am Chem Soc* 2018, *140* (2), 546–549. https://doi.org/10.1021/jacs.7b09573.

(60) Fisher, B. F.; Snodgrass, H. M.; Jones, K. A.; Andorfer, M. C.; Lewis, J. C. Site-Selective C–H Halogenation Using Flavin-Dependent Halogenases Identified via Family-Wide Activity Profiling. *Acs Central Sci* 2019, *5* (11), 1844–1856. https://doi.org/10.1021/acscentsci.9b00835.

(61) Voss, M.; Malca, S. H.; Buller, R. Exploring the Biocatalytic Potential of Fe/A-Ketoglutarate-Dependent Halogenases. *Chem European J* 2020, *26* (33), 7336–7345. https://doi.org/10.1002/chem.201905752.

(62) Hausinger, R. P. Fe(II)/α-Ketoglutarate-Dependent Hydroxylases and Related Enzymes. *Crit Rev Biochem Mol* 2008, *39* (1), 21–68. https://doi.org/10.1080/10409230490440541.

(63) Martinez, S.; Hausinger, R. P. Catalytic Mechanisms of Fe(II)- and 2-Oxoglutarate-Dependent Oxygenases*. *J Biol Chem* 2015, *290* (34), 20702–20711. https://doi.org/10.1074/jbc.r115.648691.

(64) Kim, C. Y.; Mitchell, A. J.; Glinkerman, C. M.; Li, F.-S.; Pluskal, T.; Weng, J.-K. The Chloroalkaloid (–)-Acutumine Is Biosynthesized via a Fe(II)- and 2-Oxoglutarate-Dependent Halogenase in Menispermaceae Plants. *Nat Commun* 2020, *11* (1), 1867. https://doi.org/10.1038/s41467-020-15777-w.

(65) Matthews, M. L.; Chang, W.; Layne, A. P.; Miles, L. A.; Krebs, C.; Bollinger, J. M. Direct Nitration and Azidation of Aliphatic Carbons by an Iron-Dependent Halogenase. *Nat Chem Biol* 2014, *10* (3), 209–215. https://doi.org/10.1038/nchembio.1438.

(66) Iyer, S. R.; Chaplin, V. D.; Knapp, M. J.; Solomon, E. I. O2 Activation by Nonheme FeII A-Ketoglutarate-Dependent Enzyme Variants: Elucidating the Role of the Facial Triad Carboxylate in FIH. *J Am Chem Soc* 2018, *140* (37), 11777–11783. https://doi.org/10.1021/jacs.8b07277.

(67) Hewitson, K. S.; Holmes, S. L.; Ehrismann, D.; Hardy, A. P.; Chowdhury, R.; Schofield, C. J.; McDonough, M. A. Evidence That Two Enzyme-Derived Histidine Ligands Are Sufficient for Iron Binding and Catalysis by Factor Inhibiting HIF (FIH)*. *J Biol Chem* 2008, *283* (38), 25971–25978. https://doi.org/10.1074/jbc.m804999200.

(68) Gorres, K. L.; Pua, K. H.; Raines, R. T. Stringency of the 2-His–1-Asp Active-Site Motif in Prolyl 4-Hydroxylase. *Plos One* 2009, *4* (11), e7635. https://doi.org/10.1371/journal.pone.0007635.

(69) Grzyska, P. K.; Müller, T. A.; Campbell, M. G.; Hausinger, R. P. Metal Ligand Substitution and Evidence for Quinone Formation in Taurine/α-Ketoglutarate Dioxygenase. *J Inorg Biochem* 2007, *101* (5), 797–808. https://doi.org/10.1016/j.jinorgbio.2007.01.011.

(70) Chaplin, V. D.; Hangasky, J. A.; Huang, H.-T.; Duan, R.; Maroney, M. J.; Knapp, M. J. Chloride Supports O2 Activation in the D201G Facial Triad Variant of Factor-Inhibiting Hypoxia Inducible Factor, an A-Ketoglutarate Dependent Oxygenase. *Inorg Chem* 2018, *57* (20), 12588–12595. https://doi.org/10.1021/acs.inorgchem.8b01736.

(71) Papadopoulou, A.; Meierhofer, J.; Meyer, F.; Hayashi, T.; Schneider, S.; Sager, E.; Buller, R. Re-Programming and Optimization of a L-Proline Cis-4-Hydroxylase for the Cis-3-Halogenation of Its Native Substrate. *Chemcatchem* 2021. https://doi.org/10.1002/cctc.202100591.

(72) Hibi, M.; Kawashima, T.; Kasahara, T.; Sokolov, P. M.; Smirnov, S. V.; Kodera, T.; Sugiyama, M.; Shimizu, S.; Yokozeki, K.; Ogawa, J. A Novel Fe(II)/A-ketoglutarate-dependent Dioxygenase from Burkholderia Ambifaria Has B-hydroxylating Activity of N-succinyl L-leucine. *Lett Appl Microbiol* 2012, *55* (6), 414–419. https://doi.org/10.1111/j.1472-765x.2012.03308.x.

(73) Mitchell, A. J.; Dunham, N. P.; Bergman, J. A.; Wang, B.; Zhu, Q.; Chang, W.; Liu, X.; Boal, A. K. Structure-Guided Reprogramming of a Hydroxylase To Halogenate Its Small Molecule Substrate. *Biochemistry-us* 2017, *56* (3), 441–444. https://doi.org/10.1021/acs.biochem.6b01173.

(74) Hibi, M.; Kasahara, T.; Kawashima, T.; Yajima, H.; Kozono, S.; Smirnov, S. V.; Kodera, T.; Sugiyama, M.; Shimizu, S.; Yokozeki, K.; Ogawa, J. Multi-Enzymatic Synthesis of Optically Pure B-Hydroxy A-Amino Acids. *Adv Synth Catal* 2015, *357* (4), 767–774. https://doi.org/10.1002/adsc.201400672.

(75) Qin, H.-M.; Miyakawa, T.; Jia, M. Z.; Nakamura, A.; Ohtsuka, J.; Xue, Y.-L.; Kawashima, T.; Kasahara, T.; Hibi, M.; Ogawa, J.; Tanokura, M. Crystal Structure of a Novel N-Substituted L-Amino Acid Dioxygenase from Burkholderia Ambifaria AMMD. *Plos One* 2013, *8* (5), e63996. https://doi.org/10.1371/journal.pone.0063996.

(76) Hangasky, J. A.; Taabazuing, C. Y.; Martin, C. B.; Eron, S. J.; Knapp, M. J. The Facial Triad in the α-Ketoglutarate Dependent Oxygenase FIH: A Role for Sterics in Linking Substrate Binding to O2 Activation. *J Inorg Biochem* 2017, *166*, 26–33. https://doi.org/10.1016/j.jinorgbio.2016.10.007.

(77) Müller, K.; Faeh, C.; Diederich, F. Fluorine in Pharmaceuticals: Looking Beyond Intuition. *Science* 2007, *317* (5846), 1881–1886. https://doi.org/10.1126/science.1131943.

(78) Gillis, E. P.; Eastman, K. J.; Hill, M. D.; Donnelly, D. J.; Meanwell, N. A. Applications of Fluorine in Medicinal Chemistry. *J Med Chem* 2015, *58* (21), 8315–8359. https://doi.org/10.1021/acs.jmedchem.5b00258.

(79) Liang, T.; Neumann, C. N.; Ritter, T. Introduction of Fluorine and Fluorine-Containing Functional Groups. *Angewandte Chemie Int Ed* 2013, *52* (32), 8214–8264. https://doi.org/10.1002/anie.201206566.

(80) O'Hagan, D.; Deng, H. Enzymatic Fluorination and Biotechnological Developments of the Fluorinase. *Chem Rev* 2015, *115* (2), 634–649. https://doi.org/10.1021/cr500209t.

(81) Solomon, E. I.; Brunold, T. C.; Davis, M. I.; Kemsley, J. N.; Lee, S.-K.; Lehnert, N.; Neese, F.; Skulan, A. J.; Yang, Y.-S.; Zhou, J. Geometric and Electronic Structure/Function Correlations in Non-Heme Iron Enzymes. *Chem Rev* 2000, *100* (1), 235–350. https://doi.org/10.1021/cr9900275.

(82) Neidig, M. L.; Brown, C. D.; Light, K. M.; Fujimori, D. G.; Nolan, E. M.; Price, J. C.; Barr, E. W.; Bollinger, J. M.; Krebs, C.; Walsh, C. T.; Solomon, E. I. CD and MCD of CytC3 and Taurine Dioxygenase: Role of the Facial Triad in α-KG-Dependent Oxygenases. *J Am Chem Soc* 2007, *129* (46), 14224–14231. https://doi.org/10.1021/ja074557r.

(83) Payne, J. T.; Andorfer, M. C.; Lewis, J. C. Regioselective Arene Halogenation Using the FAD-Dependent Halogenase RebH . *Angewandte Chemie Int Ed* 2013, *52* (20), 5271–5274. https://doi.org/10.1002/anie.201300762.

(84) Mecking, S.; Held, A.; Bauers, F. M. Aqueous Catalytic Polymerization of Olefins. *Angewandte Chemie Int Ed* 2002, *41* (4), 544–561. https://doi.org/10.1002/1521-3773(20020215)41:4<544::aid-anie544>3.0.co;2-u.

(85) Wang, L.; Lu, R. S.; Bau, R.; Flood, T. C. Coordination Polymerization of Ethylene by Single-Component Rhodium Catalysts in Protic Solvents. *J Am Chem Soc* 1993, *115* (15), 6999–7000. https://doi.org/10.1021/ja00068a078.

(86) Johnson, L. K.; Killian, C. M.; Brookhart, M. New Pd(II)- and Ni(II)-Based Catalysts for Polymerization of Ethylene and .Alpha.-Olefins. *J Am Chem Soc* 1995, *117* (23), 6414–6415. https://doi.org/10.1021/ja00128a054.

(87) Held, A.; Bauers, F. M.; Mecking, S. Coordination Polymerization of Ethylene in Water by Pd(Ii) and Ni(Ii) Catalysts. *Chem Commun* 2000, *0* (4), 301–302. https://doi.org/10.1039/a908633a.

(88) Wang, C.; Friedrich, S.; Younkin, T. R.; Li, R. T.; Grubbs, R. H.; Bansleben, D. A.; Day, M. W. Neutral Nickel(II)-Based Catalysts for Ethylene Polymerization. *Organometallics* 1998, *17* (15), 3149–3151. https://doi.org/10.1021/om980176y.

(89) Younkin, T. R.; Connor, E. F.; Henderson, J. I.; Friedrich, S. K.; Grubbs, R. H.; Bansleben, D. A. Neutral, Single-Component Nickel (II) Polyolefin Catalysts That Tolerate Heteroatoms. *Science* 2000, *287* (5452), 460–462. https://doi.org/10.1126/science.287.5452.460.

(90) Connor, E. F.; Younkin, T. R.; Henderson, J. I.; Waltman, A. W.; Grubbs, R. H. Synthesis of Neutral Nickel Catalysts for Ethylene Polymerization – the Influence of Ligand Size on Catalyst Stability. *Chem Commun* 2003, *0* (18), 2272–2273. https://doi.org/10.1039/b306701g.

(91) Bauers, F. M.; Mecking, S. High Molecular Mass Polyethylene Aqueous Latexes by Catalytic Polymerization. *Angewandte Chemie Int Ed* 2001, *40* (16), 3020–3022. https://doi.org/10.1002/1521-3773(20010817)40:16<3020::aid-anie3020>3.0.co;2-7.

(92) Bauers, F. M.; Mecking, S. Aqueous Homo- and Copolymerization of Ethylene by Neutral Nickel(II) Complexes. *Macromolecules* 2001, *34* (5), 1165–1171. https://doi.org/10.1021/ma001704w.

(93) Göttker-Schnetmann, I.; Korthals, B.; Mecking, S. Water-Soluble Salicylaldiminato Ni(II)–Methyl Complexes: Enhanced Dissociative Activation for Ethylene Polymerization with Unprecedented Nanoparticle Formation. *J Am Chem Soc* 2006, *128* (24), 7708–7709. https://doi.org/10.1021/ja0619962.

(94) Wehrmann, P.; Mecking, S. Aqueous Dispersions of Polypropylene and Poly(1-Butene) with Variable Microstructures Formed with Neutral Nickel(II) Complexes. *Macromolecules* 2006, *39* (18), 5963–5964. https://doi.org/10.1021/ma061462l.

(95) Lewis, J. C. Artificial Metalloenzymes and Metallopeptide Catalysts for Organic Synthesis. *Acs Catal* 2013, *3* (12), 2954–2975. https://doi.org/10.1021/cs400806a.

(96) Abe, S.; Hirata, K.; Ueno, T.; Morino, K.; Shimizu, N.; Yamamoto, M.; Takata, M.; Yashima, E.; Watanabe, Y. Polymerization of Phenylacetylene by Rhodium Complexes within a Discrete Space of Apo-Ferritin. *J Am Chem Soc* 2009, *131* (20), 6958–6960. https://doi.org/10.1021/ja901234j.

(97) Onoda, A.; Fukumoto, K.; Arlt, M.; Bocola, M.; Schwaneberg, U.; Hayashi, T. A Rhodium Complex-Linked β-Barrel Protein as a Hybrid Biocatalyst for Phenylacetylene Polymerization. *Chem Commun* 2012, *48* (78), 9756–9758. https://doi.org/10.1039/c2cc35165j.

(98) Gu, Y. New Approaches In Artificial (Metallo)Enzymes. Ph.D. Thesis, The University of Chicago, Chicago, U.S.A., 2018.

(99) Srinivas, V.; Nakajima, Y.; Ando, W.; Sato, K.; Shimada, S. (Salicylaldiminato)Ni(Ii)-Catalysts for Hydrosilylation of Olefins. *Catal Sci Technol* 2015, *5* (4), 2081–2084. https://doi.org/10.1039/c5cy00270b.

(100) Hyster, T. K.; Knörr, L.; Ward, T. R.; Rovis, T. Biotinylated Rh(III) Complexes in Engineered Streptavidin for Accelerated Asymmetric C–H Activation. *Science* 2012, *338* (6106), 500–503. https://doi.org/10.1126/science.1226132.

(101) Mérel, D. S.; Gaillard, S.; Ward, T. R.; Renaud, J.-L. Achiral Cyclopentadienone Iron Tricarbonyl Complexes Embedded in Streptavidin: An Access to Artificial Iron Hydrogenases and Application in Asymmetric Hydrogenation. *Catal Lett* 2016, *146* (3), 564–569. https://doi.org/10.1007/s10562-015-1681-6.

(102) Chan, M. S. W.; Deng, L.; Ziegler, T. Density Functional Study of Neutral Salicylaldiminato Nickel(II) Complexes as Olefin Polymerization Catalysts. *Organometallics* 2000, *19* (14), 2741–2750. https://doi.org/10.1021/om000055+.

(103) Zhang, T.; Guo, D.; Jie, S.; Sun, W.; Li, T.; Yang, X. Influence of Electronic Effect on Catalytic Activity of Salicylaldiminato Nickel(II) Complexes. *J Polym Sci Part Polym Chem* 2004, *42* (19), 4765–4774. https://doi.org/10.1002/pola.20242.

(104) Göttker-Schnetmann, I.; Wehrmann, P.; Röhr, C.; Mecking, S. Substituent Effects in (κ 2 - N , O)-Salicylaldiminato Nickel(II)–Methyl Pyridine Polymerization Catalysts: Terphenyls Controlling Polyethylene Microstructures. *Organometallics* 2007, *26* (9), 2348–2362. https://doi.org/10.1021/om0611498.

(105) Bastero, A.; Göttker-Schnetmann, I.; Röhr, C.; Mecking, S. Polymer Microstructure Control in Catalytic Polymerization Exclusively by Electronic Effects of Remote Substituents. *Adv Synth Catal* 2007, *349* (14-15), 2307–2316. https://doi.org/10.1002/adsc.200700127.

(106) Chang, S.; Jones, L.; Wang, C.; Henling, L. M.; Grubbs, R. H. Synthesis and Characterization of New Ruthenium-Based Olefin Metathesis Catalysts Coordinated with Bidentate Schiff-Base Ligands. *Organometallics* 1998, *17* (16), 3460–3465. https://doi.org/10.1021/om970910y.

(107) Cokol, N. K.; Kaya, S.; Balci, M. A New Synthon for the Synthesis of Aminoinositol Derivatives. *Tetrahedron Lett* 2017, *58* (28), 2732–2735. https://doi.org/10.1016/j.tetlet.2017.05.099.

(108) Mallin, H.; Hestericová, M.; Reuter, R.; Ward, T. R. Library Design and Screening Protocol for Artificial Metalloenzymes Based on the Biotin-Streptavidin Technology. *Nat Protoc* 2016, *11* (5), 835–852. https://doi.org/10.1038/nprot.2016.019.

(109) Inard, C.; Fourcade, E.; Baron, R.; Tovar, D.; Chaisemartin, L.; Blonski, C.; Faye, J.-C. Syntheses of Functionalized Biotin N-1‘ Derivatives: New Tools for the Control of Gene Expression with Small Molecules. *Bioconjugate Chem* 2006, *17* (4), 1030–1035. https://doi.org/10.1021/bc060010a.

(110) Corona, C.; Bryant, B. K.; Arterburn, J. B. Synthesis of a Biotin-Derived Alkyne for Pd-Catalyzed Coupling Reactions. *Org Lett* 2006, *8* (9), 1883–1886. https://doi.org/10.1021/ol060458r.